IOWA STATE UNIVERSITY
Digital Repository

Graduate Theses and Dissertations

Iowa State University Capstones, Theses and Dissertations

2014

Evaluation of the need for longitudinal median joints in bridge decks on dual structures

Zhengyu Liu
Iowa State University

Follow this and additional works at: https://lib.dr.iastate.edu/etd

 Part of the Civil Engineering Commons

Recommended Citation
Liu, Zhengyu, "Evaluation of the need for longitudinal median joints in bridge decks on dual structures" (2014). *Graduate Theses and Dissertations*. 14204.
https://lib.dr.iastate.edu/etd/14204

This Thesis is brought to you for free and open access by the Iowa State University Capstones, Theses and Dissertations at Iowa State University Digital Repository. It has been accepted for inclusion in Graduate Theses and Dissertations by an authorized administrator of Iowa State University Digital Repository. For more information, please contact digirep@iastate.edu.

www.manaraa.com

Evaluation of the need for longitudinal median joints in bridge decks on dual structures

by

Zhengyu Liu

A thesis submitted to the graduate faculty

in partial fulfillment of the requirements for the degree of

MASTER OF SCIENCE

Major: Civil Engineering (Structural Engineering)

Program of Study Committee:
Brent M. Phares, Major Professor
Terry Wipf
Kejin Wang

Iowa State University
Ames, Iowa
2014

Copyright © Zhengyu Liu, 2014. All rights reserved.

www.manaraa.com

TABLE OF CONTENTS

www.manaraa.com

www.manaraa.com

www.manaraa.com

www.manaraa.com

LIST OF FIGURES

Page

www.manaraa.com

www.manaraa.com

www.manaraa.com

www.manaraa.com

www.manaraa.com

www.manaraa.com

LIST OF TABLES

Page

www.manaraa.com

ACKNOWLEDGEMENTS

I would like to thank my committee chair, Brent M Phares, and my committee members, Terry Wipf and Kejin Wang for their guidance and support throughout the course of this research.

In addition, I would also like to thank my friends, colleagues, the department faculty and staff for making my time at Iowa State University a wonderful experience. I want to also offer my appreciation to those who were willing to participate in my surveys and observations, without whom, this thesis would not have been possible.

Finally, thanks to my family for their encouragement.

www.manaraa.com

ABSTRACT

In the State of Iowa, bridge widths are typically limited to 60-ft. Although the justification for 60-ft is somewhat unknown, there is a desire, in some cases, to build wider bridges. For example, when dual bridges are constructed in urban areas they are frequently constructed very close to one another. In essence, this close construction results in a "joint" between bridges which is known to trap water and other debris which in some cases has led to accelerated deterioration. At the same time, integral abutment bridges are in wide use (in Iowa and beyond), since they have no expansion joints to allow leaking of chloride-contaminated water that can corrode the bottom of the deck and the adjacent girders. Thus, the practice of limiting bridge width and introducing a "joint" between dual bridges goes against other current practices. However, because there is concern that increased bridge width results in an increased propensity for cracking, there is resistance to commonly constructing wider bridges.

The primary objective of this project is to determine the effect of bridge width on deck cracking in bridges. Other parameters, such as bridge skew, girder spacing and type, abutment type, pier type and number of bridge spans were also studied. To achieve the above objectives, one bridge was selected to conduct live-load and long-term testing. The data obtained from both field tests were used to calibrate a three-dimensional (3D) Finite Element Model (FEM). Three different types of loading-live loading, thermal loading and shrinkage loading-were applied and used to calibrate the analytical model. A parametric study was then conducted using the calibrated FEM.

The general conclusions are as follows:

- Longitudinal and diagonal cracking in the deck near the abutment on an integral abutment bridge is due to the temperature differences between the abutment and the deck.

www.manaraa.com

- Based upon a limited review of bridges in the Iowa DOT inventory, it appears that, regardless of bridge width, longitudinal and diagonal cracks are prevalent in integral abutment bridges but not in bridges with stub abutments.
- The parametric study results show that bridge width and skew have minimal effect on the strain in the deck bridge resulting from restrained thermal expansion. In other words, integral abutment bridges will show similar cracking regardless of width.
- Pier type, girder type, girder spacing and number of spans also appear to have no influence on the level of restrained thermal expansion strain in the deck near the abutment.
- FEM results showed that an effective solution to reduce cracking in the deck might be to place an isolation pad between the soil and back side of abutment.

www.manaraa.com

CHAPTER 1. INTRODUCTION

1.1 Background

Nationally, longitudinal joints are commonly used in dual structure bridge decks for the sake of ease of construction, staged-construction, construction of wide bridges, etc. Among other reasons, the Iowa Department of Transportation (DOT) requires the use of longitudinal joints to reduce/eliminate deck cracking in wide bridges. This deck cracking can be induced by transverse contractions due to temperature change, shrinkage, and live loads. Longitudinal deck joints are thought to provide a relief point and to reduce the overall amount of shrinkage that must be accommodated. Unfortunately, these longitudinal joints have been known to begin leaking and allow chloride contaminated water to reach the bottom of the deck overhang and the adjacent girders. This can be problematic when the joint is narrow and located between median barrier rails where chloride contaminated snow and debris can be trapped for a long period. On weathering steel bridges, the constant exposure to moisture combined with limited air circulation prevents the natural formation of the protective patina. Thus, minimization or elimination of using longitudinal joints may significantly lessen the aforementioned problems. A preliminary search of bridge design manuals from several state DOTs indicates that state DOTs are not in agreement with regard to the maximum width of the continuous deck, which ranges from 60 to 120 ft.

1.2 Objective and Scope

The main objective of this research is to determine the maximum width of a continuous deck that can be used without negatively impacting performance. To achieve this objective,

www.manaraa.com

analytical techniques including finite element analysis (FEA) were used to investigate the behavior of decks with various widths under typical loadings. Experimental testing was conducted in order to provide validation of the analytical models, specifically.

One bridge was selected based upon bridge inspection results to conduct live-load and long-term testing. The data obtained from both field tests were used to calibrate a three-dimensional (3D) Finite Element Model (FEM). Three different types of loading-live loading, thermal loading and shrinkage loading-were applied. The crack pattern from the FEM was compared to the crack pattern from bridge inspection results to identify the primary crack-induced loading. The validated model was then extrapolated to various other configurations to study the influence of those parameters.

1.3 Final Products

Based on the outcome of analytical and experimental investigations, the influence of various parameters, which include bridge width, bridge skew, abutment type, pier type, girder type, girder spacing and number of spans was studied. In addition to a summary of the results (including identification of structurally significant parameters), this report also includes recommendations for means and methods for potentially reducing deck cracking due to thermal loads.

www.manaraa.com

CHAPTER 2. LITERATURE REVIEW/SURVEY

2.1 Literature Review

2.1.2 Cracking of integral abutment bridge

Cracking in continuous bridge decks has been a concern of bridge designers and owners for decades. Various contributing factors have been identified, but their relationships are not fully understood (TRS1105 2011). Research has been conducted to study the cracks in continuous decks of integral abutment bridges, but most focus on transverse cracks rather than longitudinal and diagonal cracks.

Martin and Burke summarized the issues associated with integral abutment bridges, including early-age cracking of concrete, erosion of roadway shoulders, embankments, and backfill adjacent to bridge abutments, casting connections between moving members, and construction errors. They found that diagonal deck cracks located at acute corners of integral-type bridges are occasionally reported, and some uniformly spaced straight cracks are located over and perpendicular to the concrete diaphragms. (Martin and Burke 1999)

2.1.1 Integral abutment bridge advantage

Integral abutment bridges have been gaining popularity since the first integral abutment bridge was built in the state of New York in the late 1970s. The most prominent advantage of the integral abutment bridge is the elimination of expansion joints. Expansion joints typically leak chloride contaminated water that reaches and corrodes the bottom of the deck and the girders. Damaged and leaking bridge deck joints are a problem which effectively shortens the service life

www.manaraa.com

of many bridges (Kunin and Alampalli 2000). Purvis summarized performance data for commonly used expansion joint systems, and also introduced examples of selection criteria and design guidelines in his synthesis report. He concluded that there should be a high priority for state DOTs to reduce or eliminate deck joints whenever possible, although joints are sometimes unavoidable. (Purvis 2003)

Beyond reduced initial costs and long-term maintenance expenses, and the elimination of costly expansion joints and bearings, Kunin summarized that the benefits offered by integral abutment bridges also includes decreased impact loads, improved riding quality, simplified construction procedures, reduced substructure cost and increased structure continuity to resist seismic events and overloading. (Kunin and Alampalli 2000)

2.1.3 Reasons that induce cracks on bridge decks

Russell and Gerken reported that, rather than dead and live loadings, the major loadings that induce transverse cracks on a jointless bridge are temperature, creep and shrinkage loadings. Temperature loading includes daily temperature changes and seasonal temperature changes. Daily temperature changes can induce a temperature gradient through the depth of the bridge, while seasonal temperature changes cause changes in total structure length between summer and winter. Shrinkage and creep of concrete girders and the deck introduce forces into the structures and also produce interaction effects with temperature and humidity variations. (Russel and Gerken 1994)

Frosch and Blackman completed an investigation to determine the factors affecting transverse and longitudinal bridge deck cracking. During laboratory work, the contribution of stay-in-place steel formwork was studied. Further, the effects of reinforcement bar spacing and epoxy thickness on crack width and spacing were evaluated. They concluded that the observed

www.manaraa.com

longitudinal cracking was caused by a combination of factors, including restrained shrinkage and a construction detail associated with the stay-in-place formwork for the deck. (Frosch, Blackman and Radabaugh 2003)

Stringer and Burgueno used experimentally calibrated non-linear finite-element models to predict cracks in jointless bridge decks with integral abutments and semi-integral abutments. A parametric study was conducted using the finite-element model to study the influential factors on bridge deck cracking. During the bridge inspection phase, they found that few longitudinal cracks were observed on steel girder bridges. These results confirmed that the more restraint present in the bridge system, the greater the build-up of the restrained tensile forces will be and the more cracking will occur. The result of the study was that longitudinal cracking can be attributed to bridge geometry, and is not due to restrained concrete shrinkage. They also concluded that changing the amount of reinforcement and reinforcement distribution has no significant effect on deck cracking. Using larger shear studs at a larger spacing was found to slightly improve performance. (Strainge and Burgueno 2012)

Paul and Laman built 2D and 3D models to investigate forces and stresses induced by thermal loading in the superstructure of pre-stressed concrete integral abutment bridges. A preliminary study was conducted to compare the response of a central Pennsylvania Bridge with numerical 2D and 3D model results. The results from this parametric study showed that (1) the largest thermally-induced superstructure force and stress occurred near the abutment; (2) the bridge length and abutment height can influence thermally-induced superstructure force; (3) the number of spans can affect thermally-induced superstructure forces; (4) thermally-induced superstructure forces are comparable to those caused by live load. The research results also indicated that calculated thermally-induced stresses at the bottom of the beam and top of the

www.manaraa.com

deck slab exceeded the tensile strength of the beam and slab concrete near the abutment, which suggests that cracks would occur in those regions. (Paul, Laman and Linzell 2005)

Fu and Feng used a calibrated finite element model to study corner cracking in the concrete decks of skewed bridges. Twenty straight and twenty skewed bridges were inspected in terms of corner cracking in the deck, and the results show no obvious causal relation. Two skewed decks were selected for field testing and the results were used to calibrate finite element models. The results from the parametric study using the calibrated finite element models indicated that the main cause of skew deck corner cracking is thermal and shrinkage load. (Fu, et al. 2007)

2.2 Survey

To supplement the literature search briefly summarized above, a search of state DOTs design manuals related to bridge width limitations was conducted. A survey of state DOTs related to deck cracking performance was also conducted. The results of these additional information searches are summarized in the following.

2.2.1 Bridge width limitation

The bridge design manuals from several state DOTs indicate that state DOTs are not in agreement with regard to the maximum width of continuous decks in integral abutment bridges, which ranges from 60 to 120 ft. Nevada DOT (2008) requires the use of longitudinal joints for the decks of multiple-span bridges with large skews. Illinois DOT (2012) has different guidelines for non-staged and staged construction, as shown in Table 1.

www.manaraa.com

Table 1. Bridge width limitations on using longitudinal open joints by state DOTs

Transportation Agencies		Deck Width	Skew and Span Configuration
D.C. DOT (2009)		> 88 ft	…
Montana DOT (2002)		> 88 ft	…
Nevada DOT(2008)		> 120 ft	Muliple-span bridges with large skews
Illinois DOT (2012)	No stage construction	> 120 ft (Center-to-center distance of exterior girders)	…
	Stage construction	> 120 ft (Total width of the staged pours)	
Minnesota DOT (2012)		> 100 ft	…
Iowa DOT (2012)		> 60 ft	…

2.2.2 Deck cracking performance

A survey was conducted of DOTs from the mid-central states in the United States in August 2014. The purpose of this survey was to collect information regarding bridge width limitations and deck cracking performance. The questions in the survey and the responses from the eight states are listed in Table 2. In summary:

- No limitations on bridge width were reported, although some states (Illinois, Michigan) do require the use of open joints or construction joints when bridges exceed a certain width.
- No DOT thinks that deck cracking can be attributed to bridge width.
- DOTs are using varying approaches to control the cracks in the deck in the early stages.
- Some DOTs think that substructure elements such as columns, bearings or piles may be influenced by bridge width.

www.manaraa.com

Table 2. Summary of survey

DOTs	Q1. What, if any, limitations does your state have on bridge width?	Q2. Has there ever been observed deck cracking that was attributed to total bridge width? If so, please describe.	Q3. Besides limiting bridge width, have you used other techniques to control the development of deck cracking?	Q4. Are there other bridge components whose design and/or behavior are influenced by total bridge width?
North Dakota	No	I do not think anyone is looking.	The rate that the deck is placed. Wet cure	No
South Dakota	No	None of any significance.	None specifically to control longitudinal cracking.	Substructure components, especially columns in frame bents.
Minnesota	No	Not that can be attributed mainly to width of the bridge.	Transverse fixity is provided for only the interior 2/3 of the bearings Deck sequences are required for decks wider than 90 feet. High performance concrete, night pours, and fibers have been used.	Substructures and bearings.
Illinois	No. When the distance between fascia girders is greater than 90ft - a 1" open joint is required.	Deck cracking issues do exist but can't be attributed to width alone.	Pouring sequences. Fibers, HPC, Type K cement, etc. Lower the maximum ambient temperature for deck casting. Limiting LL deflection to something more restrictive than L/800.	Substructures, bearings, joints.
Wisconsin	No	Not sure if we've seen cracking directly attributable to deck width.	7 day wet cure for normal deck concrete 14 day wet cure for high-performance concrete decks.	Longer piers
Kansas	No	Not width. The different shrinkage rate between the pile-lower abutment beam and upper abutment beam-deck.	Add additional transverse reinforcement.	Deck drainage design
Michigan	No. Bridge width greater than 100'-0" requires a longitudinal open/expansion joint.	Our deck cracking problems have been attributed to the acute corners on bridges with an excessive skew.	Nighttime casting of superstructure concrete	Not that I can think of…
Nebraska	No	No	Using minimum placing and finishing rate to prevent setting before continuous spans are placed	Substructures (pile bearings) and bearings.

www.manaraa.com

CHAPTER 3. FIELD TESTING

3.1 Introduction

The purpose of the field testing conducted as part of this research was to provide data to be used during the calibration of a finite element model (FEM) which will be subsequently described. During field testing, two types of tests were conducted on a bridge near Waterloo, Iowa: Bridge short-term and long-term. In this chapter, the process followed to select the bridge for field testing is described. Additionally, the instrumentation plans for the short-term, live-load test and the long-term test are described and illustrated.

3.2 Bridge Inspection

To select the most suitable bridge for field testing, several factors including safety, structure type, structure geometry, traffic condition, and crack condition were considered. In total, five bridges were selected by the Iowa DOT for initial consideration and inspection as these bridges had varied locations, ages, element types, bridge geometries, and crack conditions. The cracking condition in the deck from these five bridges were generically compared in terms of the effect from the factors such as abutment type and bearing type. The key results of these inspections are summarized in Table 3.

Based upon the bridge inspection results and further discussion with the project Technical Advisory Committee (TAC), Bridge #605220 was selected for the following reasons. (1) The crack pattern on its deck is typical. (2) The traffic condition on the bridge and under the bridge are suitable for live-load testing and instrumentation work can be conducted without completely stop traffic on the bridge nor under the bridge.

www.manaraa.com

Table 3. Results of bridge inspection for selection of field testing bridge

Bridge FHWA No.	Bridge Location	Type	Deck Width (ft)	No. of spans	Abutment type	Bearing type	Cracks		Traffic	Year built
							Inspection Report	Our Inspection (Cracks near abutment):		
012411	Mills Civic Parkway Over I-35	PPCB	196	2	Integral	Fixed	Noted cracking problem	Diagonal cracks near the corners and longitudinal cracks in the center region along deck width. 1/3 of bridge on each side Length: 3-6 ft. Spacing: 8-10 ft.	Heavy Complex traffic paths; Curved lanes	2001
605220	Iowa-21 over US-20	PPCB	81	4	Integral	Fixed	Longitudinal cracks (especially near the abutments)	Diagonal cracks near the corners and longitudinal cracks in the center region along deck width. 1/3 of bridge on each side Length: 3-15 ft. Spacing: 2-3 ft.	State highway Straight lanes	1983
604730	Blairsferry road over I-380	PPCB	84	4	Integral	Fixed	Longitudinal cracks (especially near the abutments) Hollow areas on the bottom of crack	Diagonal cracks near the corners and longitudinal cracks in the center region along deck width. 1/3 of bridge on each side Length: 3-15ft. Spacing: 2-4 ft.	Complex traffic paths; Curved lanes Far away	1980
042740	I-235 over the Des Moines River	CWPG	75.9	10	Stub	Expansion	Noted longitudinal cracking problem	None Found	Heavy Interstate highway Straight lanes	1964
042891	I-235 over East 15th street	CWPG	71	3	Integral	Fixed	A few scattered hairline transverse cracks	One or two (6-8 ft)	Heavy Interstate highway Straight lanes	2004

* PPCB: pre-stressed concrete beam; CWPG: continuous welded plate girder

www.manaraa.com

Figure 1 shows the general configuration of Bridge #605220 which is a four-span bridge with a small 1.5 degree skew. Figure 2 and Figure 3 shows an overall cross-sectional view and the cross-section details in a typical bay. The bridge consists of an integral abutment and 12 pre-stressed concrete girders. In general, the bridge is in very good condition. Figure 4 to Figure 6 shows the photographs of bridge geometry and crack conditions on the top of the deck. With respect to degradation/damage that might be attributed to the width of the deck, the only observable evidence was cracking of the deck. The crack patterns on the top and bottom surface of the deck of Bridge #605220 are shown in Figure 7 and Figure 8, respectively. Of interest in these sketches is (1) the amount of cracking observed and (2) the orientation of the cracks. It was generally observed that cracks near the centerline of the bridge were less numerous than at the edges and that cracks near the centerline tended to be orientated longitudinally and those near the edges tended to be oriented at closer to 45 degrees with the bridge centerline.

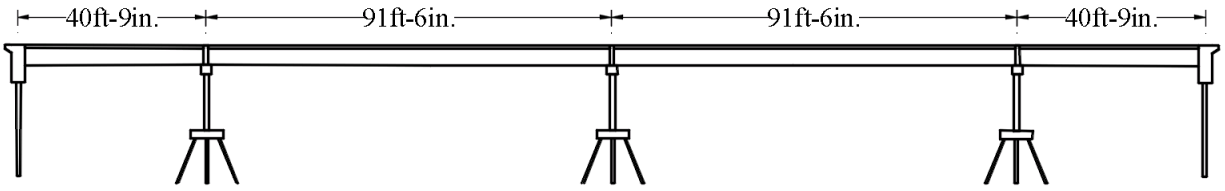

Figure 1. Side view of Bridge #605220

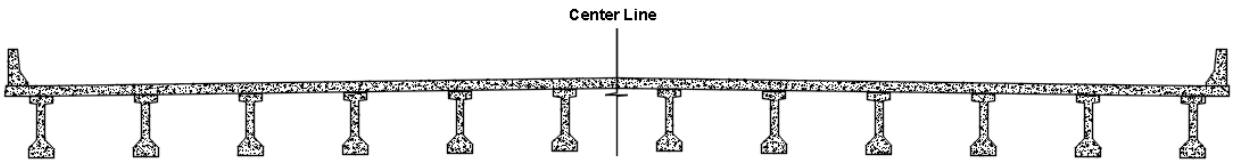

Figure 2. Cross-section view of Bridge #605220

www.manaraa.com

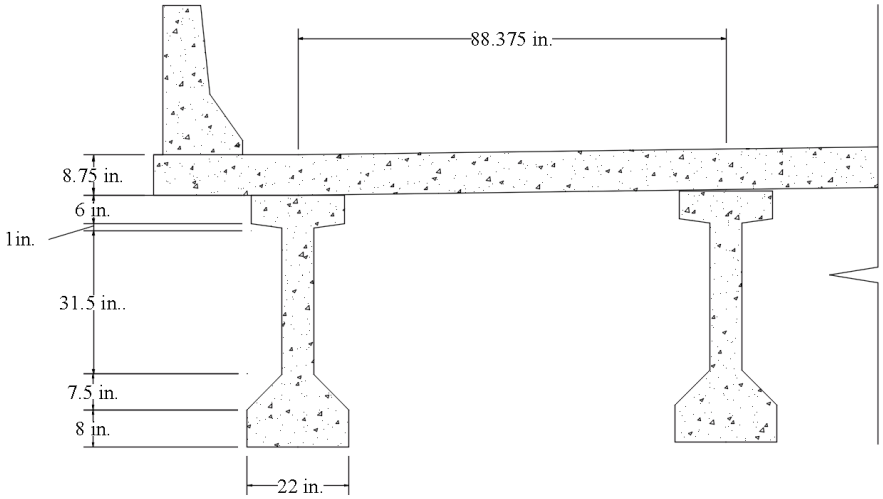

Figure 3. Cross-section details in a typical bay

Figure 4. Bottom view of the bridge

www.manaraa.com

Figure 5. Longitudinal cracks at middle of deck top

Figure 6. Transverse cracks at the corner of deck

www.manaraa.com

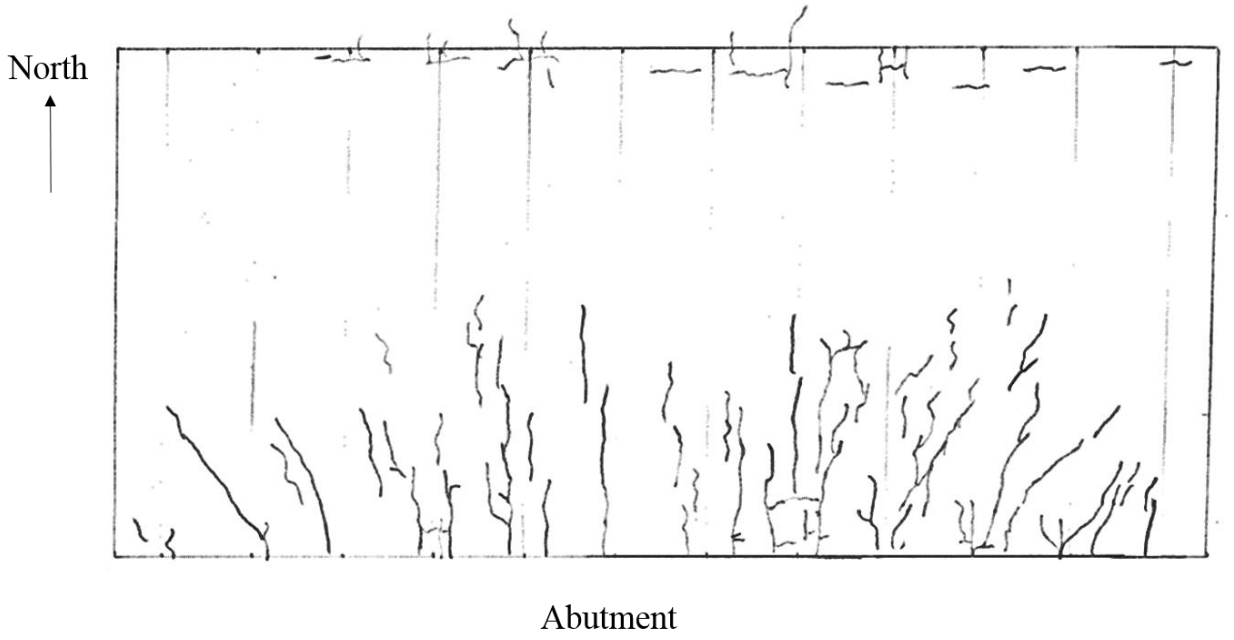

Figure 7. Crack map on top of deck on south side of Bridge #605220

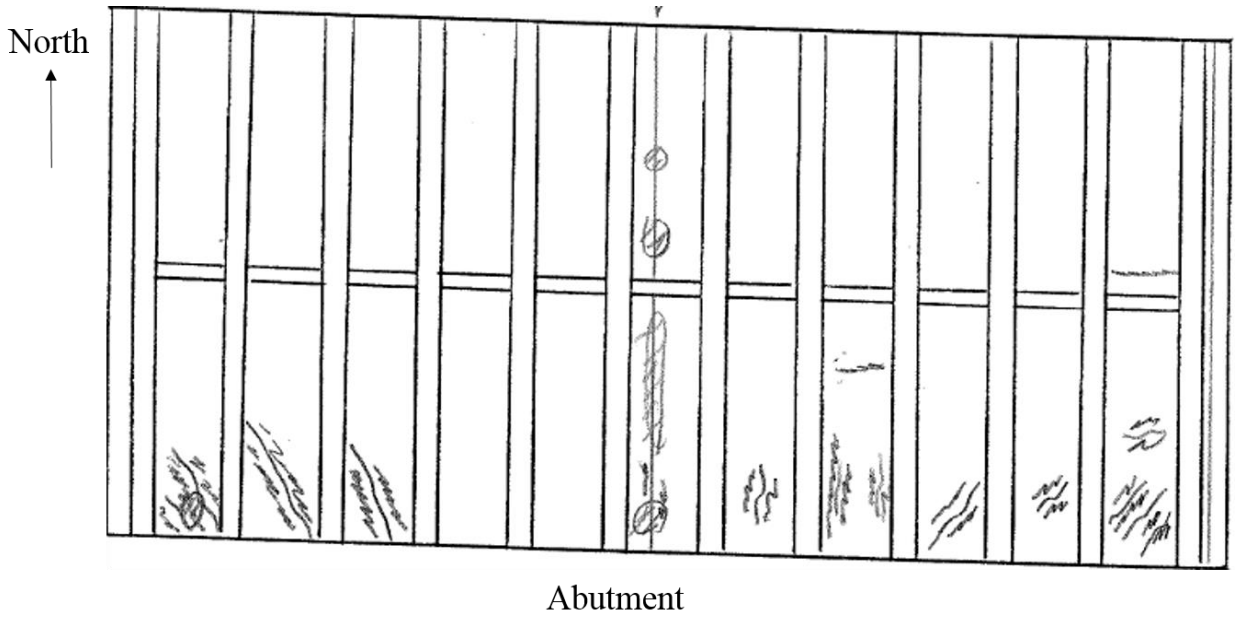

Figure 8. Crack map at bottom of deck on south side of Bridge #605220

www.manaraa.com

3.3 Live Load Testing Instrumentation Plan and Operation

3.3.1 Truck information and load case information

During live-load testing, a three-axle Iowa Department of Transportation snooper truck was driven across the bridge at a crawl speed to induce a pseudo-static load on the bridge. During passage of the truck, the bridge response was measured using a series of subsequently described strain transducers. The gross vehicle weight of the truck was approximately 54,800 lb. The approximately weight supported by each axle is illustrated in Figure 9.

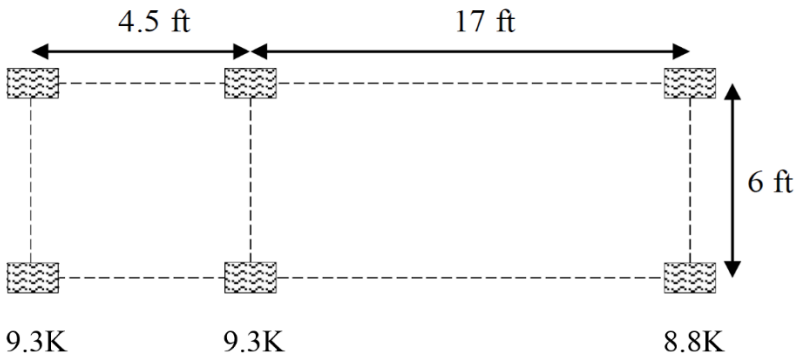

Figure 9. Snooper truck details

In total, five load cases were utilized to obtain the strain data which was used for general study of bridge behavior and for calibration of the subsequently described FEM. The transverse location of the vehicle in each load case is shown in Figure 10. In each load case, the truck moved from south to north at approximately 3 mph.

www.manaraa.com

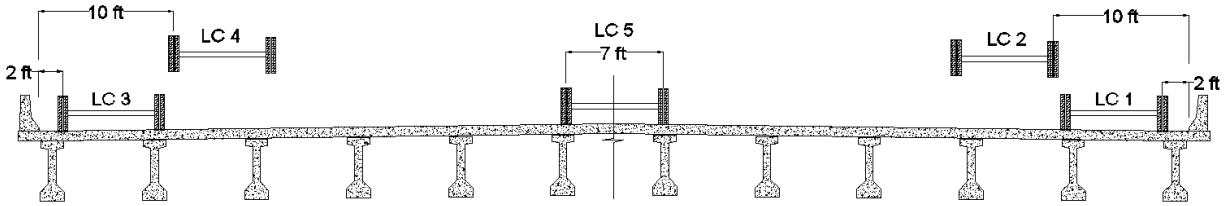

Figure 10. Transverse load position: vehicle traveled from south to north

3.3.2 Instrumentation plan and operation

During live-load testing, Bridge Diagnostic, Inc. (BDI) transducers were used to measure the load-induced strain at both the top and the bottom flanges of the girders. Three cross-sections were selected to install strain transducers: near the abutment section (54 in. from the surface of the south abutment), the pier section (54 in. from the south side of the southernmost pier), and at mid-span of the second span from the south end of the bridge. The locations of these three instrumentation sections are shown in Figure 11.

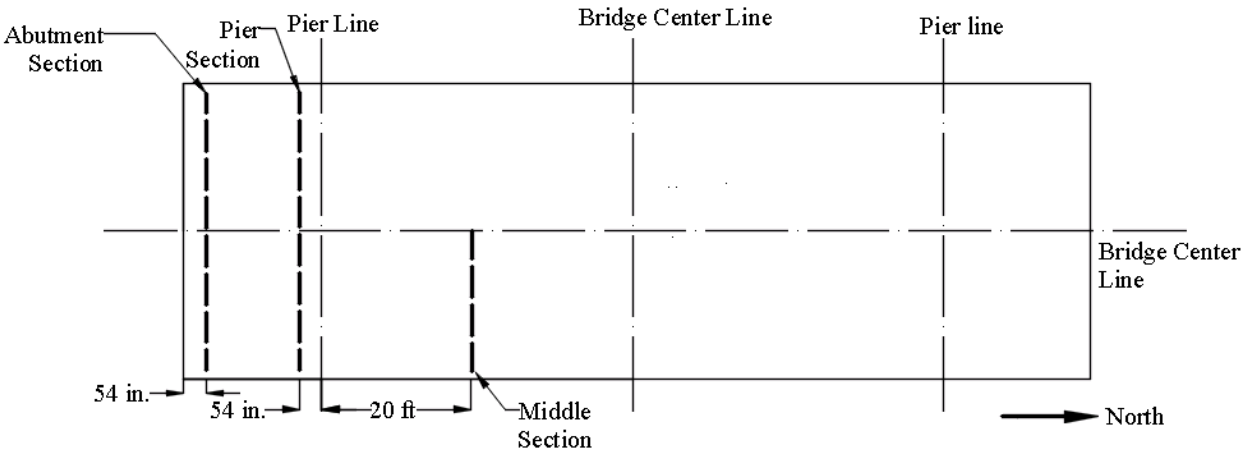

Figure 11. Locations of the three instrumentation sections

In total, 60 BDI transducers were installed during the live-load testing. Twenty-four transducers were placed on the abutment section and pier section respectively, and twelve transducers were placed on the mid-span section. On each girder in each section, one transducer

www.manaraa.com

was attached on the side of the top flange, and a second transducer was attached at the bottom surface of the bottom flange. The strain gauge locations and associated gauge labels are shown in Figure 12. The gauge label which consists of three parts which designates pertinent gauge location information in terms of girder number, cross-section section, and the location on flange. For example, gauge label "G1-A-T", "G1" means the first girder on the west side of the bridge; "A" means the abutment section; and "T" means that the gauge is on the top flange of the girder.

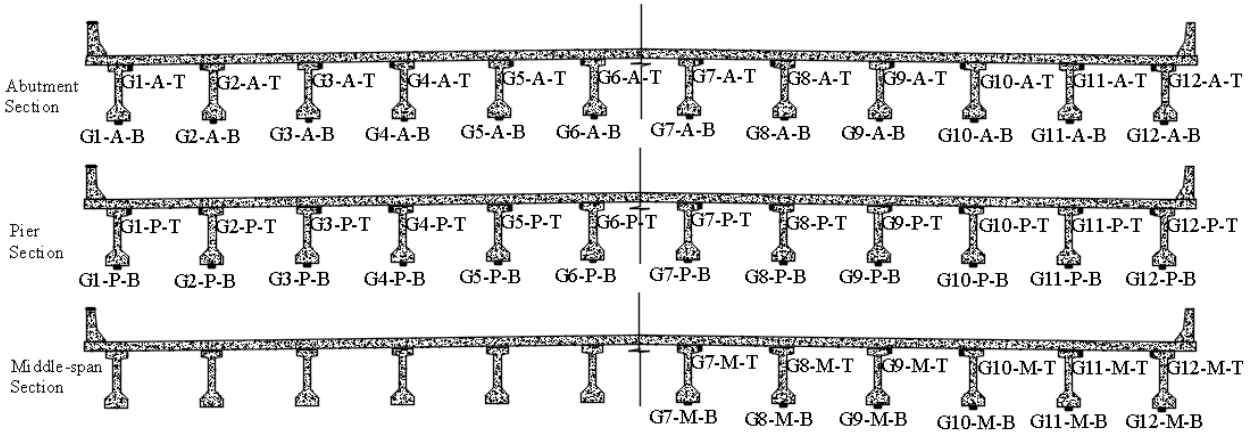

Figure 12. BDI transducers locations on cross section

After collecting the live-load test data, Bridge Diagnostics Inc. (BDI) WinGraf software was used to zero the data, convert the strain versus time data to strain versus truck position data set and to plot the results.

3.4 Long-term Testing Instrumentation Plan and Operation

The objective of the long-term testing was to study the behavior of the bridge deck due to temperature change, and to provide strain, displacement, and temperature data for the calibration of the FEM for the same temperature changes. Since the bridge inspection results indicated that most cracks were observed on both the top and bottom of the deck near the abutment region, the long-term testing focused on studying the behavior of the bridge in those areas.

www.manaraa.com

Strain Data Measurement

During long-term testing, Geokon Model 4000 vibrating strain gauges were used to measure the load-induced strain on the bottom of the deck. For the strain gauges instrumentation, three sections - abutment section, middle-span section and pier section were selected to capture the strain data. The abutment section (Figure 13) is 54 in. from the surface of the south abutment. Six bays near the east side of the bridge were selected to install the strain gauges. In each bay the strain gauge was attached in the middle of the bay between the two girders. The middle-span section (Figure 14) is located in the middle of the first span on the south side of the bridge. The pier section (Figure 15) is 54 in. from the south side of the first pier in the south side of the bridge. In both the middle span section and the pier section, the vibrating strain gauges were attached in the 1st bay, 3rd bay and 5th bay on the east side of the bridge.

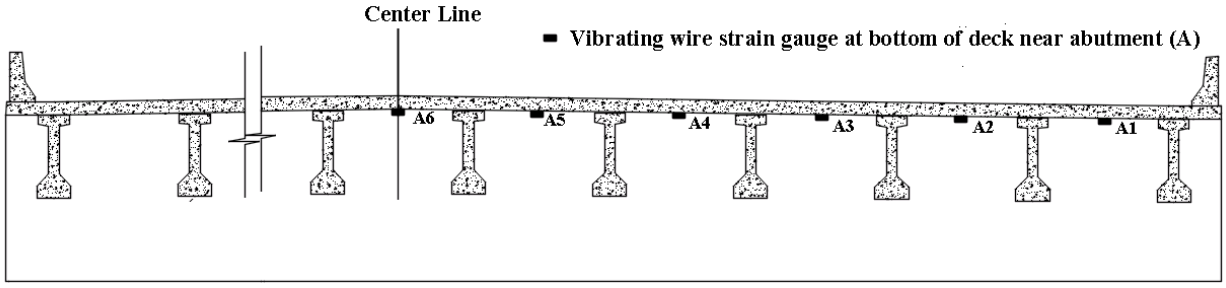

Figure 13. Instrumentation layout in abutment section for long term testing

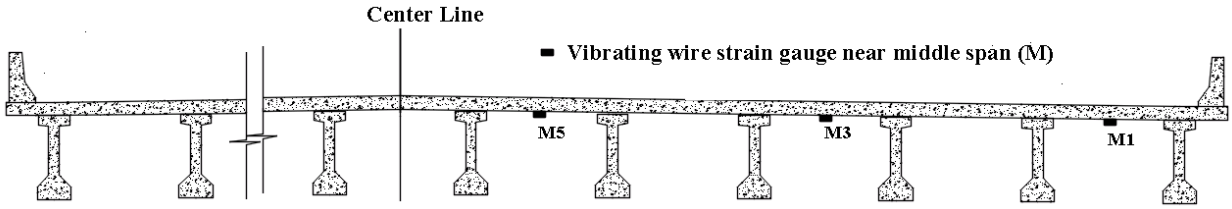

Figure 14. Instrumentation layout in middle span section for long term testing

www.manaraa.com

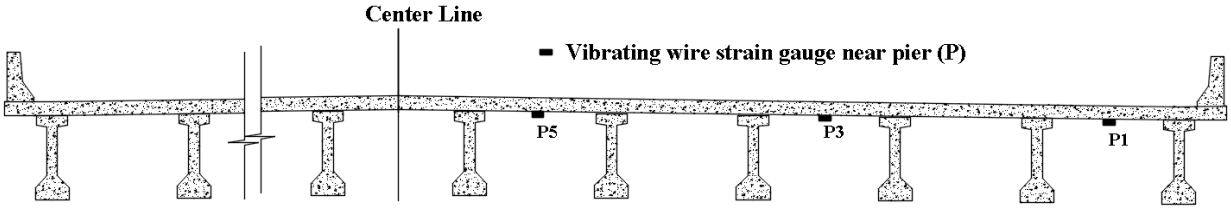

Figure 15. Instrumentation layout in pier section for long term testing

Figure 16 shows a photograph vibrating strain gauge mounted to the bottom of concrete deck prior to the installation of the protective cover.

Figure 16. Vibrating wire strain gauge at the bottom of deck

Displacement Data Measurement

Four Geokon Model 4427 vibrating-wire long-range displacement meters were used to measure the relative displacement in the first span of the bridge due to the thermal effects in both longitudinal and transverse directions. The positions of these four displacement transducers are shown in Figure 17. Two displacement meters were installed at the bottom of the deck in two exterior bays near the first interior girder in order to measure the relative longitudinal displacement in the first span on the south side of the bridge. The other two displacement meters were used to measure relative displacement in the transverse direction. One of them was placed

www.manaraa.com

at the bottom of the girder on the surface of the abutment on the south side of the bridge. The other one was installed at the bottom of the girder on the surface of the pier in the first span on the south side. Figure 18 shows a photograph of a vibrating-wire long-range displacement meter attached on the bottom of the girder near pier that measures the relative displacement in the transverse direction.

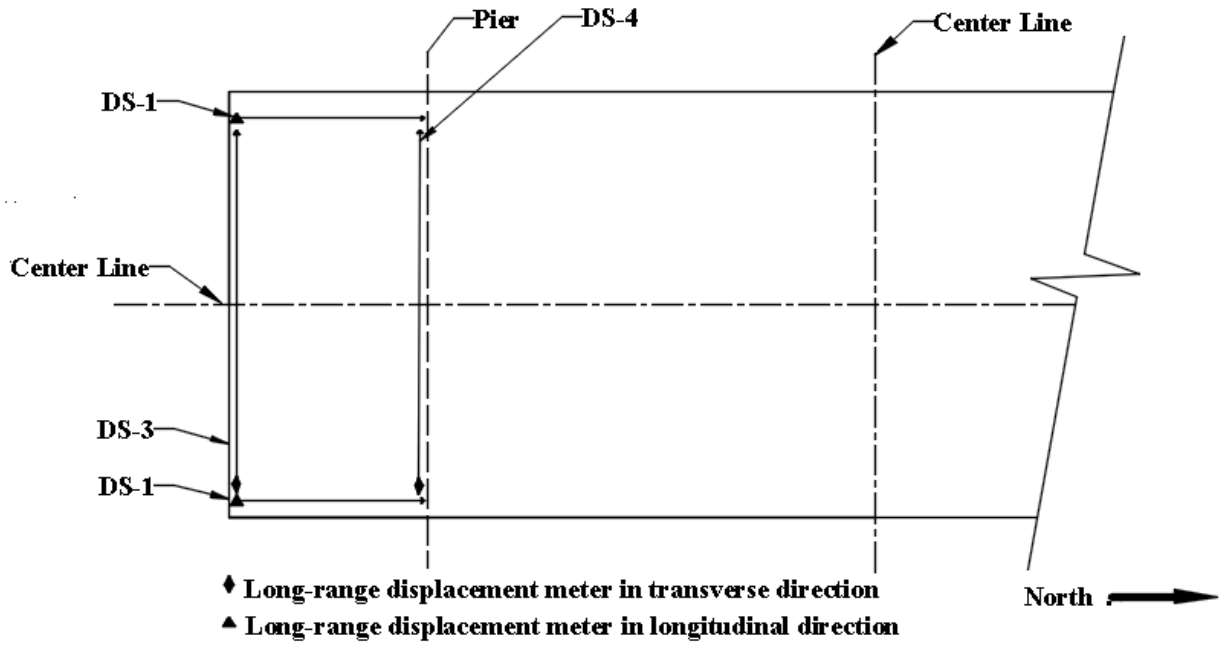

Figure 17. Instrumentation layout of long-range displacement meter (top view)

Figure 18. Vibrating wire long-range displacement meter

www.manaraa.com

Temperature Data Measurement

For temperature measurement, two type of gauges were used during the long-term testing. Part of the temperature data were collected from the thermistor housed within each of the vibrating strain gauges (shown in Figure 13, Figure 14 and Figure 15). After installation of the vibrating strain gauge, a plastic cover (shown in Figure 19) was used to cover the vibrating strain gauge and create an isolated space so that the temperature data from the vibrating strain gauge represents the temperature at the bottom surface of the deck.

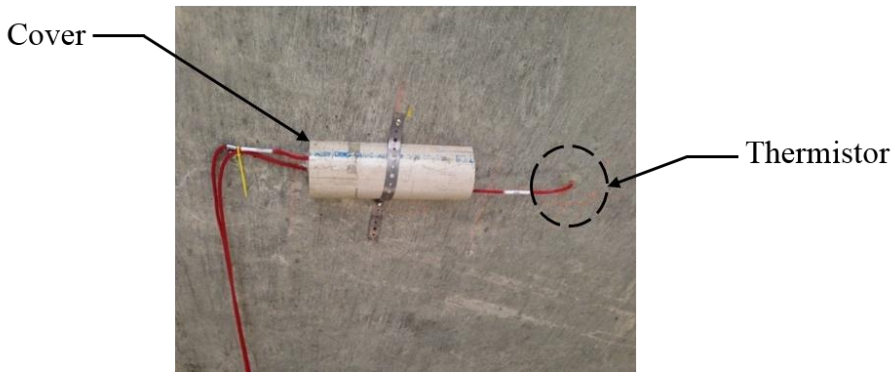

Figure 19. Relative position between strain gauge and thermistor in one bay

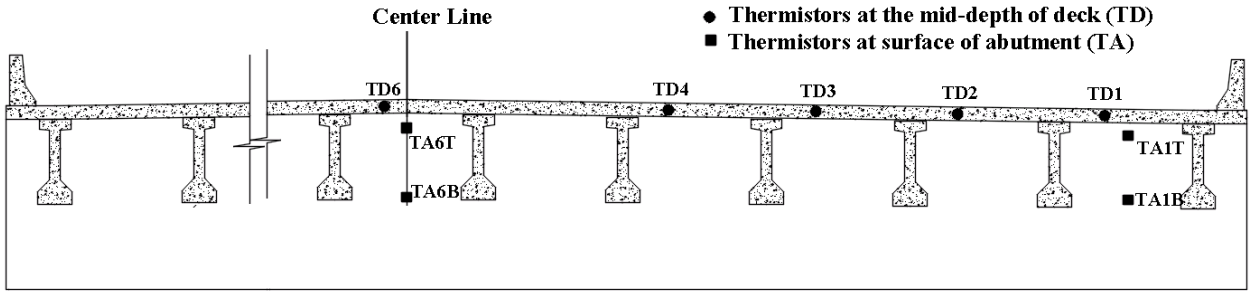

Figure 20. Thermistor in the middle depth of the deck and the abutment

In addition to the temperature at the bottom surface of the deck, the temperature inside the deck and within the abutment were also measured using a Geokon 3800 thermistor placed at mid-depth of the deck and just below the surface of the abutment. The relative position between the cover of the vibrating strain gauge and Geokon 3800 thermistors is shown in Figure 19.

www.manaraa.com

During long-term testing, five such thermistors were installed into the deck and 54 in. from the surface of the abutment (shown in Figure 20). Figure 21 shows a photograph of a thermistor attached within the deck. The locations of the four thermistors installed in the abutment are shown in Figure 20.

Figure 21. Thermistors at the bottom of deck

www.manaraa.com

CHAPTER 4. FIELD TESTING RESULTS

4.1 Live-Load Testing Results

Since Bridge #605220 has a skew of only 1.5 degrees, and field testing demonstrated that the bridge effectively acted in a symmetric manner, only the results from LC1, LC2 and LC5 are presented in this section (see Section 3.3 for LCs definitions). Figure 22 shows how the girder strain varied with truck position when the truck was transversely positioned in LC1 (see Section 3.3 for the load case information and Figure 12 for the details of gauge locations). The results from the first three girders on the east side of the bridge are presented, since only the gauges on those girders are close to the vehicle path and have significant readings (all other girders had minimal/negligible responses). Figure 23 shows the live-load test results from LC2. Figure 24 shows the live-load test results from LC5. For both LC2 and LC5, only the strain values from the four girders that are close to the truck path are presented. Results are shown at three sections – abutment, pier and middle sections, and the detail instrumentation plan was shown in Figure 12 in Chapter 3.

As shown in Figure 25, the strain values in the top flange gauges are very small indicating that the cross-section neutral axis is very near the top flange. For future reference, during calibration of the FEM (Chapter 5), only the strain value from the bottom gauges in Figure 22 to Figure 24 were used, since only these gauges have significant readings (e.g., larger than 5 microstrain).

www.manaraa.com

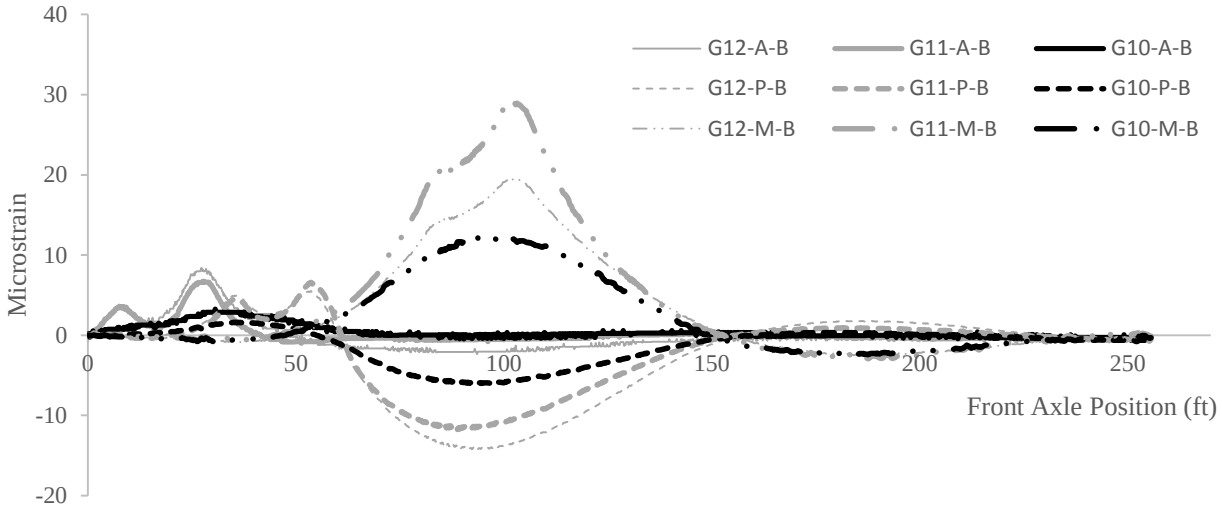

Figure 22. Strain vs. vehicle position from bottom gauges in LC1

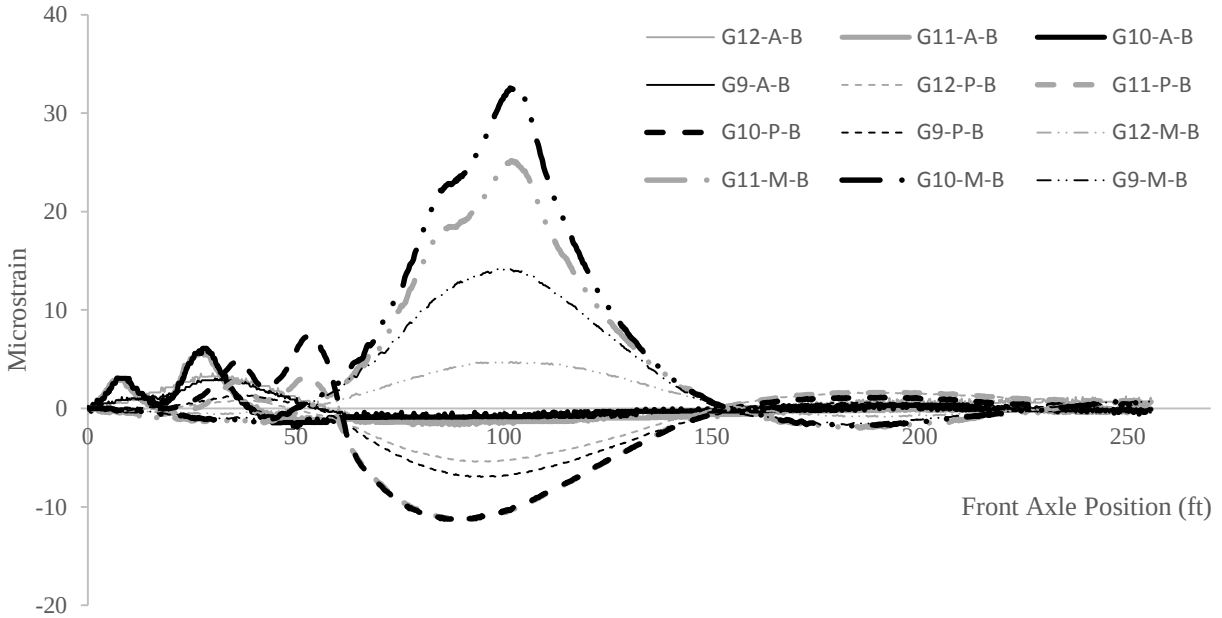

Figure 23. Strain vs. vehicle position from bottom gauges in LC2

www.manaraa.com

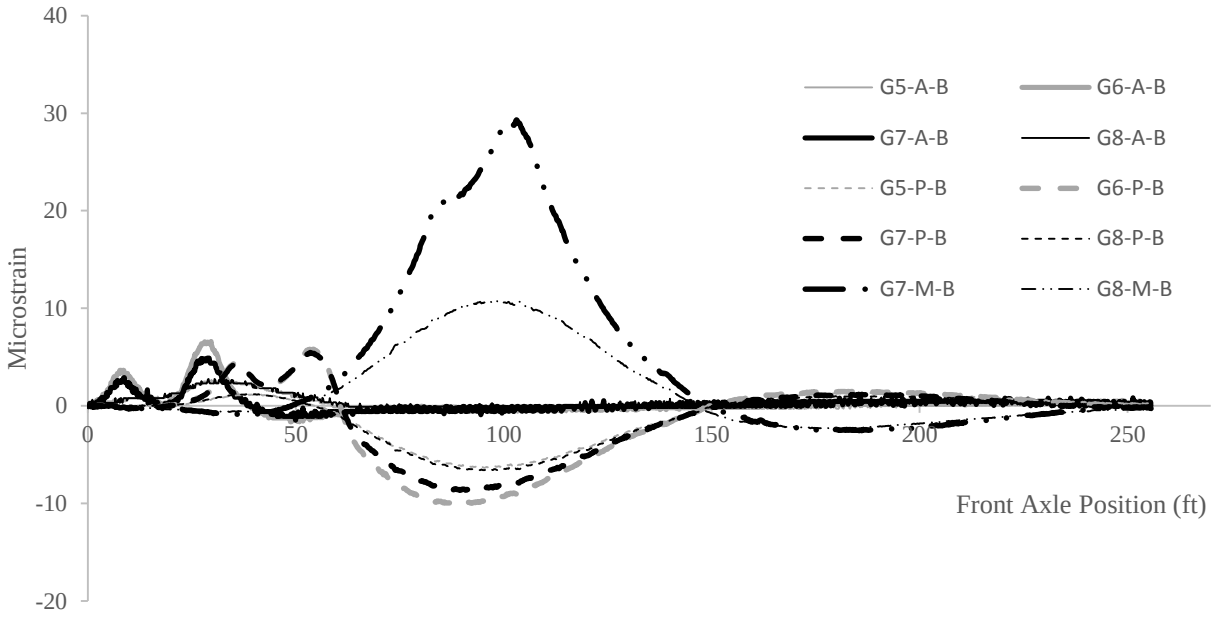

Figure 24. Strain vs. vehicle position from bottom gauges in LC5

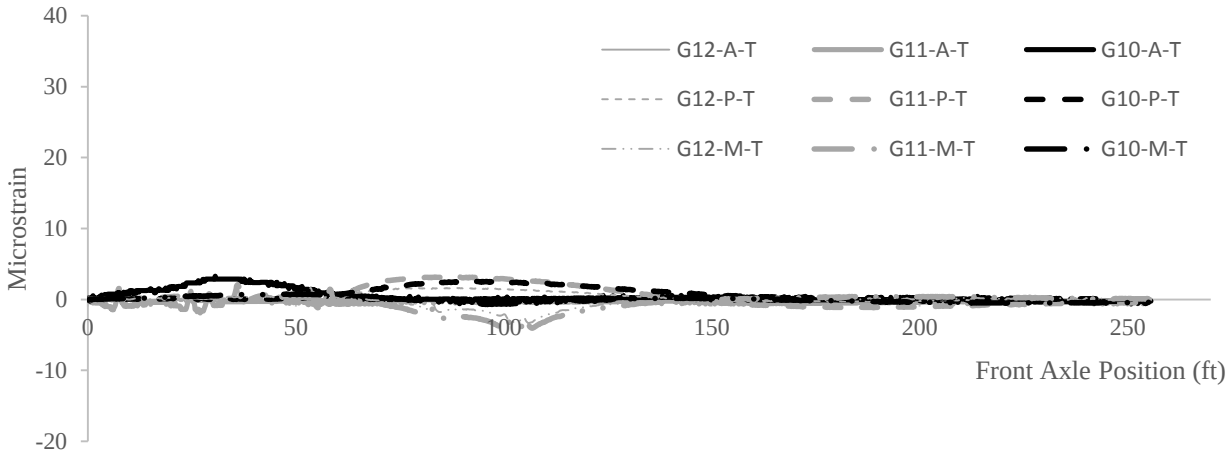

Figure 25. Strain vs. vehicle position from top gauges in LC1

www.manaraa.com

4.2 Long-Term Testing Results

Temperature Data

Figure 26 to Figure 28 show three bottom of deck temperature relationships. In Figure 26 and Figure 27, the average temperature at the mid-span and pier section vs. the average temperature at the abutment section are plotted (see section 3.4 for details of instrument location). Figure 28 shows the relation between the average temperature at the middle depth of the deck in the abutment section and the average temperature at the bottom of the deck in the abutment section. Since the slopes in these figures are one, it can be concluded that temperature at the bottom of the deck can be regarded as uniform from the abutment section to the pier section and the temperature changes that occur at the mid-depth of the deck are the same as the bottom of the deck (note that this will be of importance during calibration of the FEM). A further comparison between the deck bottom temperature and the mid-depth deck temperature reveals that the temperature at the bottom of the deck is very close to the temperature at the mid-depth of the deck at night, while during a sunny day, the maximum temperature difference is just two degrees.

www.manaraa.com

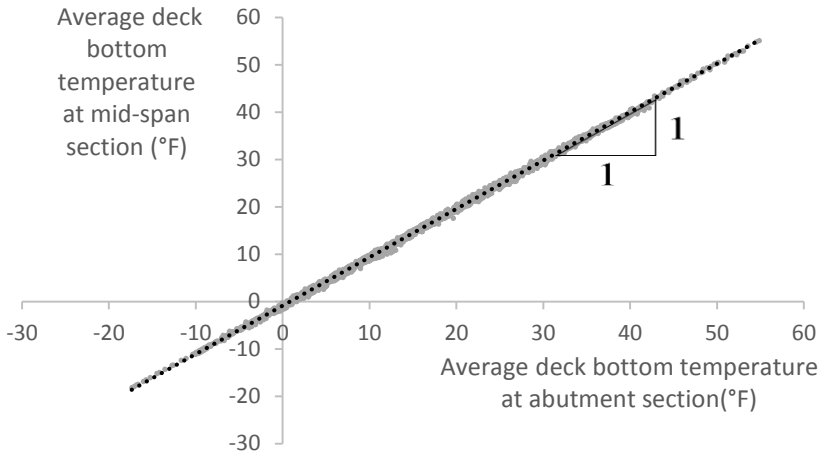

Figure 26. Average deck bottom temperature at mid-span section vs. average deck bottom temperature at abutment section

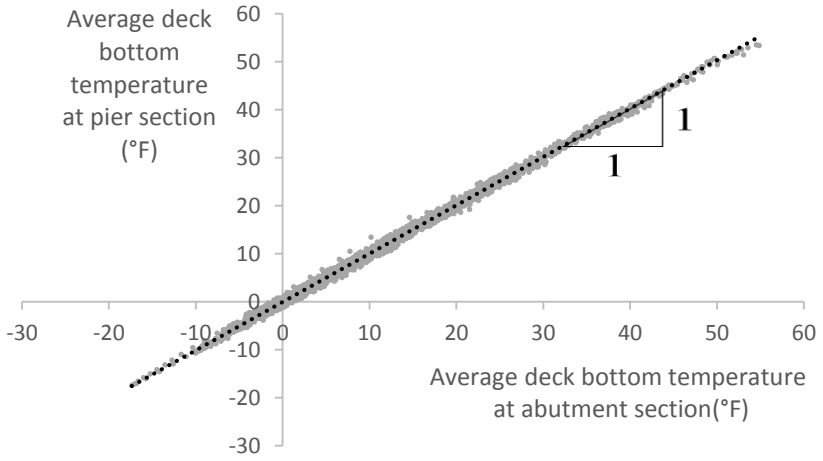

Figure 27. Average deck bottom temperature at pier section vs. average deck bottom temperature at abutment section

www.manaraa.com

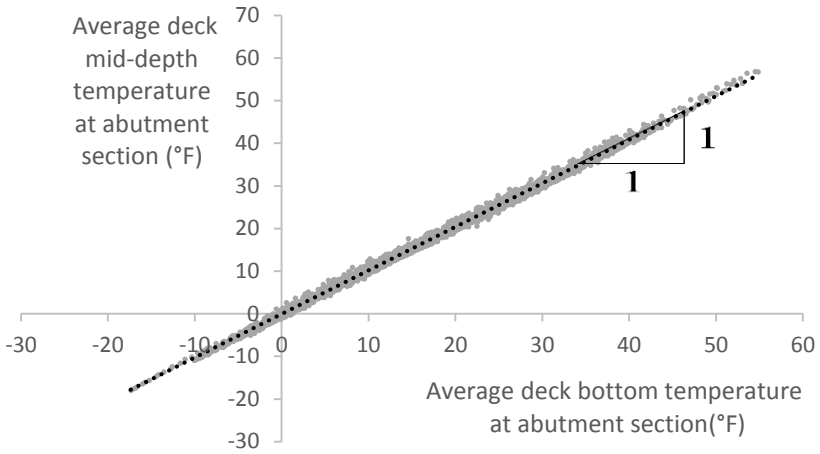

Figure 28. Average deck mid-depth temperature at abutment section vs. average deck bottom temperature at abutment section

To study the relation between temperature and strain and displacement, four one-day time periods were selected for more in depth analysis. Figure 29 shows the temperature changes with time during these four time periods.

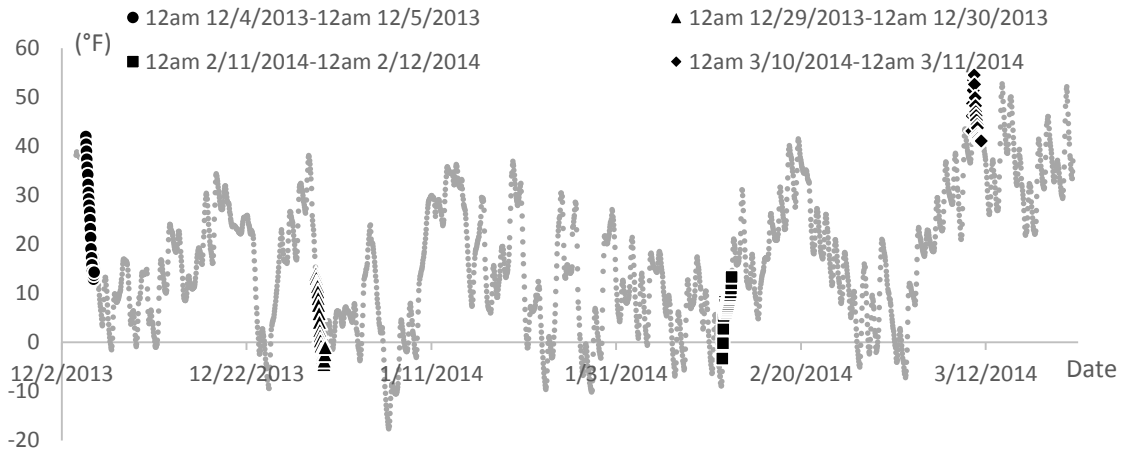

Figure 29. Average temperature at the bottom of deck vs. time

Figure 30 shows the relation between the temperatures at the abutment three inches below the bottom of the deck, and average temperature at the bottom of the full deck. Figure 31 shows the relation between the temperatures at the abutment 4ft-3in. below the bottom of the

www.manaraa.com

deck, and average temperature at the bottom of the full deck (see Figure 20 in Chapter 3 for the details of gauge locations). In Figure 30 and Figure 31, the data can be fitted by a line with a slope of 0.67, which indicates that the temperature change at the abutment is about 2/3 of the temperature change on the deck. In other words, when the temperature on the deck increases 30°F, the temperature on the abutment will increase around 20°F. As was mentioned previously, this temperature relationship will be utilized during calibration of the FEM.

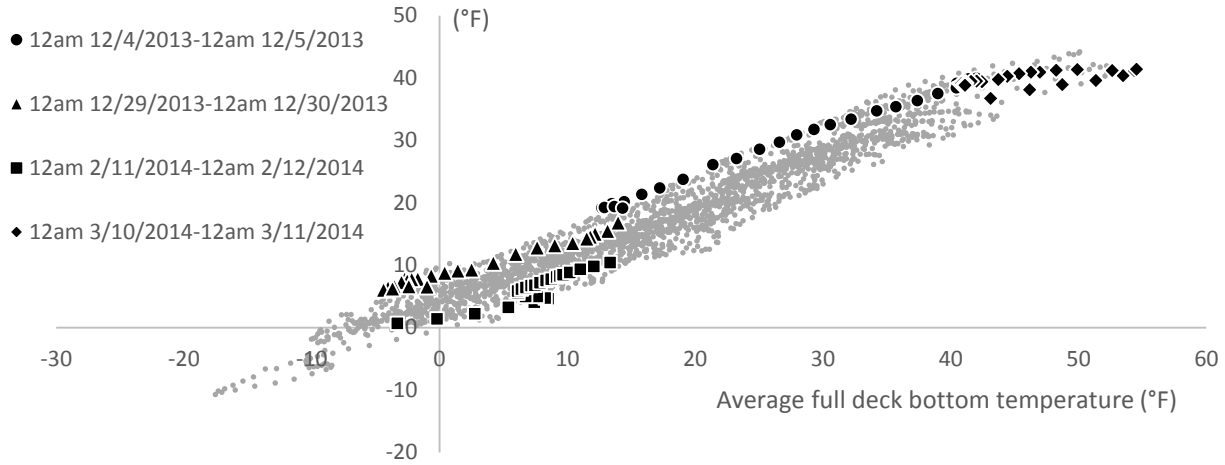

Figure 30. Average temperature on the abutment three inches below the deck (from TA1T and TA6T) vs. average temperature at the bottom of the full deck

www.manaraa.com

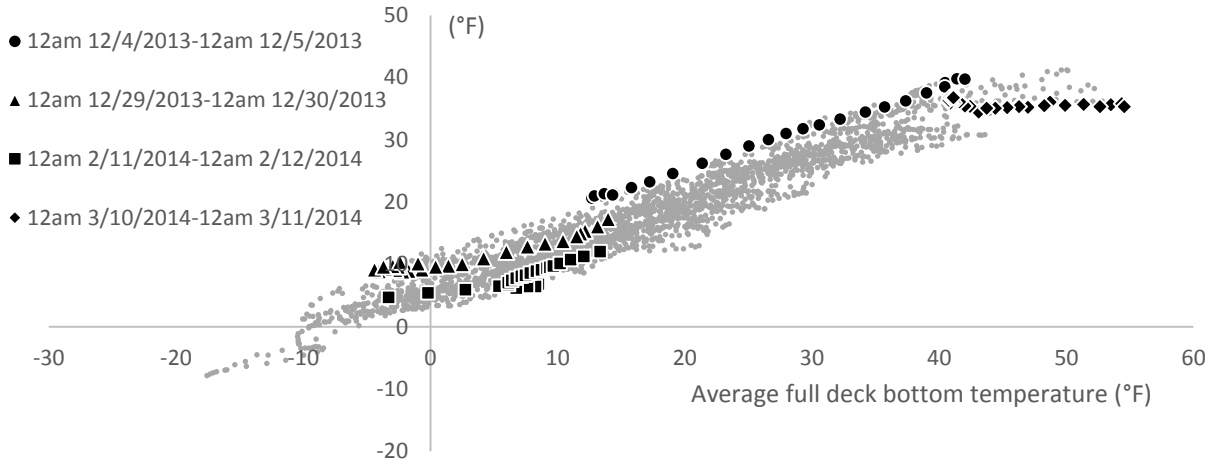

Figure 31. Average temperature on the abutment 4ft-6in. below the deck (from TA1B and TA6B) vs. average full deck bottom temperature

Strain Data

Figure 33 to Figure 44 show the strain vs. average temperature at the bottom of the deck plots for all strain gauges installed on the bottom of the bridge deck. As discussed in the previous section, the temperature at the bottom of the bridge deck was observed to be quite uniform. The temperature on the horizontal axes in Figure 33 to Figure 44 is the average temperature of all the strain gauges at the bottom of the deck.

From these strain vs. temperature plots, it can be seen that within most of the daily periods, a uniform slope between the strain changes and temperature changes is apparent. This slope can be used to calculate the strain value change for any temperature change. However, the strain corresponding to a certain temperature in a different time period is different. For example in Figure 33, when the average temperature at the bottom of the deck is zero, the corresponding strain in the second daily period is about 50 microstrain, while in the third daily period, the strain is about -10 microstrain. One of the reasons for this difference could be the soil temperature

www.manaraa.com

changes at the back of the abutment during different seasons, since the temperature changes in soil will be smaller and slower than the air temperature change. The soil far below the ground will maintain a relatively stable temperature during the whole year. The temperature change at the soil side of the abutment was not measured during long-term testing.

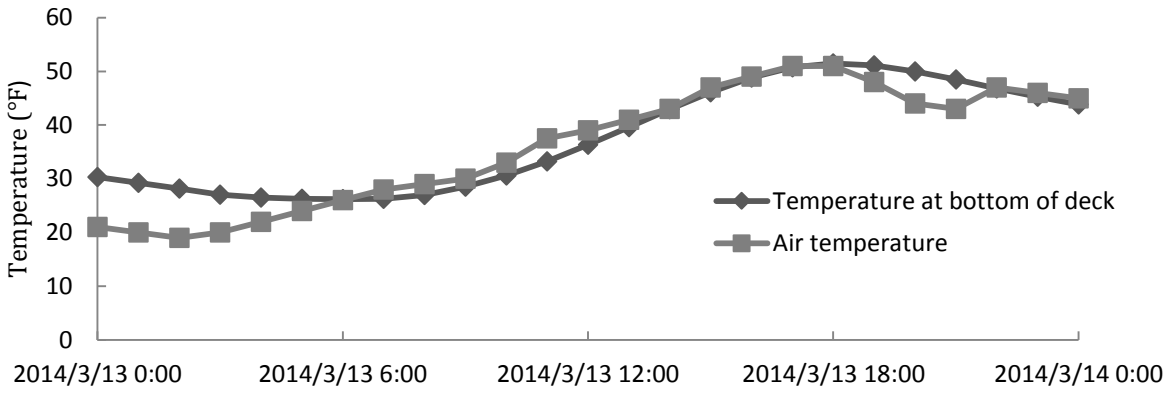

Figure 32. Comparison between the air temperature and the temperature at the bottom surface of deck

Although the long-term testing result shows that the maximum difference between the average temperature at the bottom of the deck and the average temperature at the middle depth of the deck was just two degrees, the road surface temperature data from Iowa DOT show that in the Waterloo region, the road surface temperature can be 30°F higher than the air temperature on a sunny afternoon. A comparison between the bottom deck temperature and air temperature shows that the maximum difference between both temperatures was just two degrees (shown in Figure 32). As a result of this phenomena the strain loop in the fourth time period (for example in Figure 33) is due to the large temperature difference between the top and bottom surface of the deck in the afternoon. A further observation on the strain data reveals that the peak strain value in the fourth time period occurred between 12 p.m. and 4 p.m.

www.manaraa.com

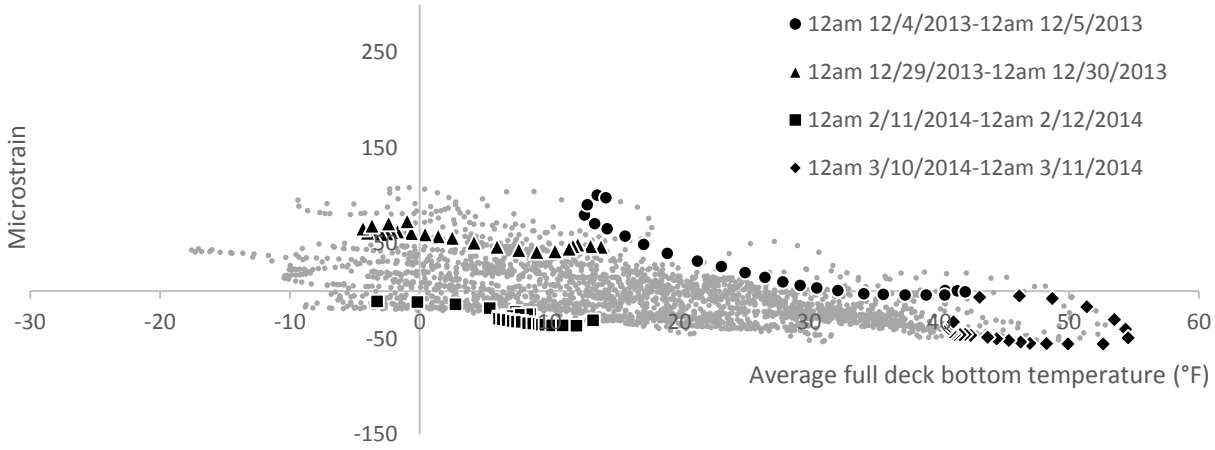

Figure 33. Strain from strain gauge A1 vs. average temperature at the bottom of the full deck

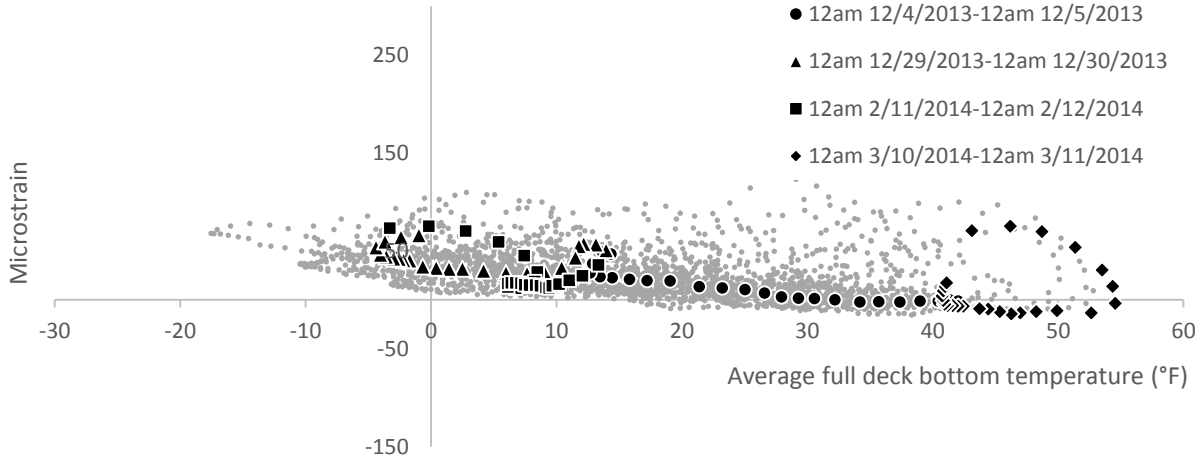

Figure 34. Strain from strain gauge A2 vs. average temperature at the bottom of the full deck

www.manaraa.com

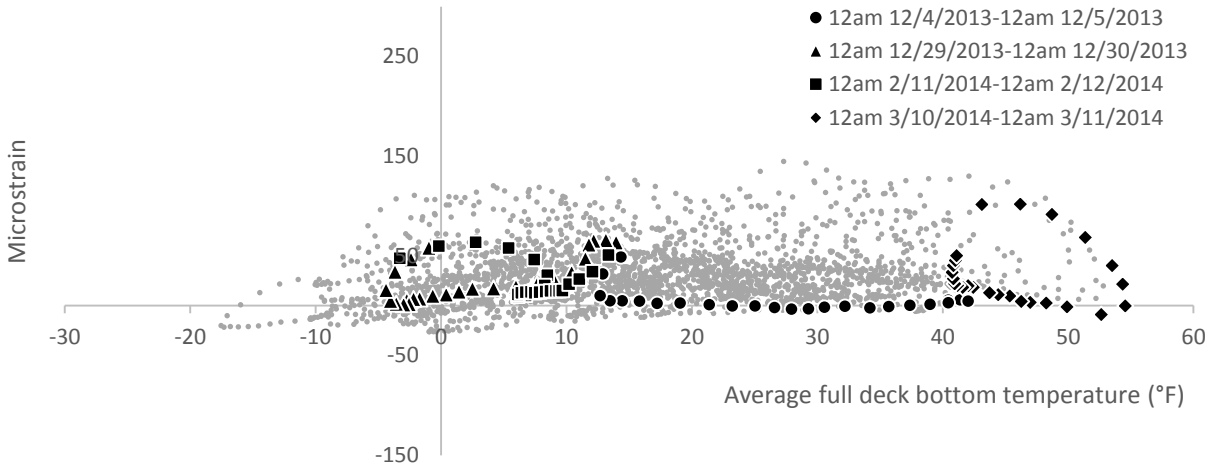

Figure 35. Strain from strain gauge A3 vs. average temperature at the bottom of the full deck

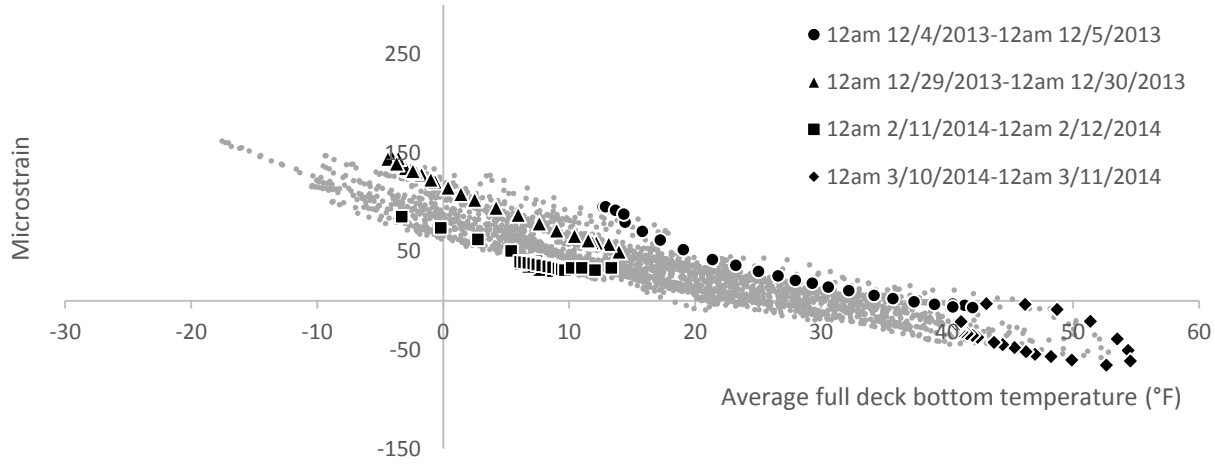

Figure 36. Strain from strain gauge A4 vs. average temperature at the bottom of the full deck

www.manaraa.com

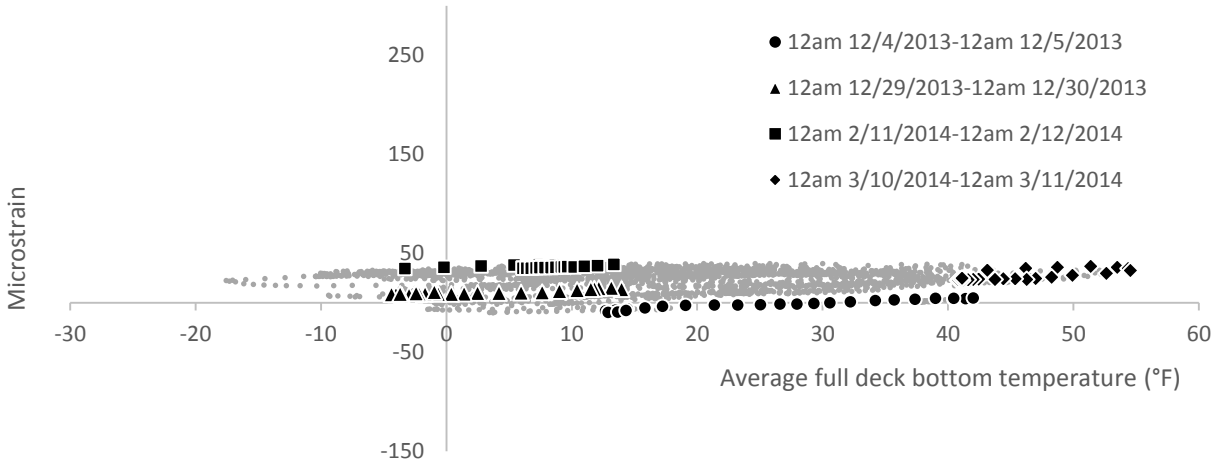

Figure 37. Strain from strain gauge A5 vs. average temperature at the bottom of the full deck

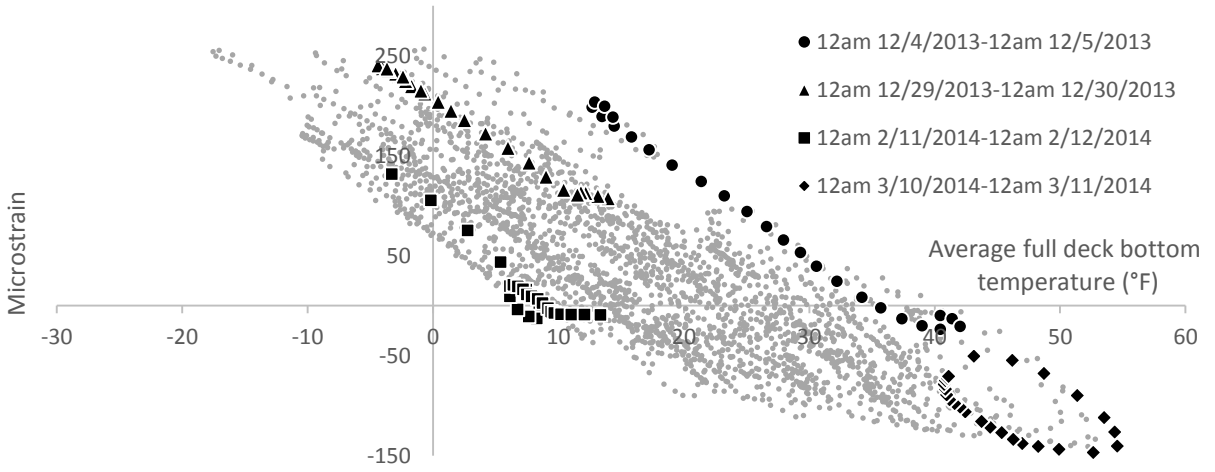

Figure 38. Strain from strain gauge A6 vs. average temperature at the bottom of the full deck

www.manaraa.com

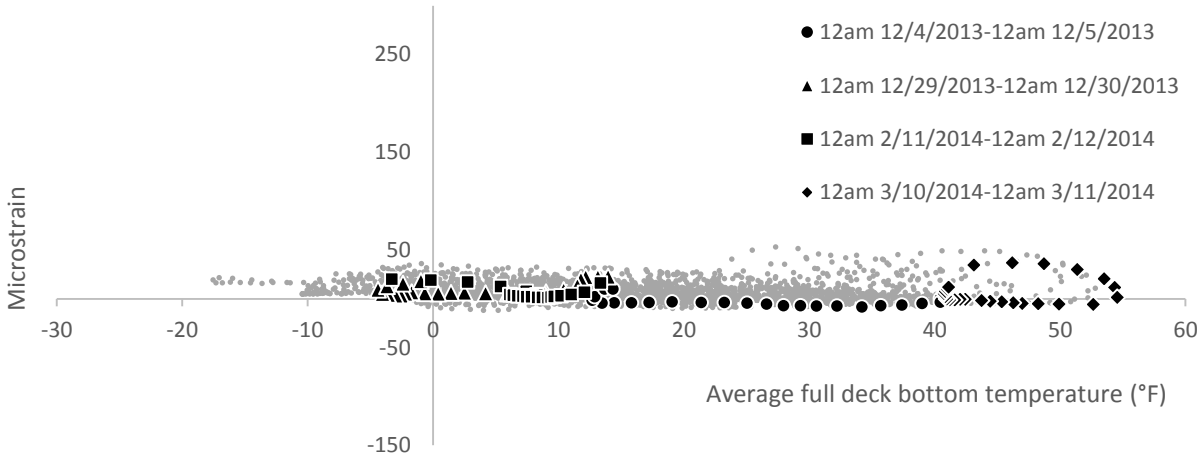

Figure 39. Strain from strain gauge M1 vs. average temperature at the bottom of the full deck

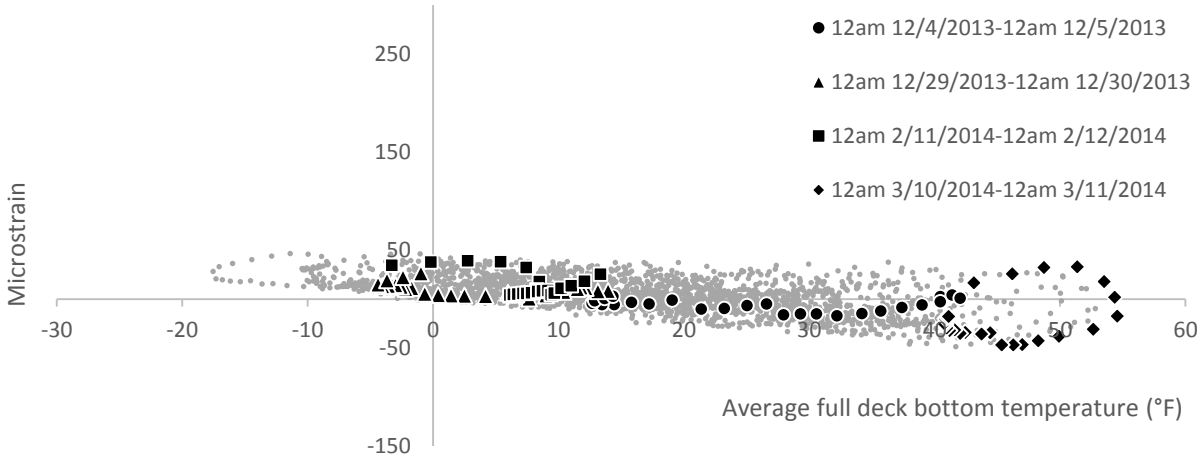

Figure 40. Strain from strain gauge M3 vs. average temperature at the bottom of the full deck

www.manaraa.com

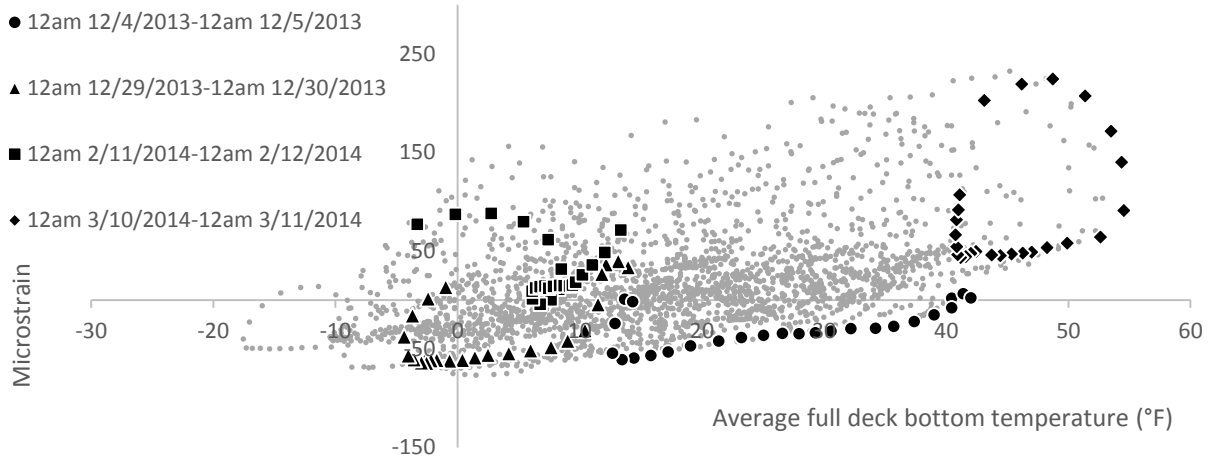

Figure 41. Strain from strain gauge M5 vs. average temperature at the bottom of the full deck

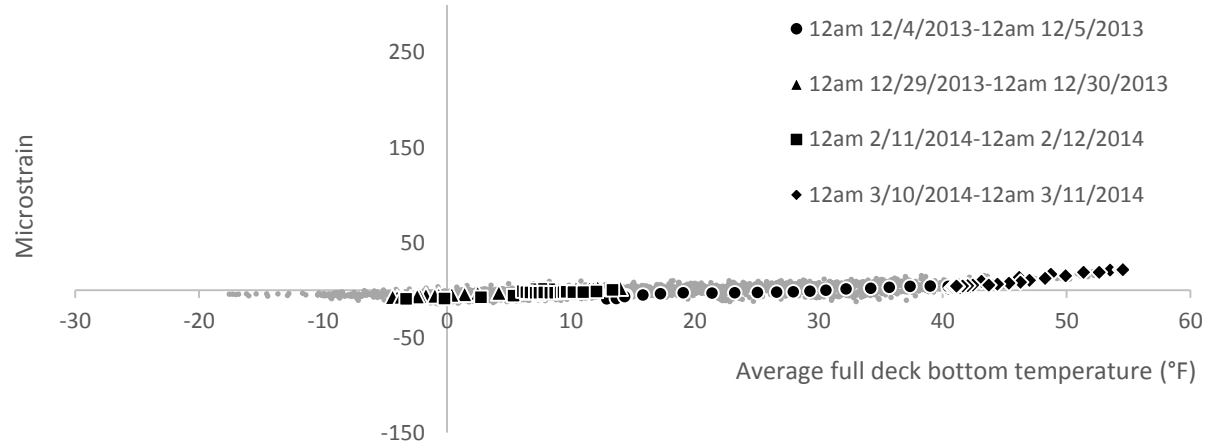

Figure 42. Strain from strain gauge P1 vs. average temperature at the bottom of the full deck

www.manaraa.com

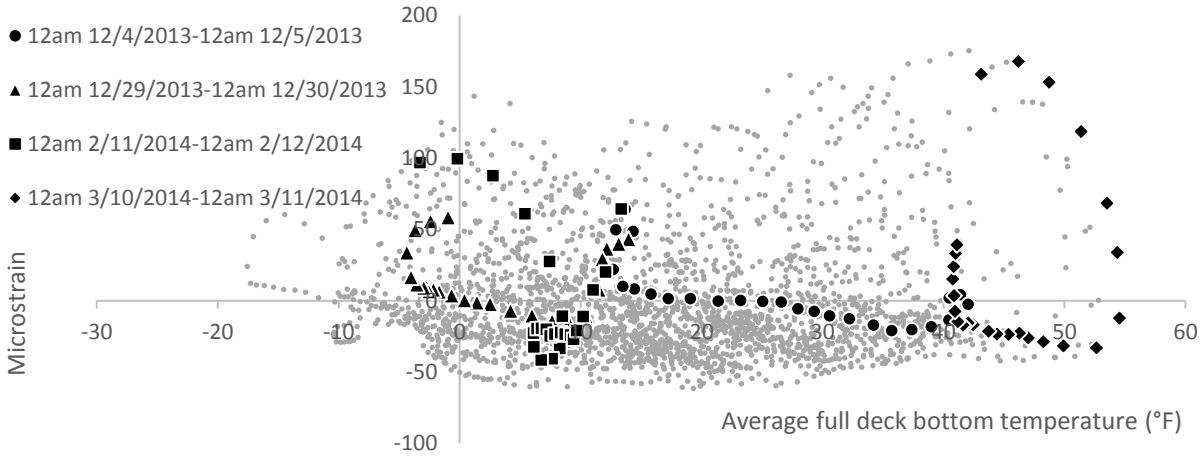

Figure 43. Strain from strain gauge P3 vs. average temperature at the bottom of the full deck

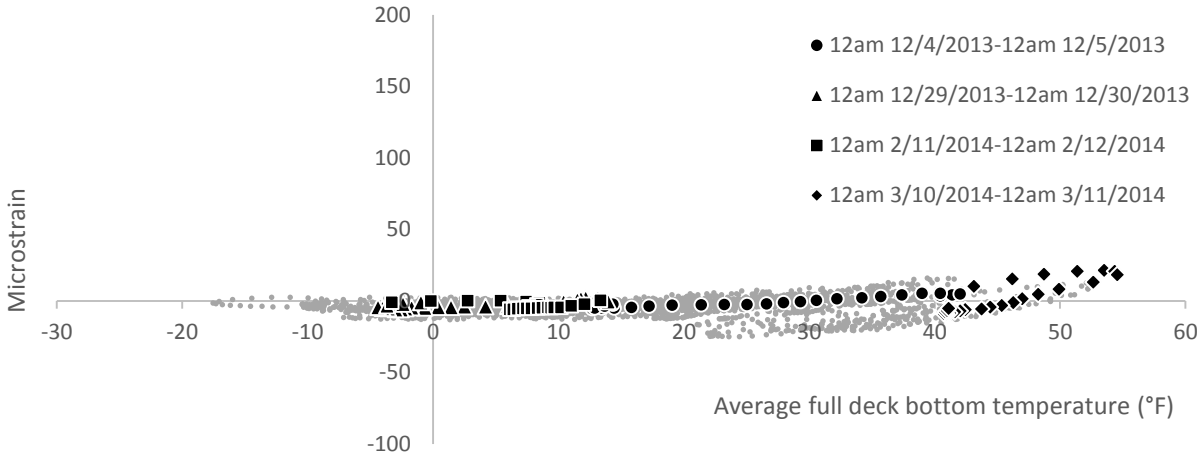

Figure 44. Strain from strain gauge P5 vs. average temperature at the bottom of the full deck

At the abutment section, the strain ranges in the first to fourth bays are around 150 microstrain (shown in Figure 33 to Figure 36). The strain value vs. temperature plot from the fifth bay (abutment section) shows a low strain range, which is from -10 to 40 microstrain (shown in Figure 37). The strain range in the sixth bay is as high as 400 microstrain (shown in Figure 38). A bridge inspection revealed that some influential cracks are near the strain gauges in these two bays. This is indicative that, among other items, high strains can be developed and then subsequently released once cracking occurs.

www.manaraa.com

For the fifth bay, a crack parallel to the girders was found at the bottom of the deck within one inch from one side of the strain gauge (shown in Figure 45). The strain gauge is near the edge of the crack and perpendicular to the crack; thus, the reading from the strain gauge will be reduced due to stress release near the edge of the crack. A similar situation was also observed in the third bay where a crack developed close to the mounting block of the strain gauge, which resulted in an irregular strain vs. temperature relation.

Figure 45. Relative position between crack and strain gauge in the fifth bay

In the sixth bay, a crack which ends eight inches from the strain gauge was found at the top surface of the deck. Figure 46 illustrates the relative position between the vibrating wire strain gauge (solid rectangular) and the crack. The high strain value in the sixth bay is probably due to the stress concentration at the end of the crack.

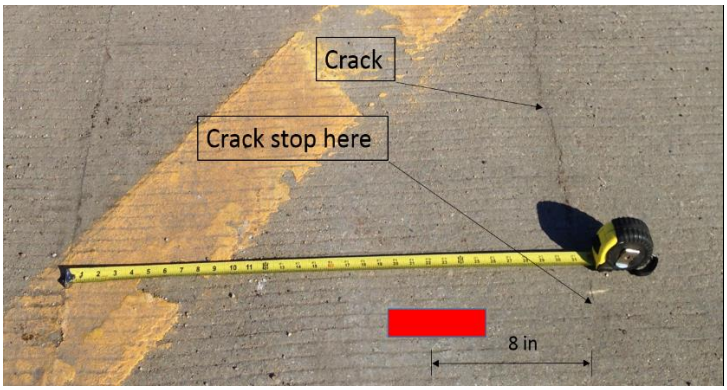

Figure 46. Relative position between crack and strain gauge in the sixth bay

www.manaraa.com

For the pier section and the middle section, the large strain readings and the small strain readings in some gauges can also be explained by the influence from nearby cracks. The gauges without influence of cracks (such as A1, A2, and A4) show reasonable and consistent strain readings, which means the strain data obtained from long-term testing are valid for the calibration of the FEM.

Displacement Data

Figure 47 to Figure 50 show the displacement data vs. temperature plots from the four displacement transducers. The locations of these four displacement transducers were shown in Figure 17 in Chapter3. The temperature on the horizontal axis in Figure 47 to Figure 50 is the average temperature at the bottom of the deck. For DS-2, DS-3, and DS-4, a very similar slope can be observed from the data in the four daily periods. These slopes can be used to evaluate the displacement changes with temperature changes for each bay. The result from DS-1 (shown in Figure 47) is much different than the other displacement transducers. No similar slope can be extracted. Generally, the displacement value increases when the temperature drops, which is counter to basic engineering concepts (e.g., expansion occurs during heating and contraction occurs during cooling). Hence, the result from DS-1 was not used to calibrate the FEM. The results from DS-2 were used to calibrate for both the west and east side of FEM.

www.manaraa.com

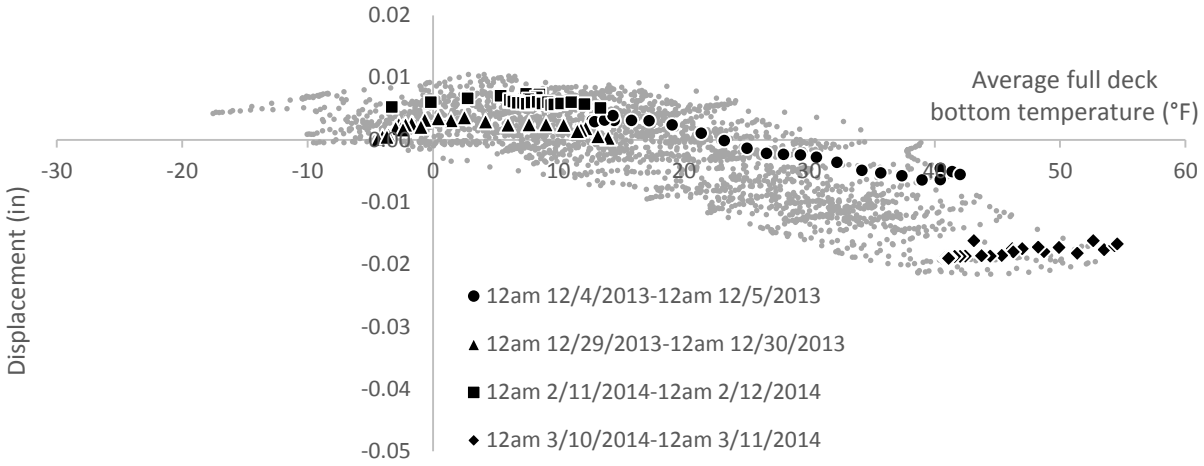

Figure 47. Displacement at DS-1 vs. average temperature at the bottom of the full deck

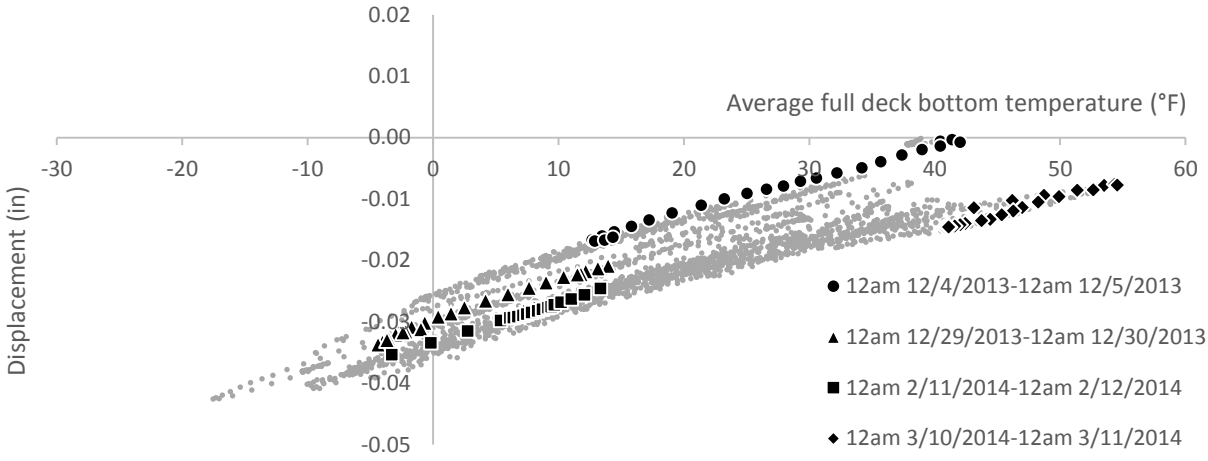

Figure 48. Displacement from DS-2 vs. average temperature at the bottom of the full deck

www.manaraa.com

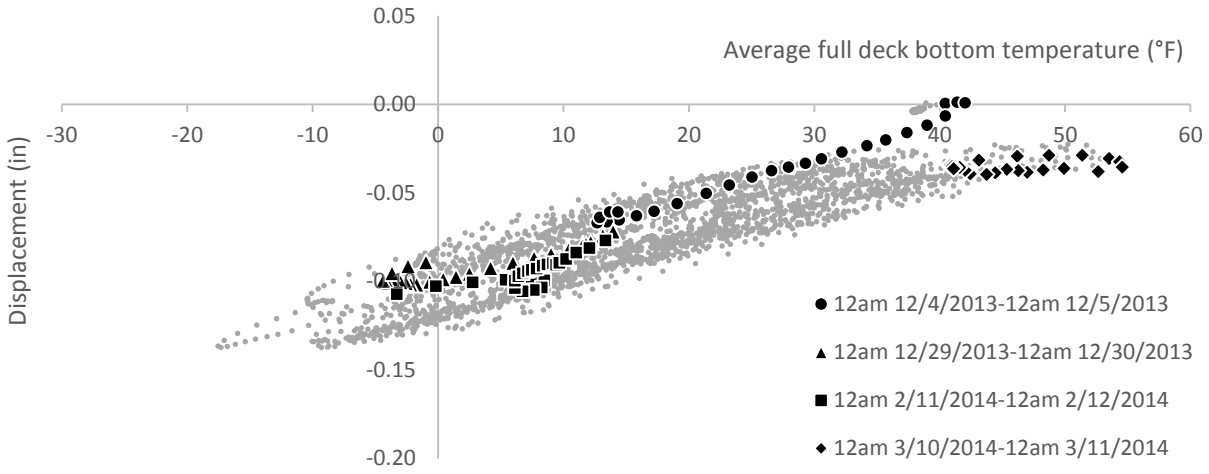

Figure 49. Displacement from DS-3 vs. average temperature at the bottom of the full deck

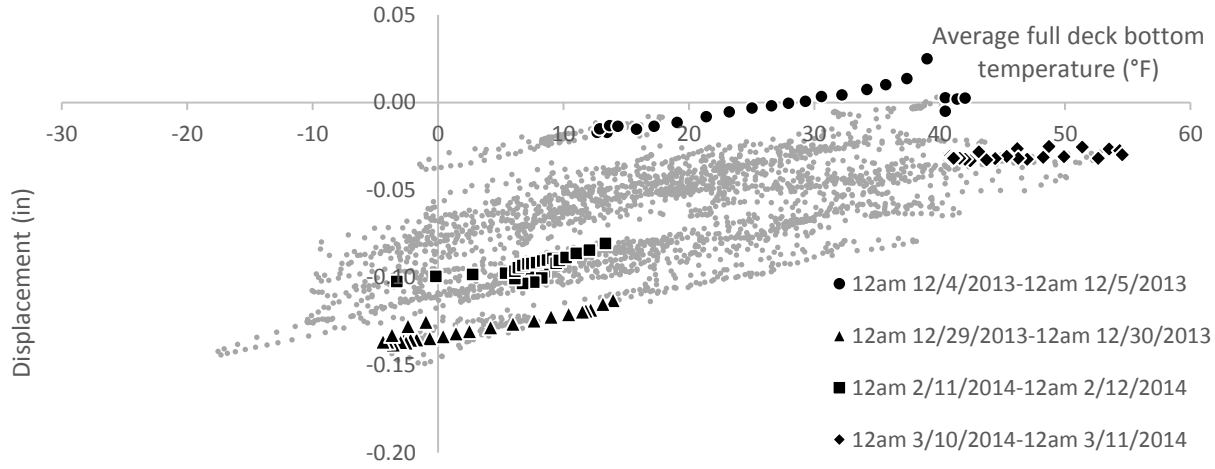

Figure 50. Displacement from DS-4 vs. average temperature at the bottom of the full deck

www.manaraa.com

CHAPTER 5. DEVELOPMENT OF BRIDGE MODEL

5.1 Introduction

In this chapter, a three-dimensional (3D) Finite Element Model (FEM) developed using the software ANSYS is described. Both live-load and long-term testing results were used to calibrate this FEM. This calibration involved incrementally altering some structural characteristics such as support conditions and material properties, until it was observed that the FEM and the field test results matched reasonably well. The bridge model developed in this research includes deck, girder, diaphragm, abutment and pier cap. Piles under the abutment and pier columns were idealized by assuming the support conditions.

5.2 Elements Used in this Study

The two element types were used to create the subsequently described FEM. The commercial software ANSYS was utilized and the specific element types used are the Shell 181 and Beam 4.

Shell 181 Element

Shell 181 is a four-node element with six degrees of freedom at each node: translations in the x, y, and z direction and rotations about the x, y, and z axis. The Shell 181 element is suitable for analyzing thin to moderately thick shell structures. In this bridge FEM, this element was used to simulate the deck, abutment, diaphragm and the web of the girders. Both isotropic and orthotropic material properties can be used in association with this element. The thickness of the element is defined at the four nodes. Further, different temperature changes can be applied to the

www.manaraa.com

top and bottom of the element allowing for the study of thermal gradient induced behaviors. Figure 51 shows the geometry and coordinates of a Shell 181 element.

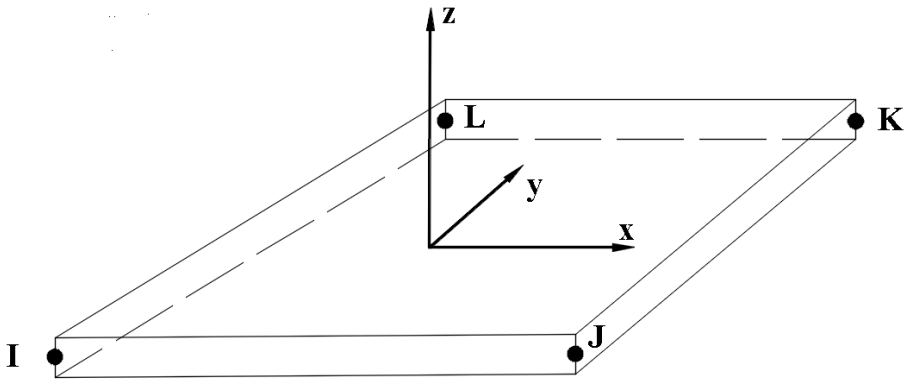

Figure 51. Shell 181 geometry

Beam 4 Element

The Beam 4 element is a two-node element with six degrees of freedom at each node: translations in the x, y, and z direction and rotations about the x, y, and z axis. It is a uniaxial element with tension, compression, torsion and bending capability. In this FEM, the Beam 4 element was used to mesh the top and bottom flange of the girders, pier caps and steel diaphragms. The section properties required for this element include: area, two moments of inertia (IZZ and IYY), two thicknesses (TKY and TKZ), the torsional moment of inertia (IXX), and pertinent material properties. Temperature loading can be input on the node of the element. Figure 52 shows the geometry and coordinates of a Beam 4 element.

www.manaraa.com

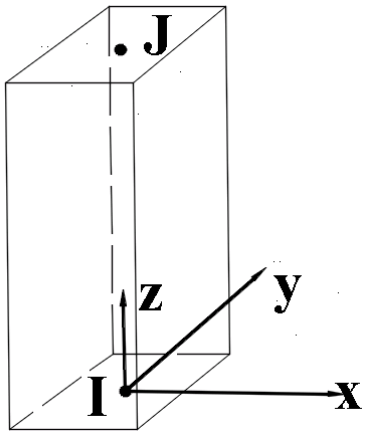

Figure 52. Beam 4 geometry

5.3 Material Properties

The bridge consists of high-strength, pre-stressed concrete for the girders, and normal concrete for the other concrete components. Based on the original design plans for the bridge, the specified compressive strength (f_c') for the pre-stressed girder is 5 ksi; and for the concrete in the other bridge components, it is specified to be 3.5 ksi. The Young's Modulus for concrete was calculated by $57000\sqrt{f_c'}$, yielding the Young's Modulus 4,000 ksi for the pre-stressed girder, and 3,400 ksi for the other concrete components.

The effect of steel reinforcement in the concrete was also taken into account, since steel reinforcement has a different thermal expansion coefficient and a higher Young's Modulus, which will increase the stiffness of each component. In the FEM, the steel reinforcing bars were smeared into the concrete. To simulate this orthotropic behavior of the bridge, an effective thermal expansion coefficient (α_{eff}) and an effective Young's Modulus (E_{eff}) were determined using Equation (1) and Equation (2) (Lowell Greimann 2014):

www.manaraa.com

$$E_{eff} = \frac{A_c E_c + A_s E_s}{A_c + A_s} \quad (1)$$

$$\alpha_{eff} = \frac{A_c E_c \alpha_c + A_s E_s \alpha_s}{A_c E_c + A_s E_s} \quad (2)$$

E_{eff} = effective linear elastic modulus of combined steel and concrete,

α_{eff} = effective thermal expansion coefficient of combined steel and concrete,

A_c = area of concrete,

A_s = area of steel,

E_c = linear elastic modulus of concrete,

E_s = linear elastic modulus of steel,

α_c = thermal expansion coefficient of concrete,

α_s =thermal expansion coefficient of steel,

Poisson's ratio (υ) for all the concrete member was taken as 0.2 was taken as 0.2. For steel member, Poisson's ratio was specified as 0.3. The effective material properties on the FEM are listed in Table 4.

www.manaraa.com

Table 4. Material properties input into the FEM

Bridge components	Element type	Direction	E (ksi)	α $(\times 10^{-6}\ in/in/F)$	υ
Deck	Shell 181	Transverse	3600	5.55	0.2
		Vertical	3370	5.50	0.2
		Longitudinal	2550	5.56	0.2
Girder-top flange	Beam 4	---	4 260	5.00	0.2
Girder-web	Shell 181	---	4 030	5.00	0.2
Girder-bottom flange (Long span)	Beam 4	---	4 530	5.20	0.2
Girder-top flange (Long span)	Beam 4	---	4 240	5.00	0.2
Abutment	Shell 181	---	3 370	5.50	0.2
Pier cap	Beam 4	---	3 530	5.55	0.2
Pier diaphragm	Shell 181	---	3 370	5.50	0.2
Pier diaphragm	Beam 4	---	29 000	6.50	0.3

5.4 Meshing and Idealized Support Conditions

Deck

Considering that the behavior of the bridge deck is the main focus of the FEM study, a fine mesh size was used to simulate the deck. Before finalizing the mesh pattern, several requirements, such as the location of live load and the location of girders, were taken into account. A convenient and acceptable element size was determined to be about six inches, with an aspect ratio near 1:1. Figure 53 shows the mesh geometry for the deck.

www.manaraa.com

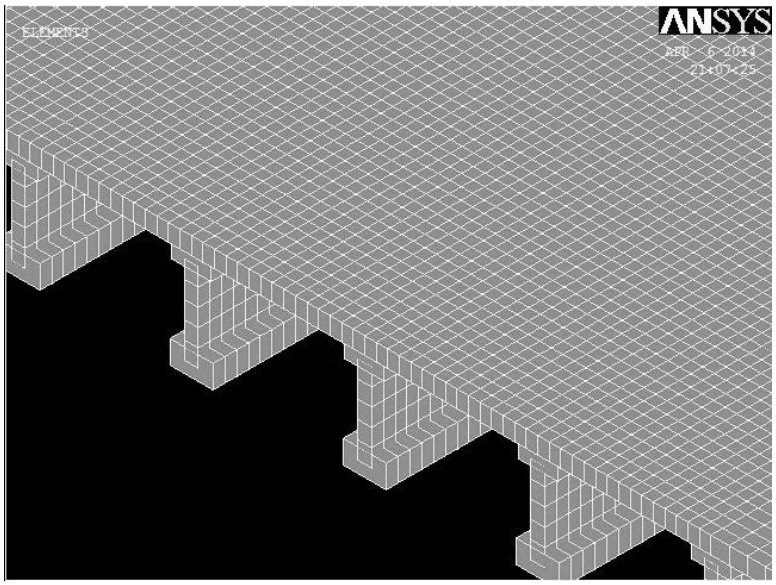

Figure 53. Meshed deck

Girder

In the FEM, two types of elements were used to model the pre-stressed concrete girder. The Shell 181 element was used to model the girder web, and the Beam 4 element was used to model both the top and bottom flanges. To simulate the shear connection between the girders and the deck a four-inch Beam 4 element with a very high stiffness was used.

Abutment - Deck, Girder

Both abutments were rigidly attached to the deck and girders. This approach allows for the simulation of the connectivity that would develop in these regions. Note that the mesh geometry for the abutment is slightly irregular (shown in Figure 54), because at the top of the abutment a fine mesh was used to match the mesh pattern on the deck, while at the bottom of the abutment, the element size was adjusted to match the pile location.

www.manaraa.com

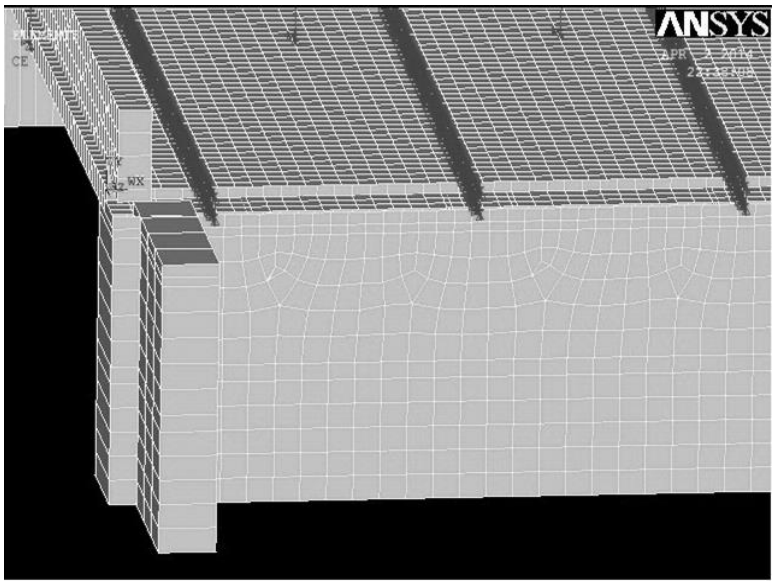

Figure 54. Meshed abutment

Girder - Pier Cap

Near the pier region, since both the bottom flange and the pier cap were simulated with beam elements, rigid links were used to connect the bottom flange of the girder and pier cap. Since Bridge #605220 has an expansion pier, the connection between the superstructure and pier cap only constrains the translation in the vertical direction and the rotations about the longitudinal and vertical directions. Hence, in the FEM, the rigid links (shown in Figure 55) that connect the girder and pier cap will only transfer the translation in the vertical direction and the rotations about the longitudinal and vertical directions from the superstructure to the substructure.

www.manaraa.com

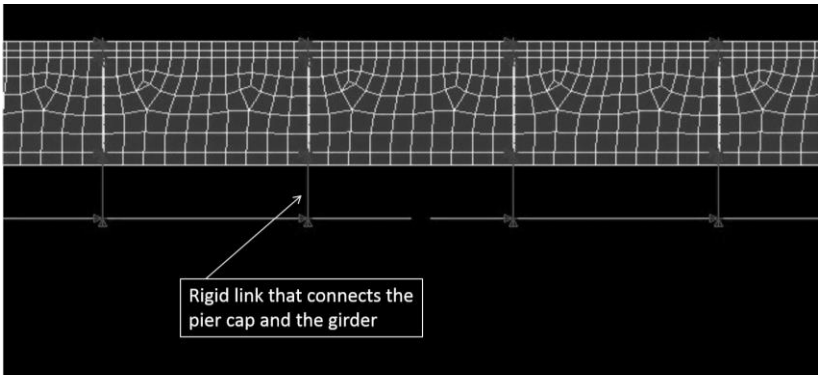

Figure 55. Rigid links that connect the bottom flange of girder and pier cap

Support Conditions

For the piles under the abutment, the bending stiffness of the pile is relatively small compared that of the other structural elements. So, the moment resistance from those piles was ignored. Also, the translation resistance from the pile in the transverse and longitudinal directions of the bridge was ignored. At each pile location under the abutment, a roller was used to replace each pile, and provided only vertical support. The pier column was also incorporated into the model. Rollers were used to replace the pier columns, and provided only vertical support. Given the many uncertainties, no consideration for soil pressure induced loads was made.

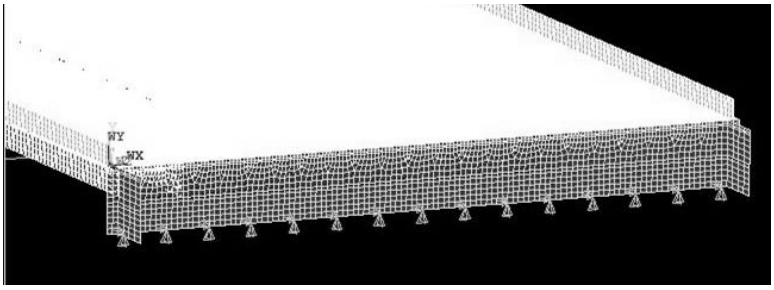

Figure 56. Roller supports used to replace the piles at the bottom of the abutment

www.manaraa.com

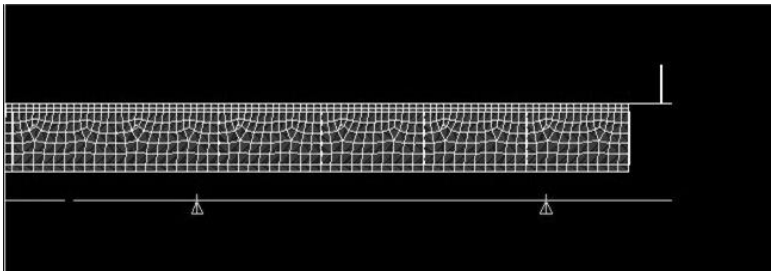

Figure 57. Roller support used to replace the pier column under pier cap

5.5 Validation and Calibration of Bridge Model

5.5.1 Calibration for live-load behavior

Live Loading

In the FEM, the load generated by the three-axle Iowa Department of Transportation dump truck was modeled with concentrated forces. The wheel spacing in the longitudinal direction and the weight carried by each wheel is shown in Figure 1 in Chapter 3.

For each load step, six concentrated forces were applied on the FEM to simulate the complete truck loading. In total, each load case consists of 58 load steps, and the spacing between each load step is five feet (shown in Figure 58).

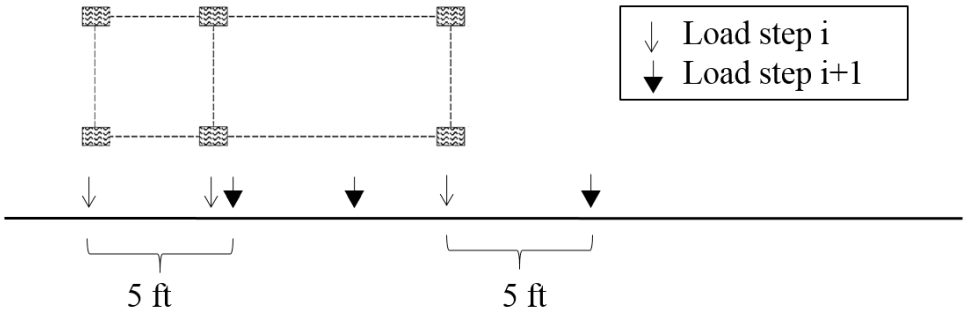

Figure 58. Load step spacing

www.manaraa.com

Calibration

Bridge #605220 has a skew of only 1.5 degrees and field testing results indicated a symmetric bridge response, so only the results from LC1, LC2 and LC5 are shown in this section. Comparisons between field testing results and FEM results for LC1 for each strain gauge located on the bottom flange of the first interior girder and exterior girder on the east side of the bridge are shown in Figure 59 and Figure 60 (see detail LC information in Section 3.3).

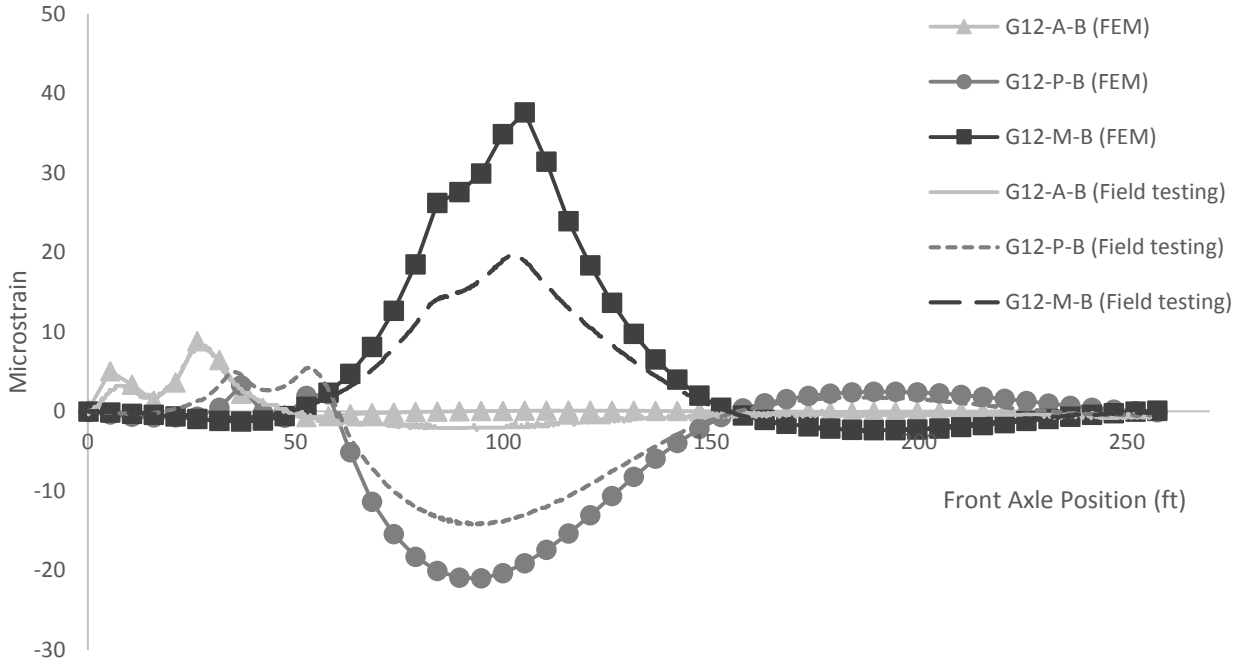

Figure 59. Comparison at the bottom flange of exterior girder in LC1 (Original E*)*

www.manaraa.com

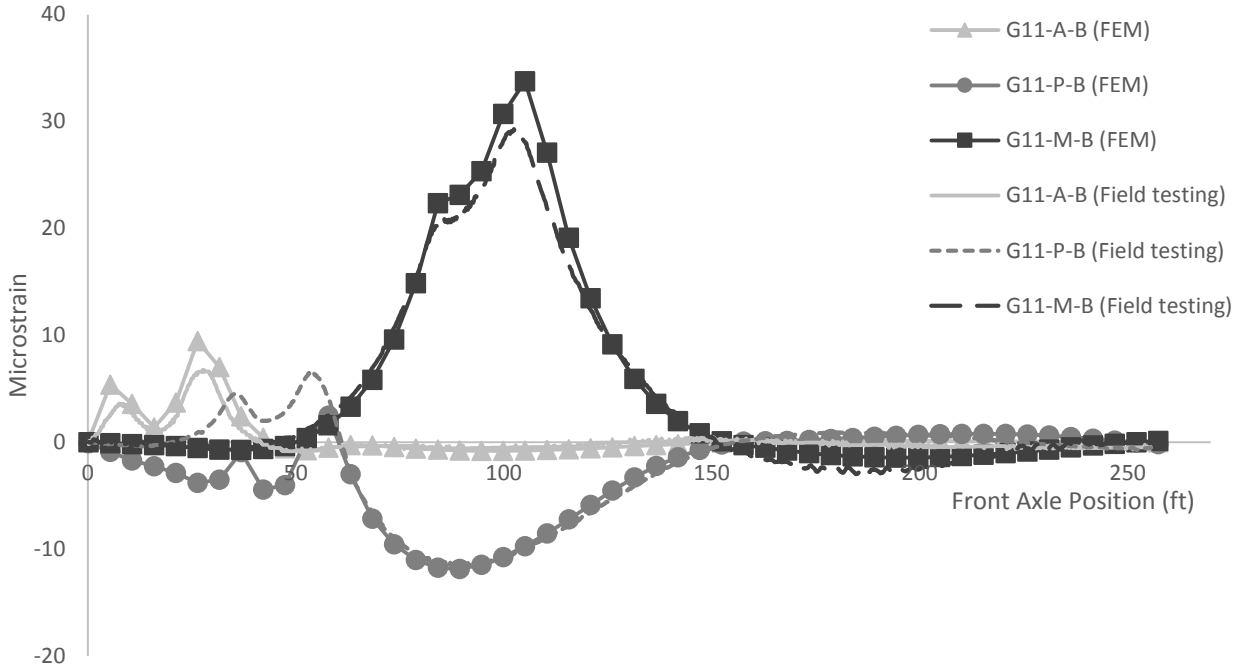

Figure 60. Comparison at the bottom flange of first interior girder in LC1 (Original E*)*

Generally, the FEM provided a higher strain value than the field testing results. Hence, the Young's Modulus was altered to calibrate the FEM. For the deck, Young's Modulus was increased from 3400 ksi to 4000 ksi. For the pre-stressed concrete girder, three Young's Modulus values (4000 ksi, 5100ksi and 7000ksi) were used to calibrate the FEM. The increase in Young's Modulus is justified because it if very likely that the concrete strength (and thus Young's Modulus) attained is higher than the minimum specified in the plans.

A very basic statistic, the percentage difference, was used to compare the results from the field testing and the FEM. For each strain gauge, the peak strain value was used to calculate the percentage with Equation (3).

$$Percentage\ difference\ = \frac{\varepsilon_{FEM} - \varepsilon_{field\ testing}}{\varepsilon_{field\ testing}} * 100\% \qquad (3)$$

The average percentage difference of each of the abutment, pier and mid-span sections was calculated for the first three girders on the east side of the bridge, because these three girders

www.manaraa.com

provide relatively high strain values. The average percentage difference of the whole bridge is the average value of these three sections, as listed in Table 5 for LC1.

Table 5 Summary of average percentage difference on each section and the whole bridge

Young's Modulus of the girder (ksi)	Abutment Section	Pier section	Mid-span section	Whole bridge
4000	14.7	23.9	33.6	24.1
5100	9.2	10.8	30.8	16.9
7000	18.6	31.3	33	27.6

The 5100 ksi Young's Modulus for the pre-stressed girder together with a 4000 ksi Young's Modulus for the deck, provided the minimum average percentage difference (16.9%) for LC 1.

After identifying the Young's Modulus combination that resulted in the minimum percentage difference for LC 1, the FEM with updated Young's Modulus values was used to conduct the numerical analysis for all five load cases. The strain vs. position plots at each gauge location of the two girders under the truck in LC1, LC2 and LC5 from the FEM with the increased Young's Modulus are shown in Figure 61 to Figure 66.

www.manaraa.com

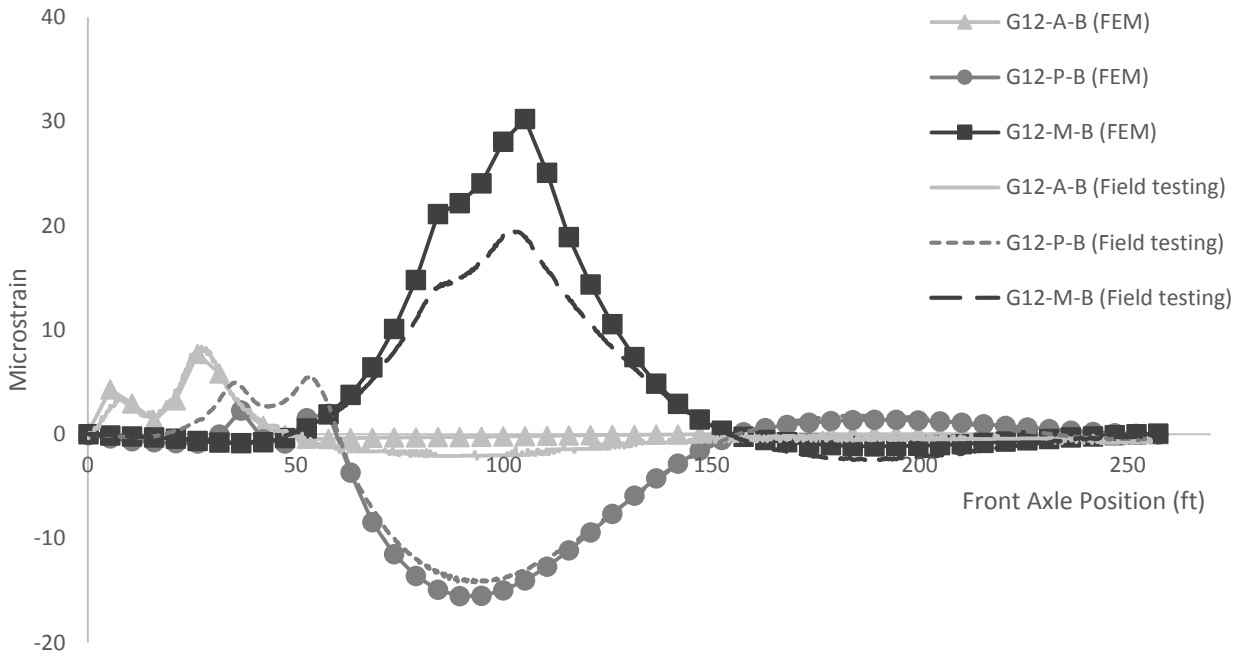

Figure 61. Comparison at the bottom flange of exterior girder in LC1

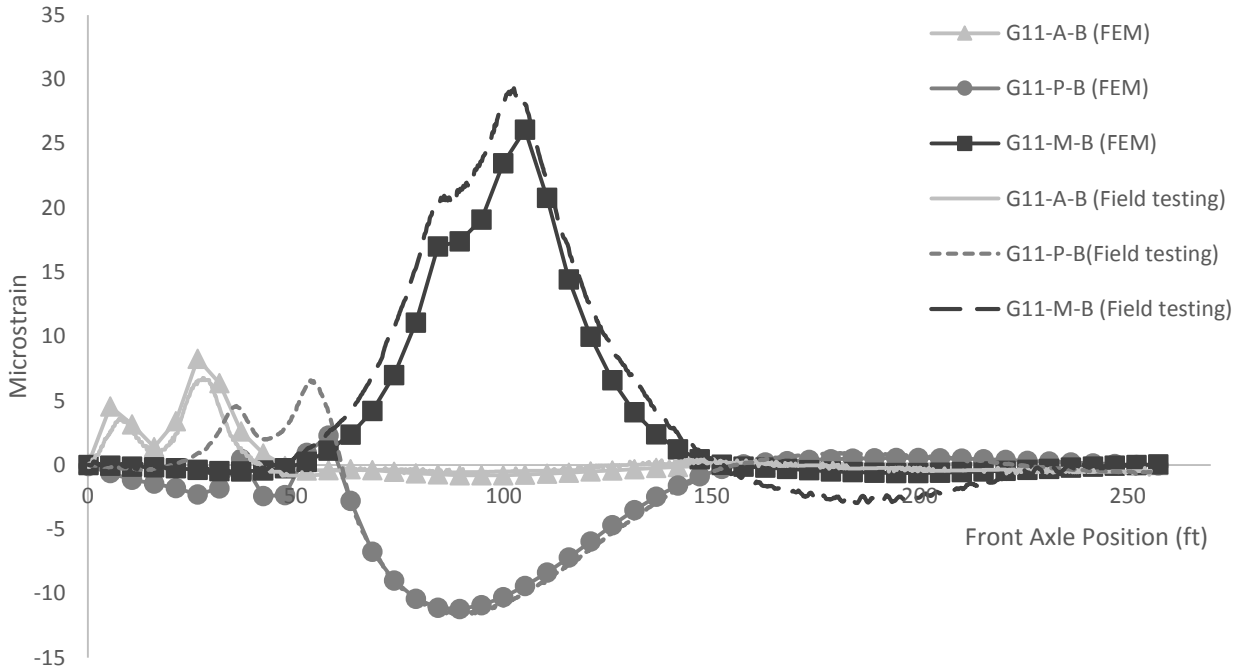

Figure 62. Comparison at the bottom flange of first interior girder in LC1

www.manaraa.com

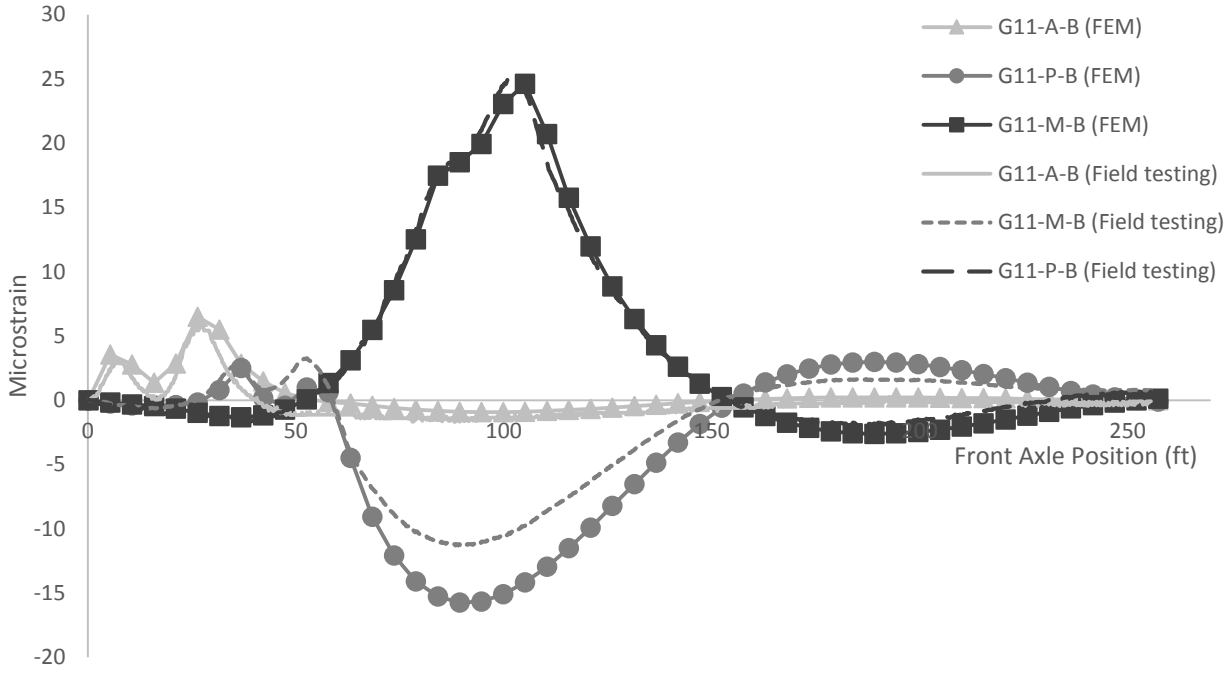

Figure 63. Comparison at the bottom flange of first interior girder in LC2

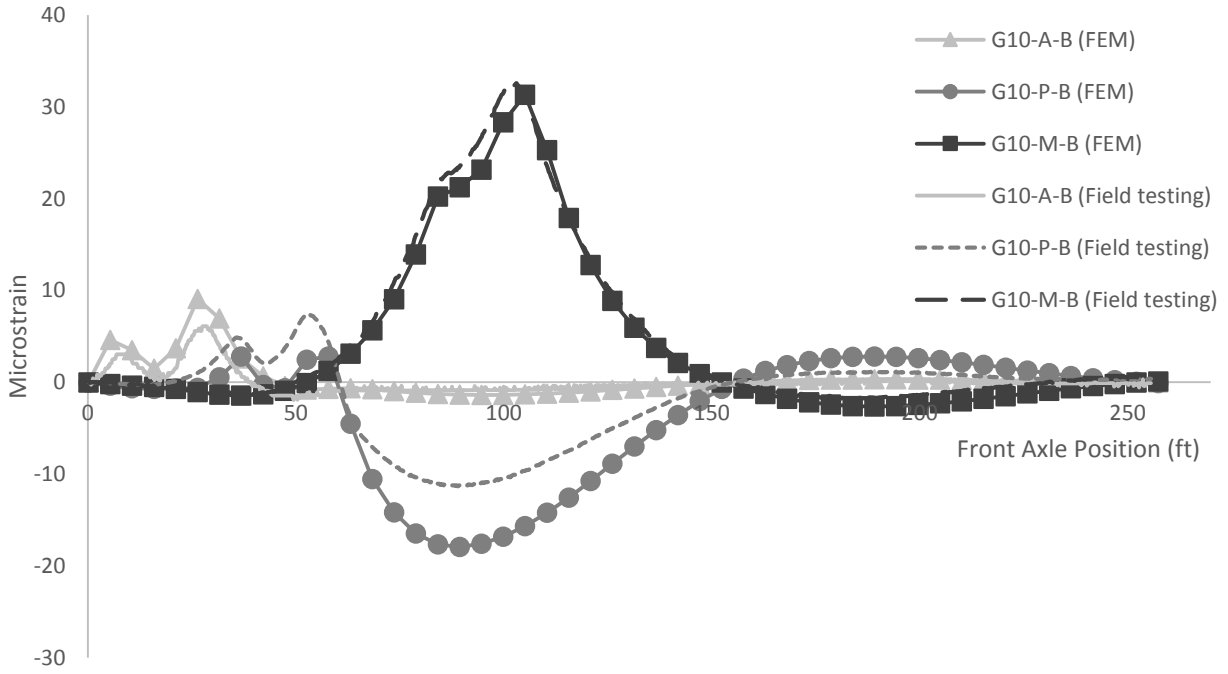

Figure 64. Comparison at the bottom flange of second interior girder in LC2

www.manaraa.com

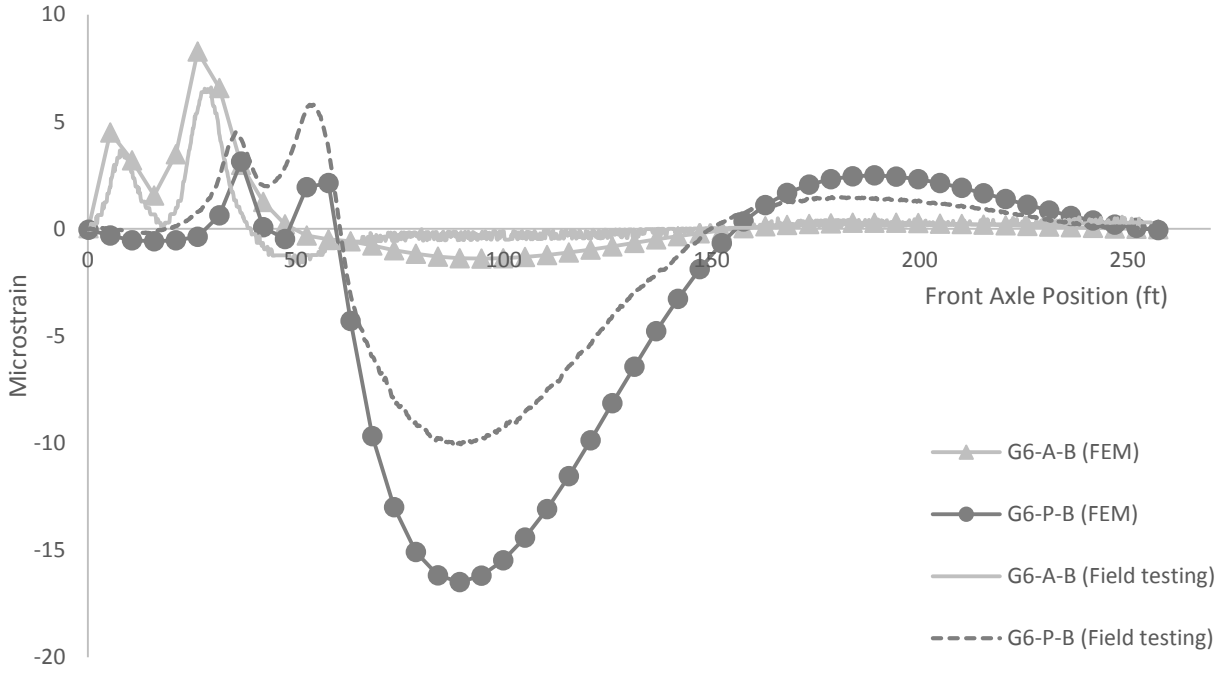

Figure 65. Comparison at the bottom flange of sixth girder from west side LC5

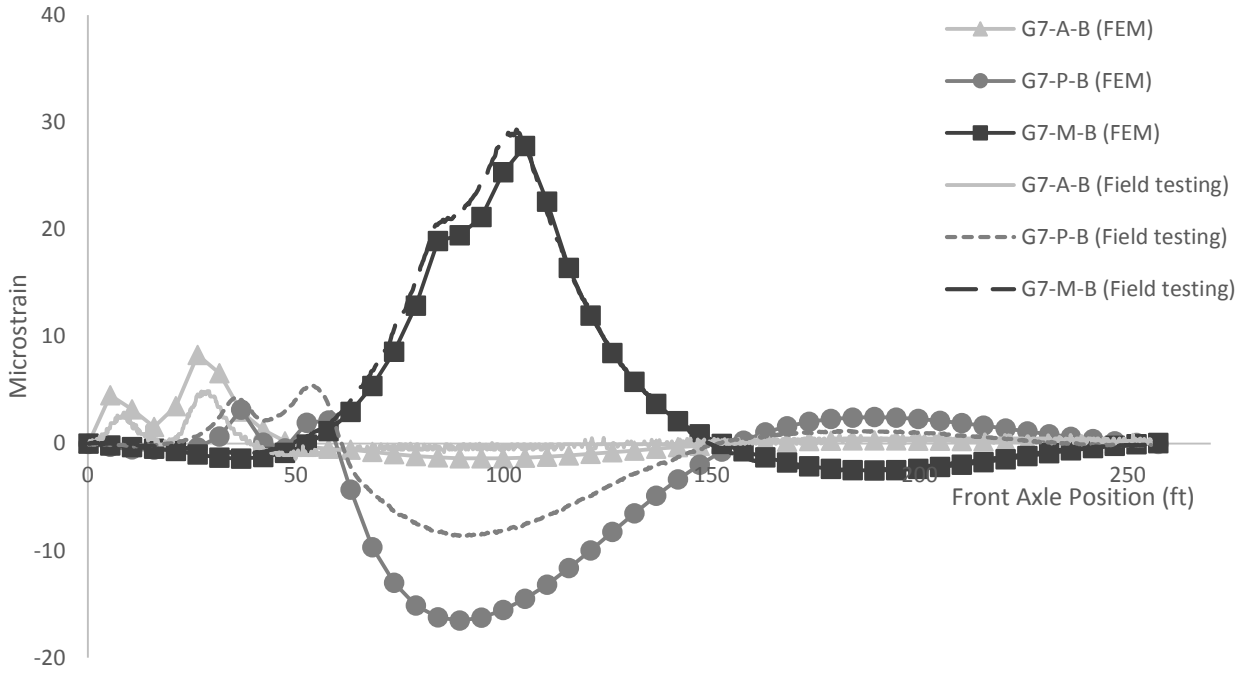

Figure 66. Comparison at the bottom flange of sixth girder from east side LC5

A further comparison between the field testing results and the FEM results in LC1 (shown in Figure 61 and Figure 62) revealed that from the FEM, the strain value in the exterior

www.manaraa.com

girder in the mid-span sections was higher than that of the first interior girder, while field testing results from the first interior girder gave a higher strain value than the exterior girder. Although not completely understood, it is believed that the observed behavior difference is likely due to the complex interaction of the barrier rail with the superstructure.

5.5.2 Validation for long-term behavior

Temperature Loading

For the FEM thermal loadings, two types of temperature changes were considered (see Section 4.2). The first is a temperature difference between the deck and the abutment. When the temperature of the deck is lower than the abutment, the deck would contract compared to the abutment; thus, tensile forces would be induced in the deck near the abutment region. The second reason is that the temperature gradient through the thickness of the deck would also produce tensile stress at the bottom of the deck. For example, when the bridge is exposed to sunshine, the temperature at the top surface of the deck would be 20°F to 30°F higher than the temperature at the bottom of the deck. As a consequence, the top layer of the deck would expand and generate tensile stress at the bottom of the deck.

During long-term testing, the temperature on the soil side of the abutment was unknown, but it is probably stable and changes very slowly. Thus, zero temperature change was assumed to have occurred in that region (shown in Figure 67).

The other temperature changes input into the FEM are shown in Figure 67 and are based upon the temperature measurement results discussed Chapter 4. Specifically, a temperature change at the bottom of deck was set to be -30°F, the temperature change on the front surface of the abutment was set to -20°F. Similarly, the temperature changes at the top surface of the deck

www.manaraa.com

on a sunny day was -10°F, assuming a 20°F temperature gradient through the deck thickness. The temperature changes for the girder, diaphragm, and pier cap were assumed to be -30°F, similar to the deck bottom temperature change.

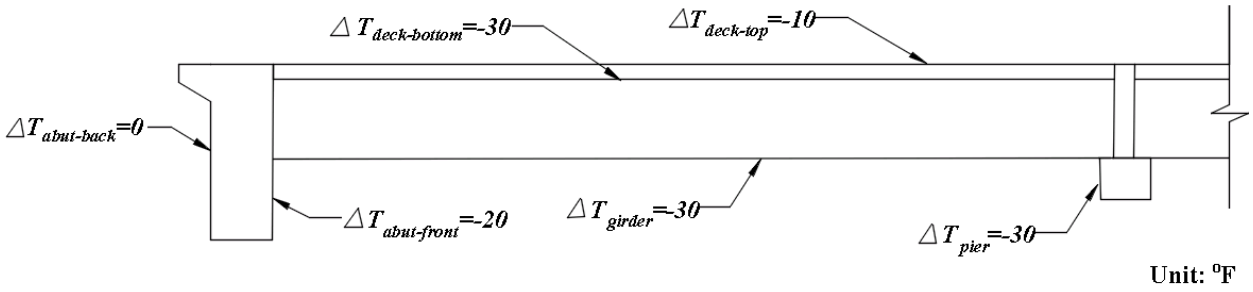

Figure 67. Temperature changes input into the FEM

Validation

After inputting the temperature changes on each component of the bridge into the FEM, the strain change at each strain gauge location at the bottom of the deck was extracted to compare with the field test results. Note that the temperature values input into the FEM represent the temperature changes, and the strain value from the FEM represents the corresponding strain changes. In Figure 68 to Figure 79, the black lines represent the results from the FEM simulation. For convenience in plotting, the initial temperature for the FEM was set to be 38°F, the same as the initial temperature of the field testing. The black lines in Figure 68 to Figure 79 therefore represent the change from the condition at 38°F.

www.manaraa.com

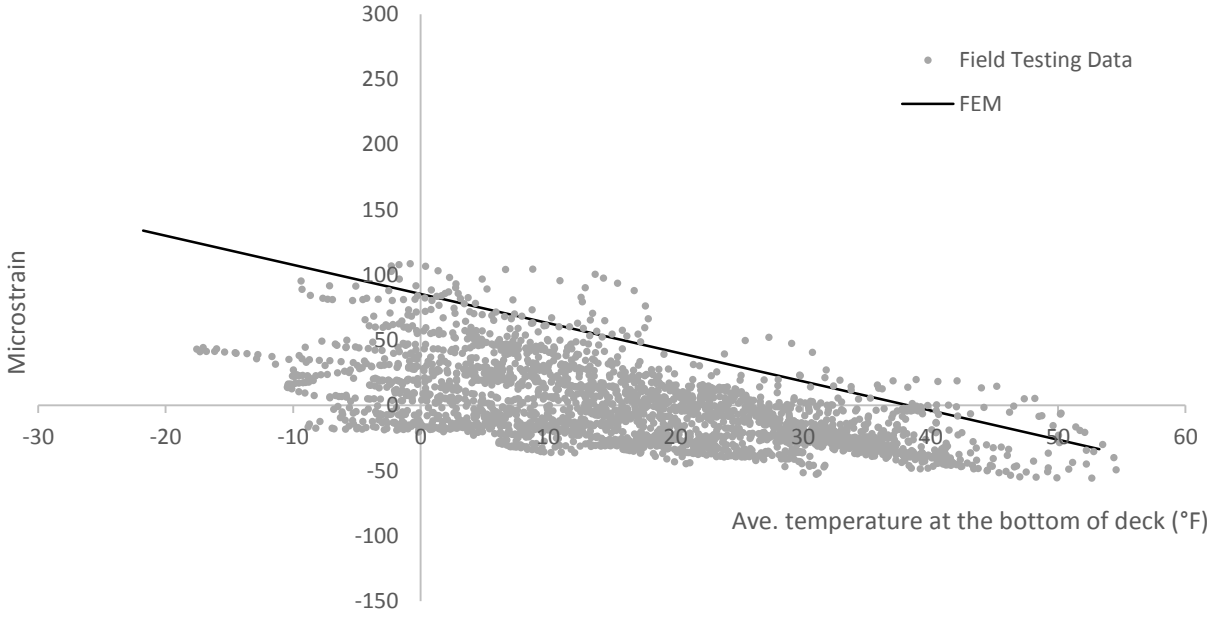

Figure 68. Results comparison for the gauge in first bay near abutment

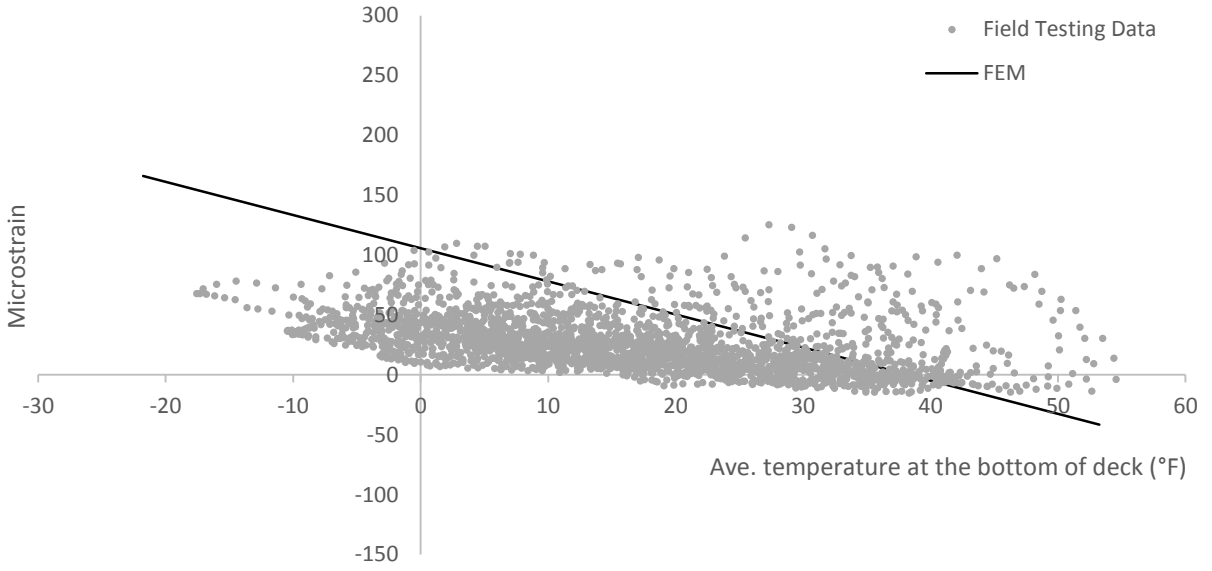

Figure 69. Results comparison for the gauge in second bay near abutment

www.manaraa.com

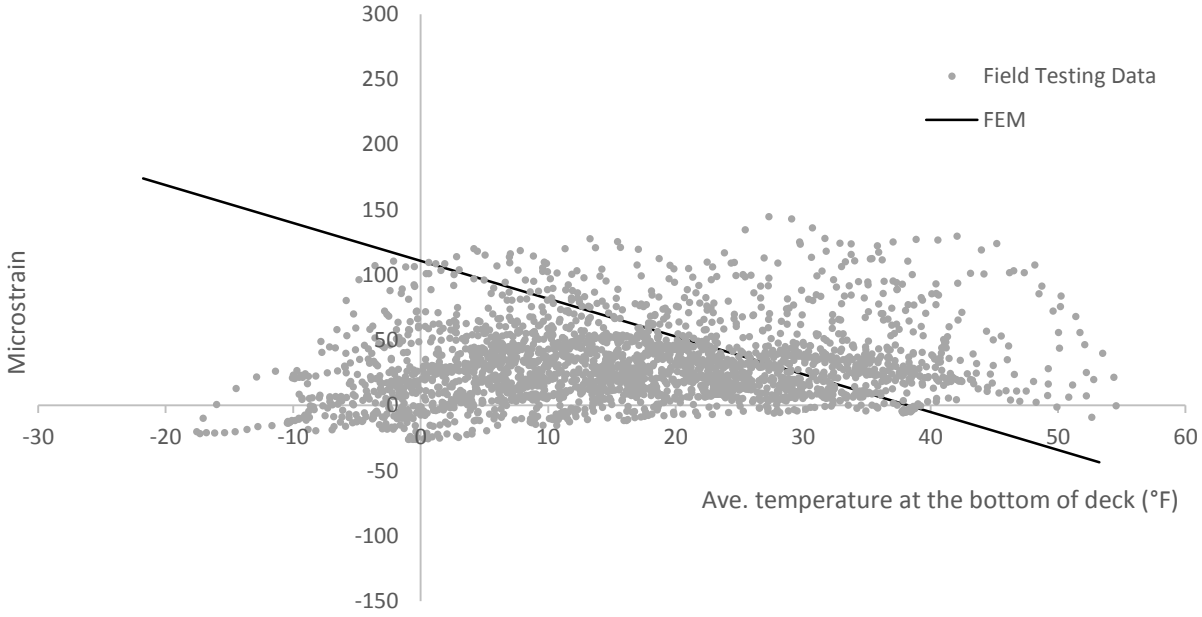

Figure 70. Results comparison for the gauge in third bay near abutment

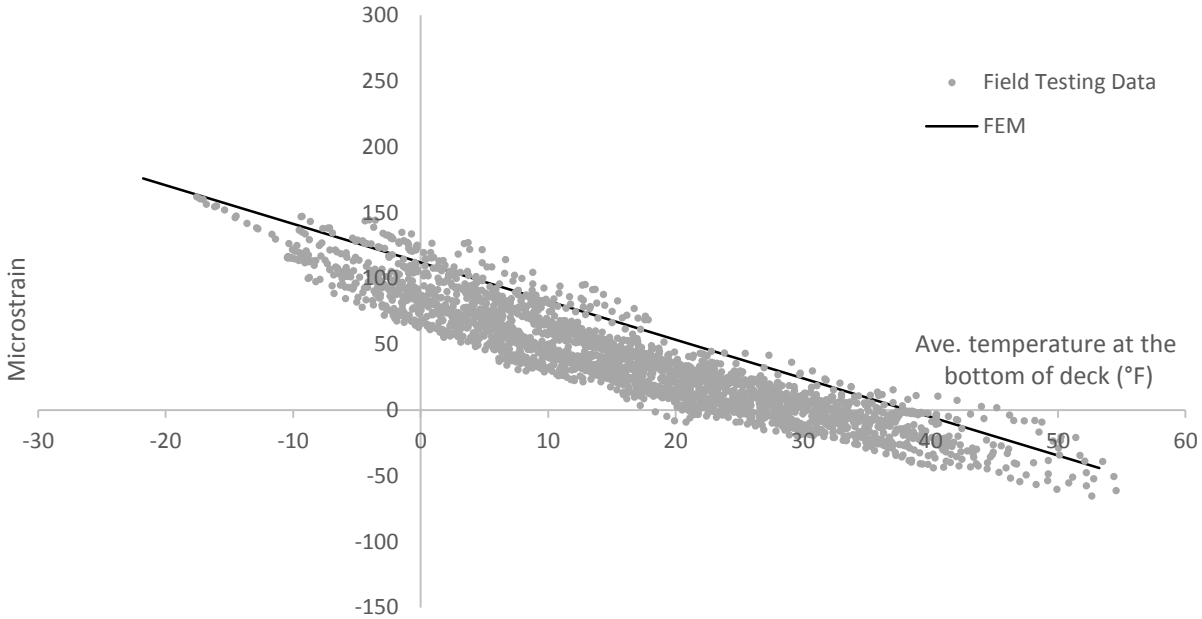

Figure 71. Results comparison for the gauge in fourth bay near abutment

www.manaraa.com

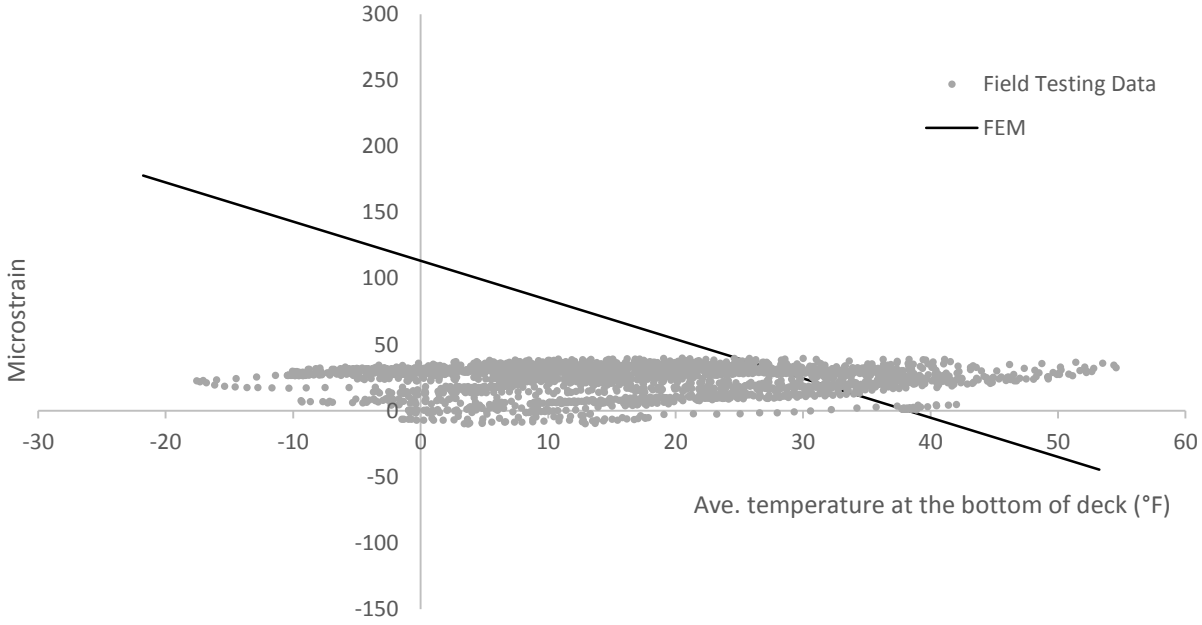

Figure 72. Results comparison for the gauge in fifth bay near abutment

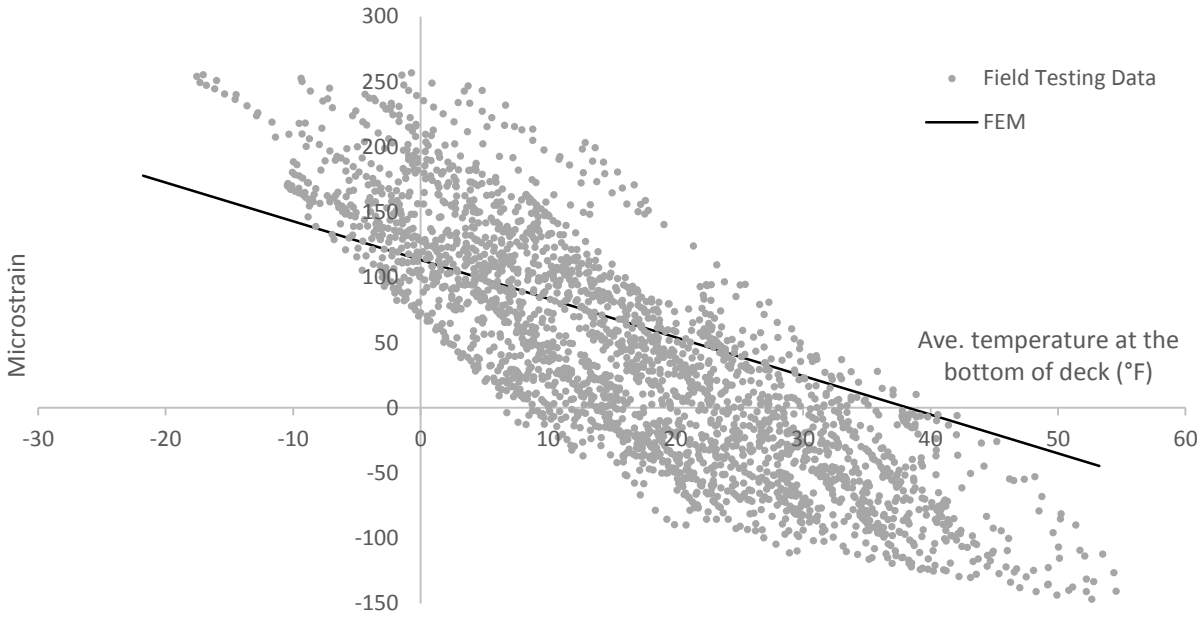

Figure 73. Results comparison for the gauge in sixth bay near abutment

www.manaraa.com

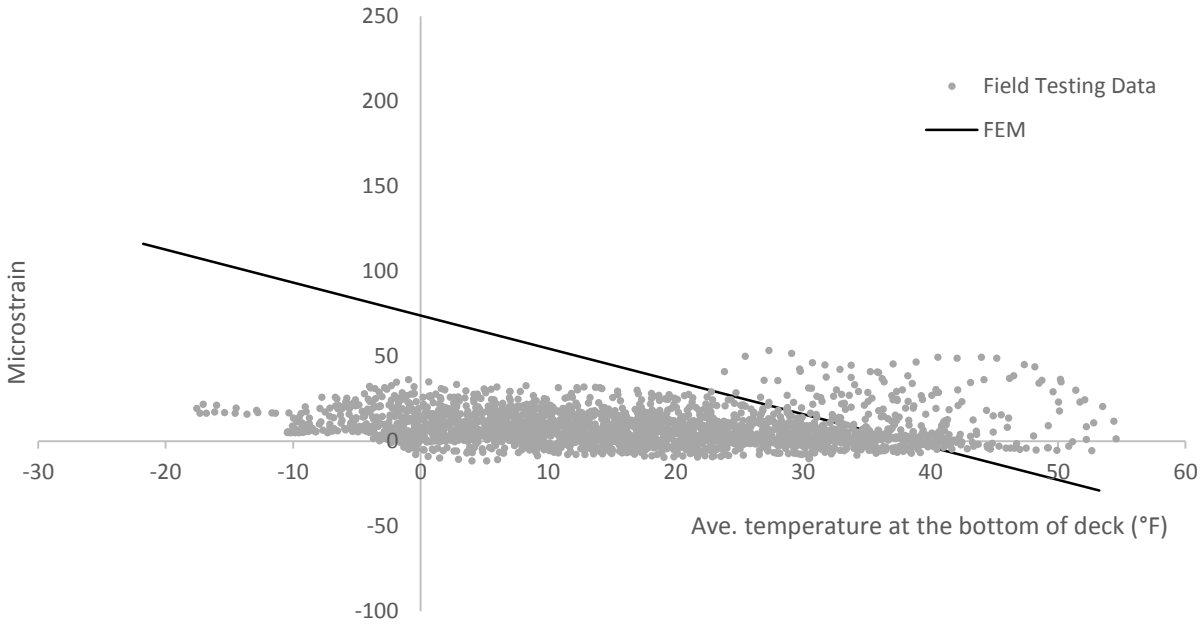

Figure 74. Results comparison for the gauge in first bay in middle span

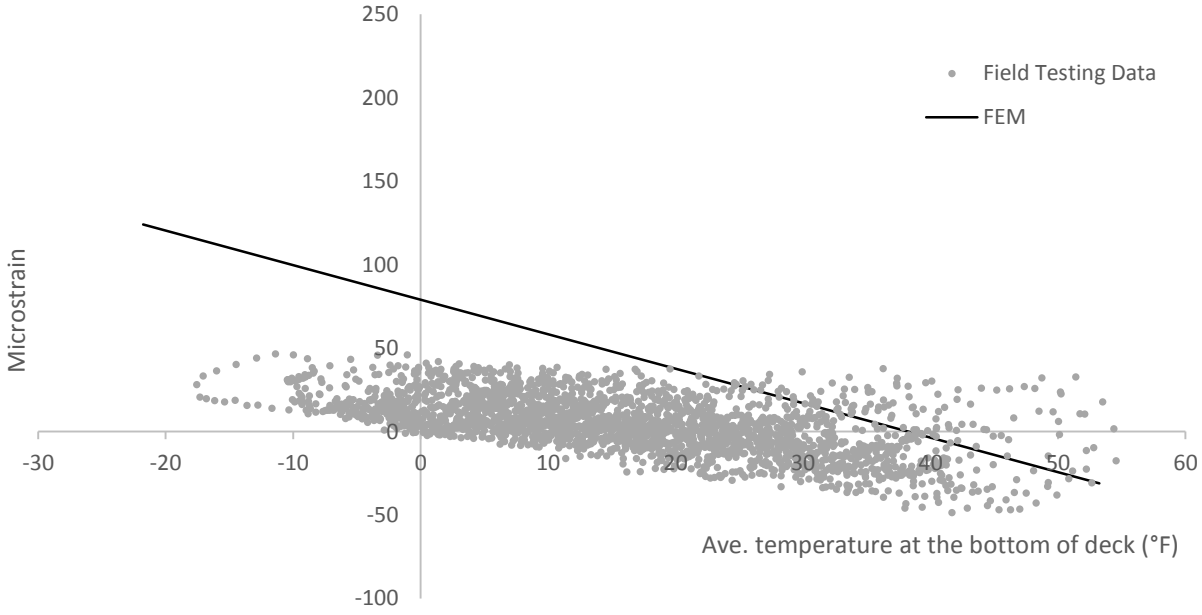

Figure 75. Results comparison for the gauge in third bay in middle span

www.manaraa.com

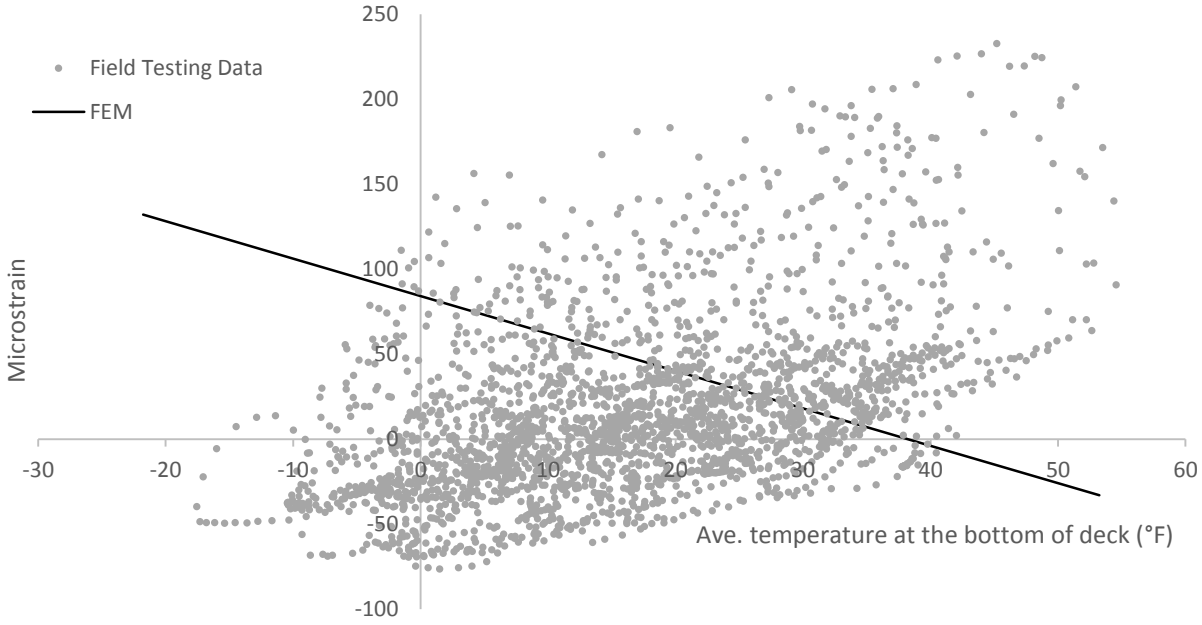

Figure 76. Results comparison for the gauge in fifth bay in middle span

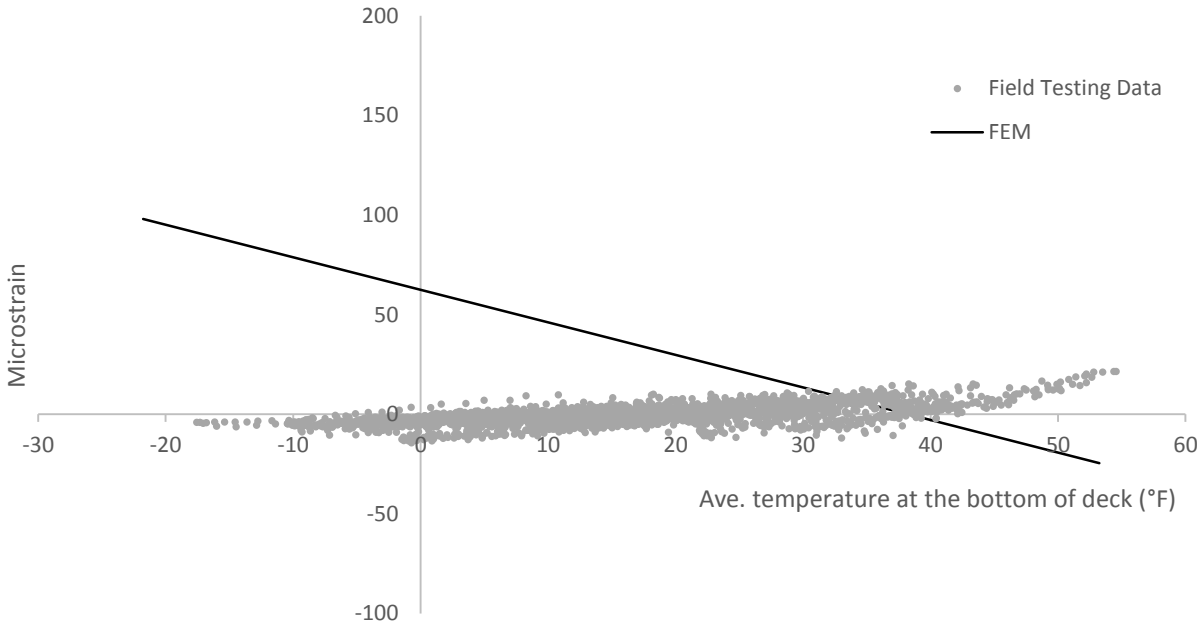

Figure 77. Results comparison for the gauge in first bay near pier

www.manaraa.com

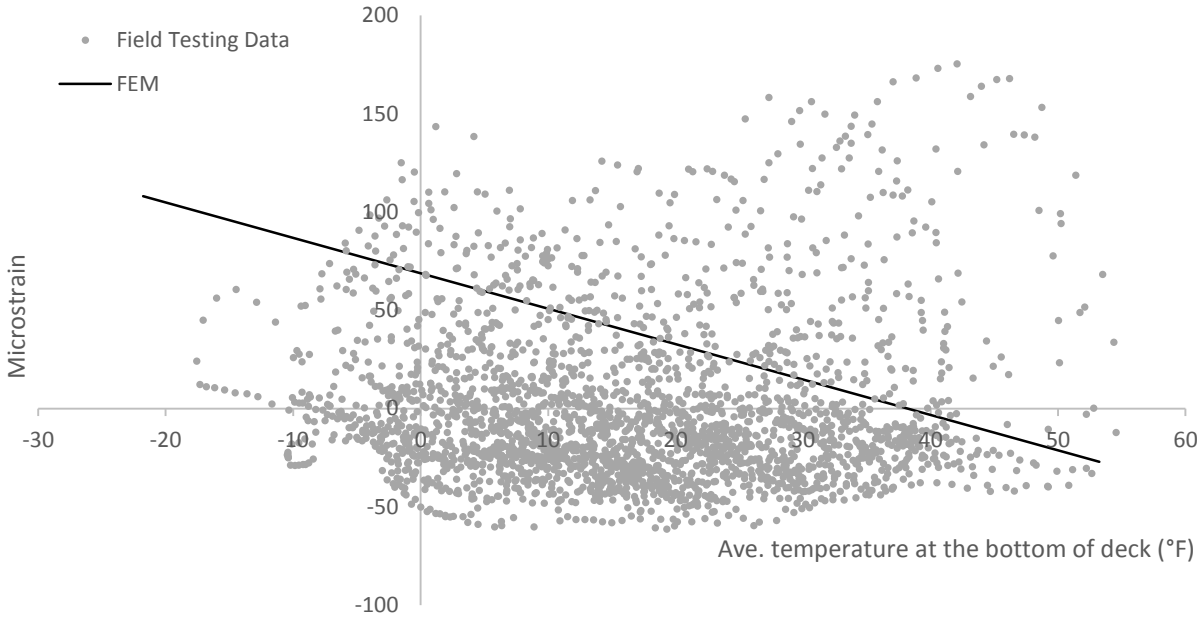

Figure 78. Results comparison for the gauge in third bay near pier

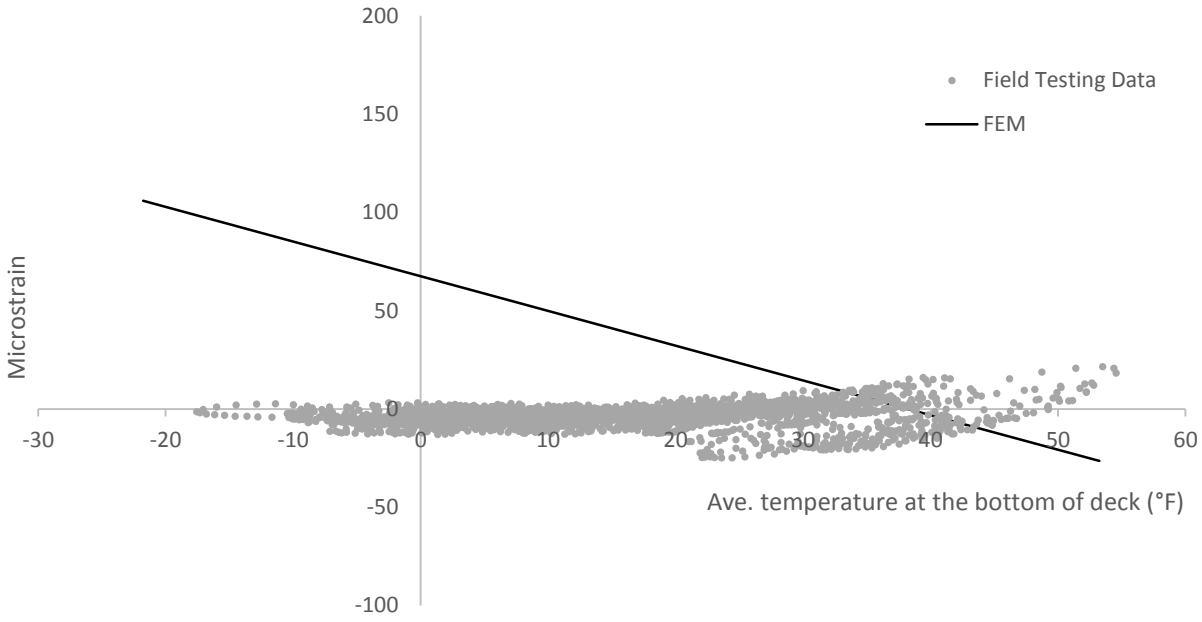

Figure 79. Results comparison for the gauge in fifth bay near pier

For the abutment section, the results from field testing reasonably match the results from the FEM, except in the third, fifth and sixth bays. As described in Section 4.2, the strain gauges

www.manaraa.com

in the third and fifth bays were installed close to the edge of a crack, which likely altered the strain pattern by reducing the strain readings. In the sixth bay, the strain gauge was placed near the end of a crack, and it is likely that high strain values due to stress concentration were measured. The comparison of displacement results between the FEM and the field testing is shown in Figure 80 to Figure 83.

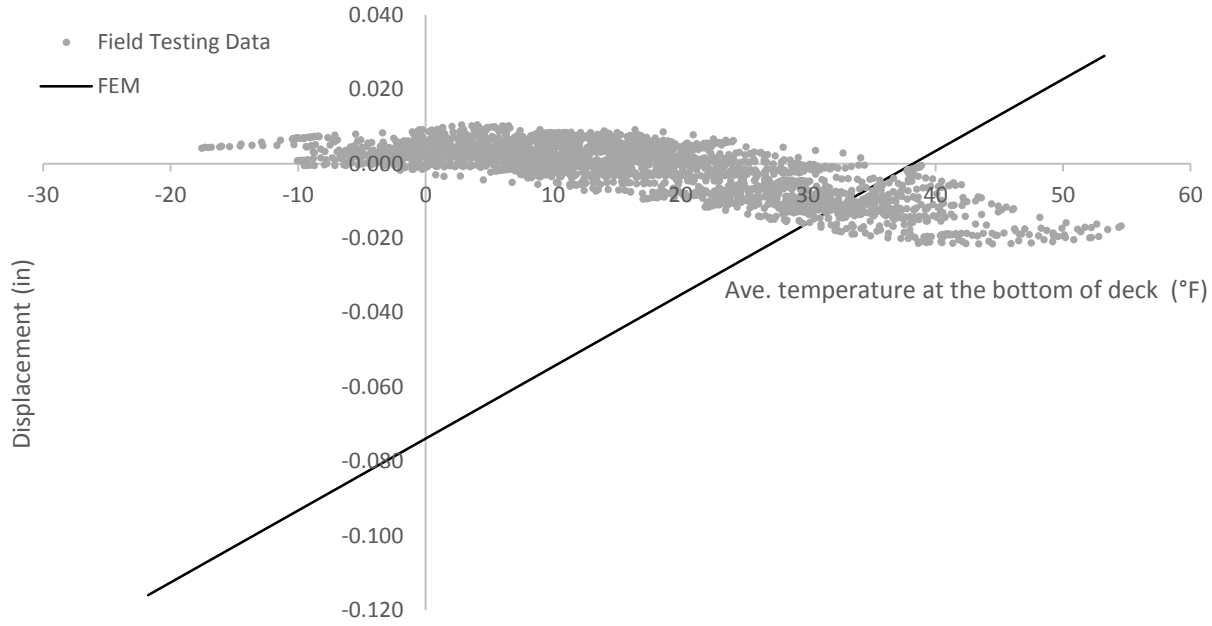

Figure 80. Results comparison for DS1

www.manaraa.com

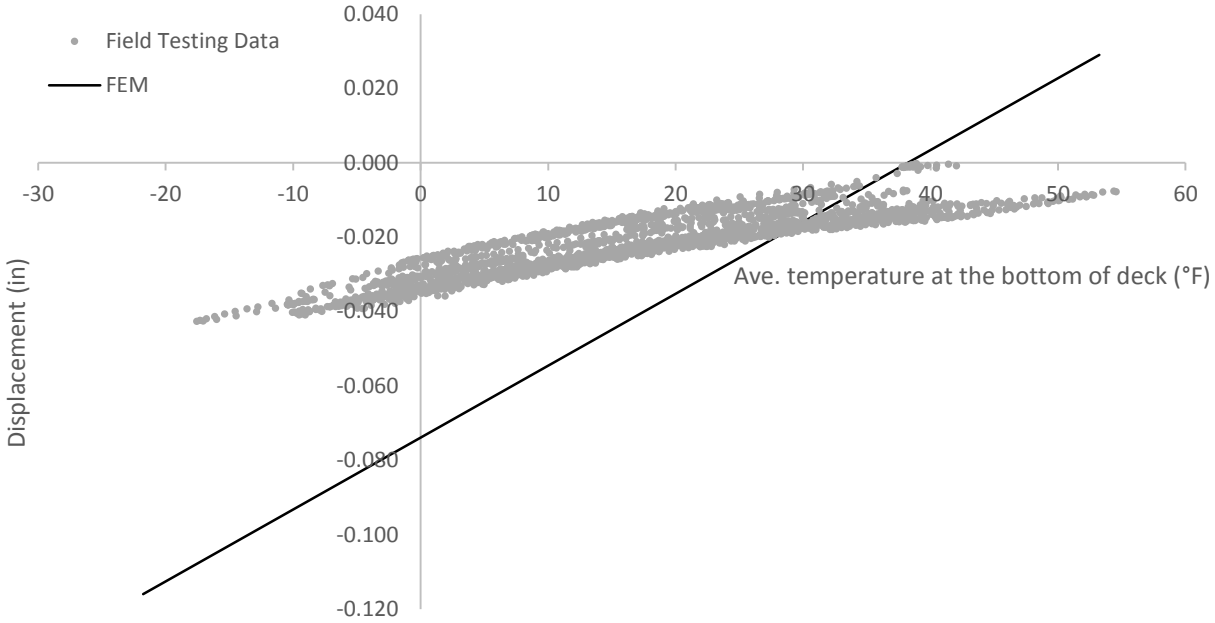

Figure 81. Results comparison for DS2

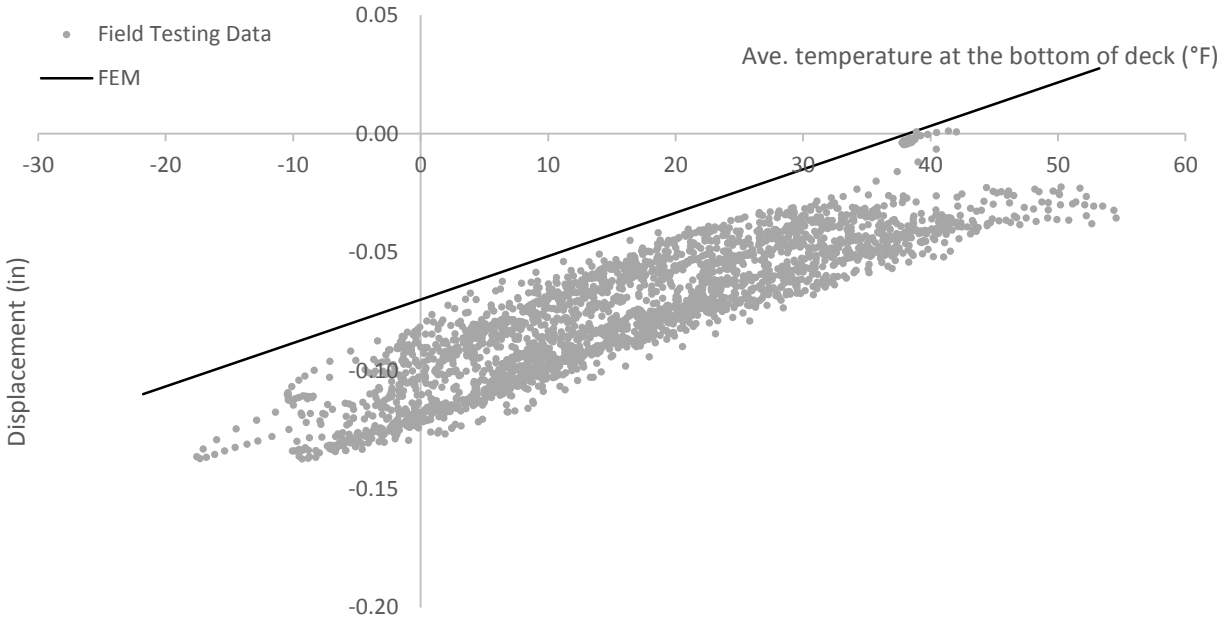

Figure 82. Results comparison for DS3

www.manaraa.com

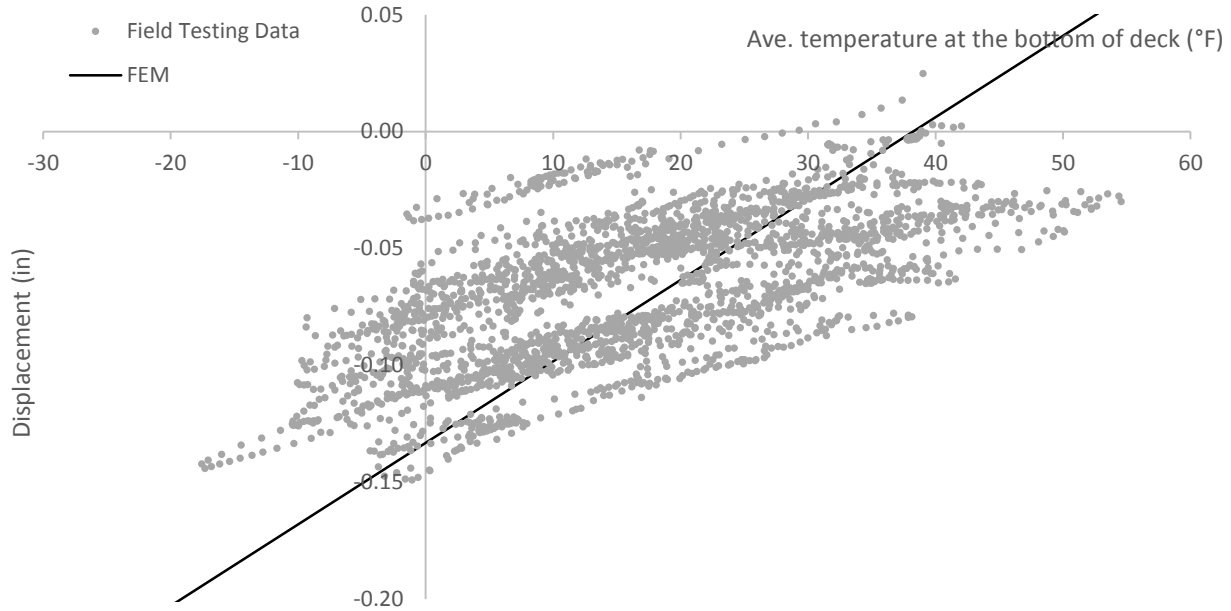

Figure 83. Results comparison for DS4

DS-1 measured the longitudinal displacement on the west side of the bridge, and the displacement data from it are considered to not be reliable (see Section 4.2).

DS-2 measured the longitudinal displacement on the east side of the bridge. The FEM results are between the field testing results and 0.8 in. calculated using $\alpha \times \Delta T \times L$.

DS-3 measured the displacement in the transverse direction near the abutment. Since both the FEM and field testing results have very similar slopes, it was deemed that no further calibration related to this behavior was required.

DS-4 measured the displacement in the transverse direction near the pier. The FEM overestimates the displacement in the transverse direction near the pier, which could be explained by two reasons. (1) Idealized support condition used to replace the pier column: a further FEM study altering the support condition at the bottom of the pier cap revealed that the pier boundary condition is not the reason. When the support condition at the bottom of the pier cap is changed from a vertical roller to a pin support which constrains the translation in the

www.manaraa.com

transverse direction, the displacement changes near the pier are reduced. However, the strain value at the bottom of the deck in the transverse section would be as high as 100 microstrain, which does not match the field testing results. (2) As a result the assumed temperature changes modelled at the pier diaphragm were regarded as the main reason that the FEM overestimated the displacement change near the pier. Since the boundary conditions at the pier have little effect on the behavior on the deck near the abutment where it has been observed that any deck width related distress might occur, only the vertical support boundary condition was used.

5.5.3 Validation for crack pattern

Annual Temperature Loading

In addition to daily temperature changes, annual temperature change was used to study the crack pattern that might result. The annual temperature change used to study this was calculated as the difference between a very cold day temperature and an assumed warm day. Using this methodology a uniform temperature of 80°F was used.

Since only the temperature at the front side of the abutment and the bottom and middle depth of the deck were measured during the long-term test, the temperature at the soil side of the abutment was unknown. Fortunately, some temperature records at the soil side of an abutment were available in the final report of "Field Monitoring of Curved Girder Bridges with Integral Abutments" (Greimann, et al. 2014). These records indicated that the temperature at the top of the steel piles remain about 35°F for the entire year. Based on temperature historical records in the Waterloo region, the minimum temperature for the cold day in winter was selected as -40°F. The temperature at the front side of abutment was calculated based on the 2/3 relation between

www.manaraa.com

the abutment temperature changes and the deck bottom temperature changes. (See detail information in Section 4.2)

The temperatures at different parts of the bridge on the cold day are shown in Figure 84. The temperature changes from the construction temperatures are shown in Figure 85.

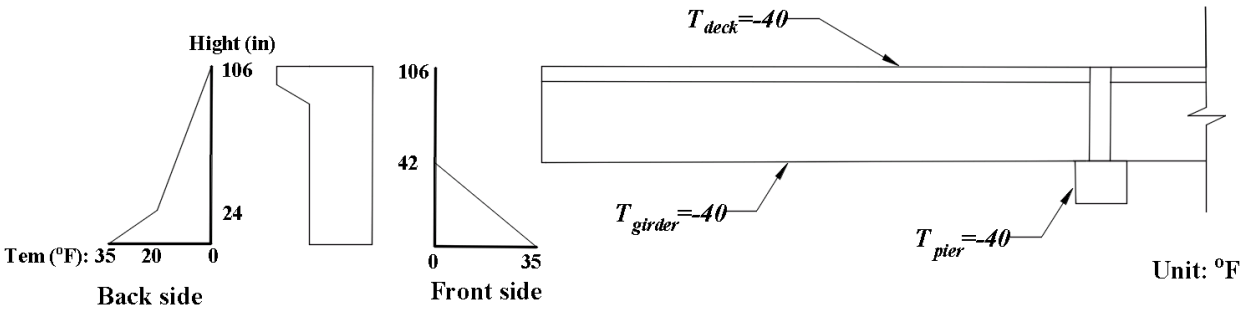

Figure 84. Assumed temperature at the cold day-calibration for crack pattern

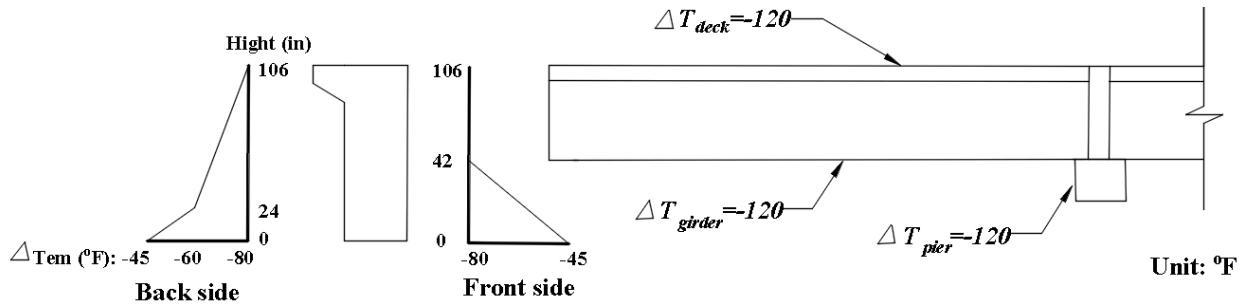

Figure 85. Temperature changes used for calibration of crack pattern

Validation

First principal strain distributions and directions on the top surface of the bridge deck were used to compare the crack pattern (see Figure 7 and Figure 8 in Chapter 3) observed during an inspection of the bridge deck to the analytical results. Based on bridge inspection results, most of the cracks on the top surface of the deck were found to start above a girder, with a higher density of cracks at the corner of the bridge. The first principal strain direction were expected to

www.manaraa.com

be perpendicular to the crack direction. As shown in the Figure 86, the maximum strain at the bridge corner is 129 ~146 microstrain, which is higher than the crack strain 132 microstrain calculated by $7.5\sqrt{f_c'}/57000\sqrt{f_c'}$. The FEM also matched the expectation for the first principal strain direction.

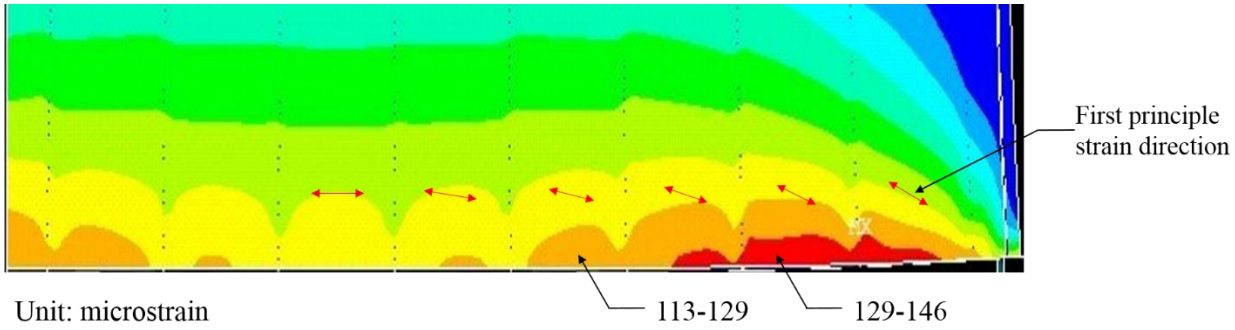

Figure 86. First principal strain contour on top surface of deck (calibration for crack pattern)

5.5.4 Validation for shrinkage

Shrinkage Loading

Strain induced by shrinkage was calculated using the relationship given by the AASHTO code and shown in Equation (4).

$$(\varepsilon_{sh})_t = -k_s k_h \left(\frac{t}{35+t}\right) 0.51 * 10^{-3} \qquad (4)$$

$(\varepsilon_{sh})_t$ – Free strain due to shrinkage at time t,

t – Drying time

k_s – Size factor relate to volume-to-area ratio (k_s=0.54 for abutment and pier diaphragm; k_s=0.71 for the deck)

k_h – Humidity factor (humidity was selected as 30% in this research; k_h=1.57)

www.manaraa.com

To simulate the maximum shrinkage strain, an infinite number of drying days was used to calculate the ultimate shrinkage strain. Using this relationship the strain caused by shrinkage loading on each free bridge component is shown in Figure 87.

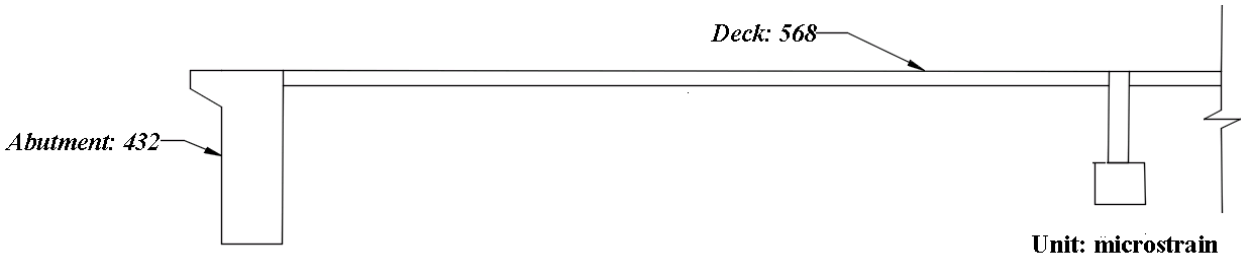

Figure 87. Shrinkage strain on each component of bridge

Shrinkage loading was applied in the FEM by an "equivalent temperature method", by which a temperature resulting in the same change in length was calculated to induce the shrinkage strain. This method has been verified and used by Stringer and Burgueno to simulate shrinkage loading on a bridge to study cracking. (Strainge and Burgueno 2012)

Free shrinkage strain was applied to the bridge through temperature loading, with the equivalent temperature calculated by Equation (5).

$$\Delta T = -\frac{(\varepsilon_{sh})_t}{\alpha} \qquad (5)$$

Since the girders were pre-stressed concrete and the majority of the shrinkage had occurred before they were shipped to the field, the girder shrinkage strain were taken as zero.

Validation

Crack maps (see Figure 7 and Figure 8 in Chapter 3) were used to compare the first principal strain distribution and direction predicted by the FEM under shrinkage loading (Figure 88). The arrows in Figure 88 represent the first principal strain vector in the vicinity region. Based on the FEM, the transverse shrinkage cracks are expected to occur away from the

www.manaraa.com

abutment. At the middle of the deck near the abutment, transverse cracks would dominate. Both phenomena do not correspond to the bridge inspection results. Hence, the shrinkage was not considered to be a primary reason for the deck cracks, and was not applied during the parametric study.

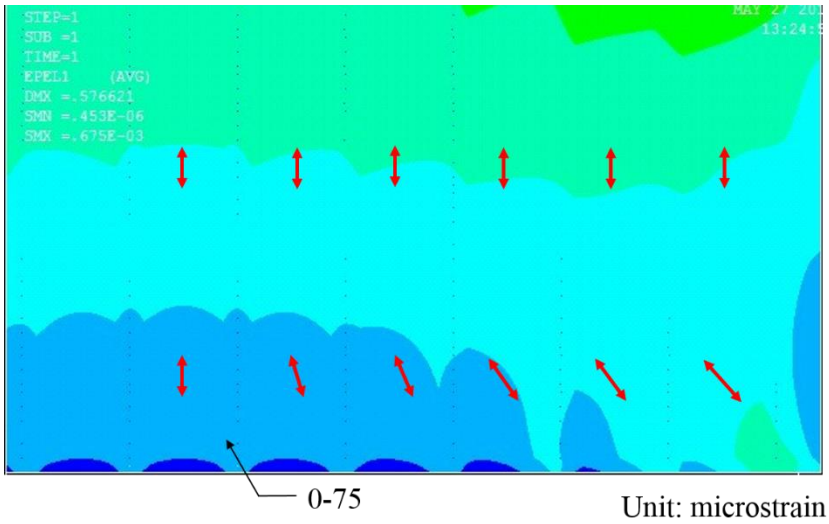

Figure 88. First principal strain contour plot with strain vector under shrinkage loading

www.manaraa.com

CHAPTER 6. PARAMATRIC STUDY ON FULL BRIDGE MODEL

6.1 Introduction

In this chapter, a parametric study performed to investigate the effect of bridge width on the tensile strain in the deck is described including a detailed study of factors that may impact the level of tensile strain in the deck, such as bridge skew, bridge width, abutment type, pier type, girder type, girder spacing and number of spans. The annual temperature change (see details in Section 5.5.3) was used as the primary loading for this parametric study in light of the results presented in the previous chapter.

6.2 Bridge Width and Skew

In this section the impact of two geometric features on deck strain are described. In total, six different bridge models were developed to study the influence of bridge skew and bridge deck width.

6.2.1 Bridge width influence on integral abutment bridge with zero skew

Strain in the Deck

Regardless of bridge width the highest stress on both the top surface and the bottom surface of the deck occurred near the abutment and it was observed that the highest stress concentration point was always 10-20 ft from the side of the bridge. Figure 89 shows the first principal strain magnitude and direction on the top surface of the deck from the three zero skew condition with variable bridge widths. Similarly, Figure 90 shows the first principal strain magnitude and direction on the bottom surface of the deck.

www.manaraa.com

As can be seen the first principal tensile strain results indicate that the maximum strain in the deck increases by 20-30 microstrain when the bridge width increases from 40-ft to 160-ft. However, it should be pointed out that tensile strain from all three models exceed the crack strain of concrete.

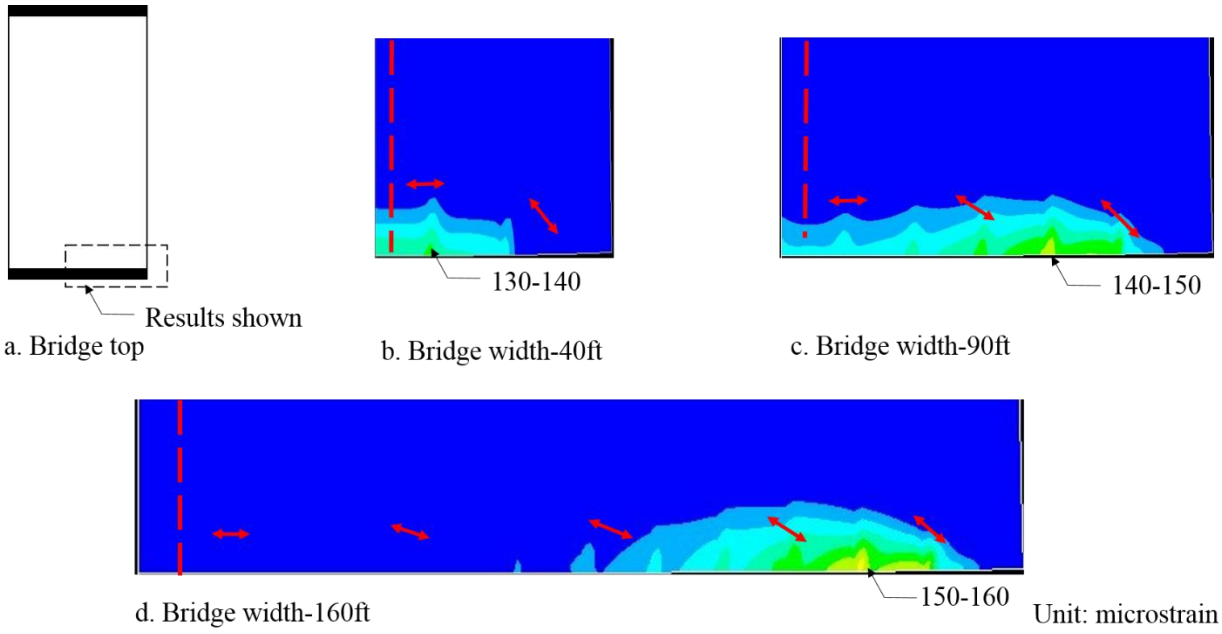

Figure 89. First principal strain on top surface of deck

www.manaraa.com

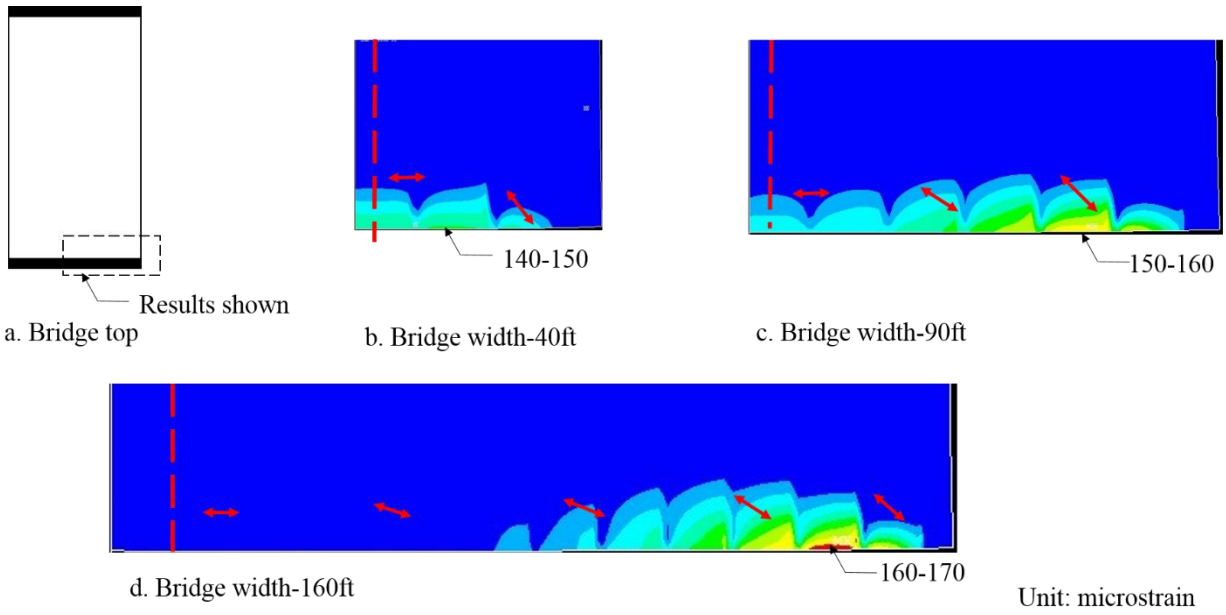

Figure 90. First principal strain on bottom surface of deck

Strain in Other Bridge Components

Besides the strain in the bridge deck, the strain in other bridge components such as the abutment and girders were also examined. Figure 91 and Figure 92 show the strain distributions on the soil and front side of the abutment, respectively. On both sides of the abutment, high strain concentrations were observed at the bottom corners of the abutments on all three bridge models. This strain concentration was not regarded as a significant issue affecting strain distribution in the deck, since the idealized support conditions at the piles are believed to be the source of this stress concentration. The next highest strain on the abutment occurred at the top of the abutment near the deck with the resulting strain magnitudes the same as those in the deck due to the imposed strain compatibility.

www.manaraa.com

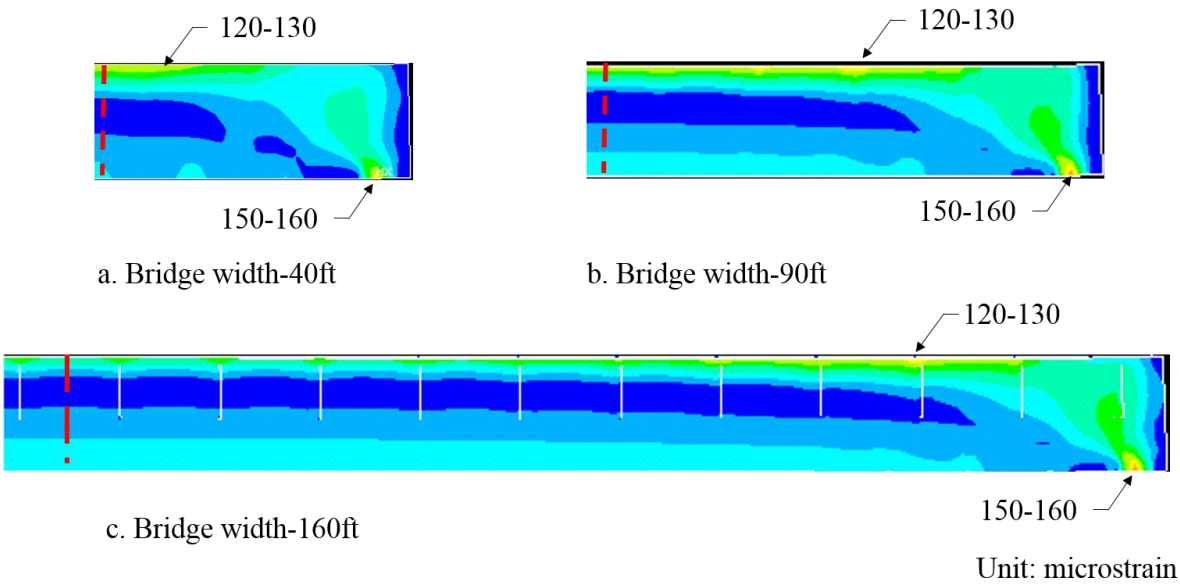

Figure 91. First principal strain distribution on the soil side of abutment

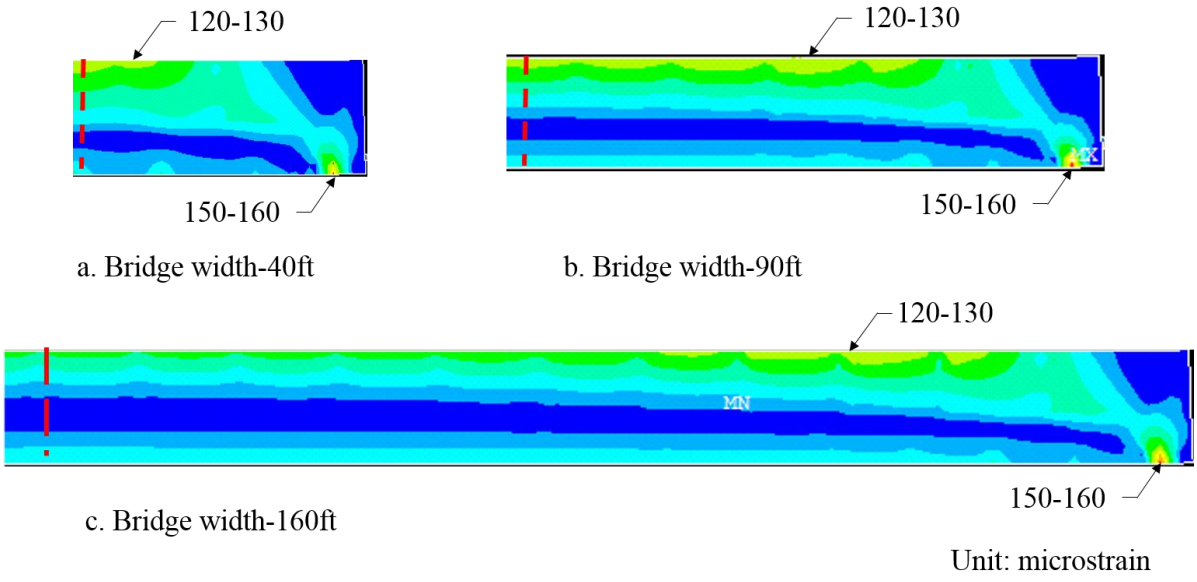

Figure 92. First principal strain distribution on front side of abutment

Based upon the FEM results from Figure 91 and Figure 92, no significant relation can be observed between the strain magnitude in other bridge components and bridge width. Thus, it appears that increasing bridge width does not induce significant deleterious effects.

www.manaraa.com

6.2.2 Bridge width influence on integral abutment bridge with 45 degree skew

Figure 93 shows the strain distribution on a 40-ft width bridge model that has 45 degrees skew. As in previous figures, the arrows represent the tensile strain direction. As the bridge which is the primary focus of this study had essentially zero skew, the crack map of Bridge #49661 shown in Figure 94 was used to provide some validation that the skewed bridge model utilized in this part of the study was realistic. Bridge #49661 was specifically selected because it is 40-ft wide (like the base model used in this work) with a 45 degree skew. As can be seen, there does appear to be good correlation between the direction of maximum tensile strain and the orientation of cracking.

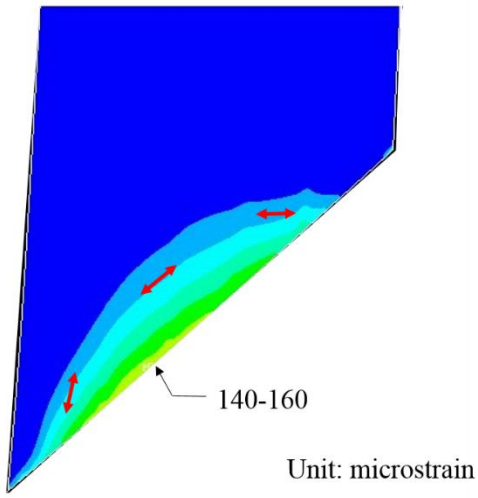

Figure 93. First principal strain distribution on 40 ft bridge with 45 degrees skew

www.manaraa.com

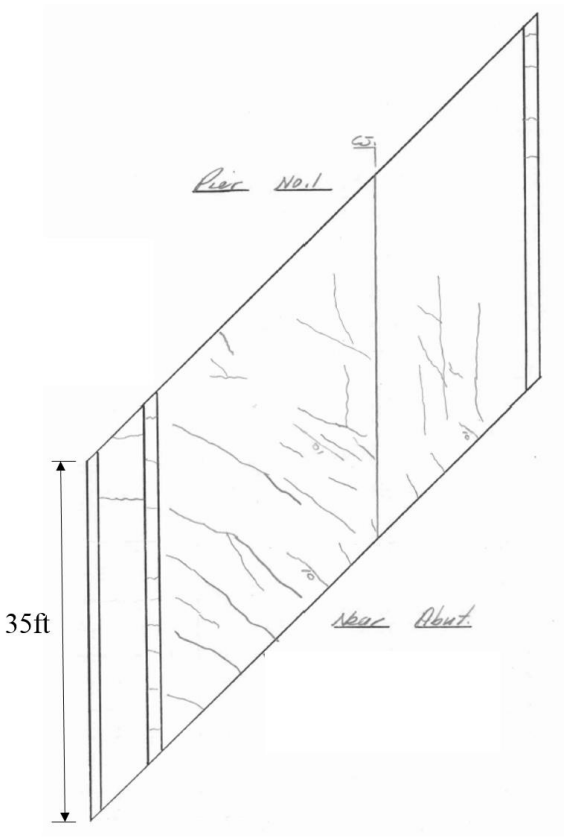

Figure 94. Crack map of Bridge #49661

Figure 95 shows three first principal strain contour plots for 45 degree skewed bridges with different bridge widths. Regardless of the bridge width, the maximum tensile strain is concentrated at the acute angle corners. The maximum strain increases from 156 to 193 microstrain as the bridge width increases from 40-ft to 160-ft.

www.manaraa.com

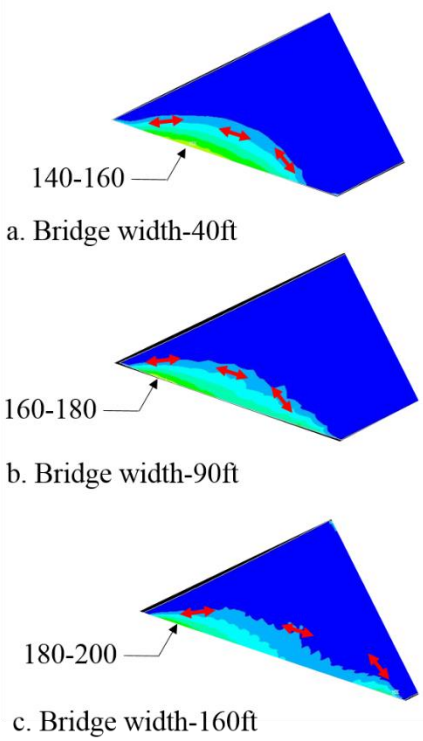

Figure 95. First principal strain contour on skew models.

6.2.3 Summary

Table 6 lists the maximum strain on the deck top surface for the skew and non-skew models. As can be seen, there does seem to be a relationship between peak thermally induced strain and both bridge width and skew.

Table 6. Maximum tensile strain on non-skew and skew bridge models

Bridge width	Non-skew	Skew-45º
40ft	140~150	140~160
90ft	150~160	160~180
160ft	160~170	180~200

www.manaraa.com

6.3 Abutment Type

To study the influence the abutment type has on the strain in the bridge deck, two non-skew bridge models with 90-ft width were modeled and compared. One bridge model had integral abutments, while the other one had stub abutments. Figure 96 compares the deck strain distributions for both the integral abutment bridge model and the stub abutment bridge model. The maximum tensile strain in the deck of the integral abutment bridge model is 130~148 microstrain, while on the stub abutment bridge model, the maximum tensile strain in the deck is 43~65 microstrain. The influence of abutment type will be further discussed in the subsequent chapter.

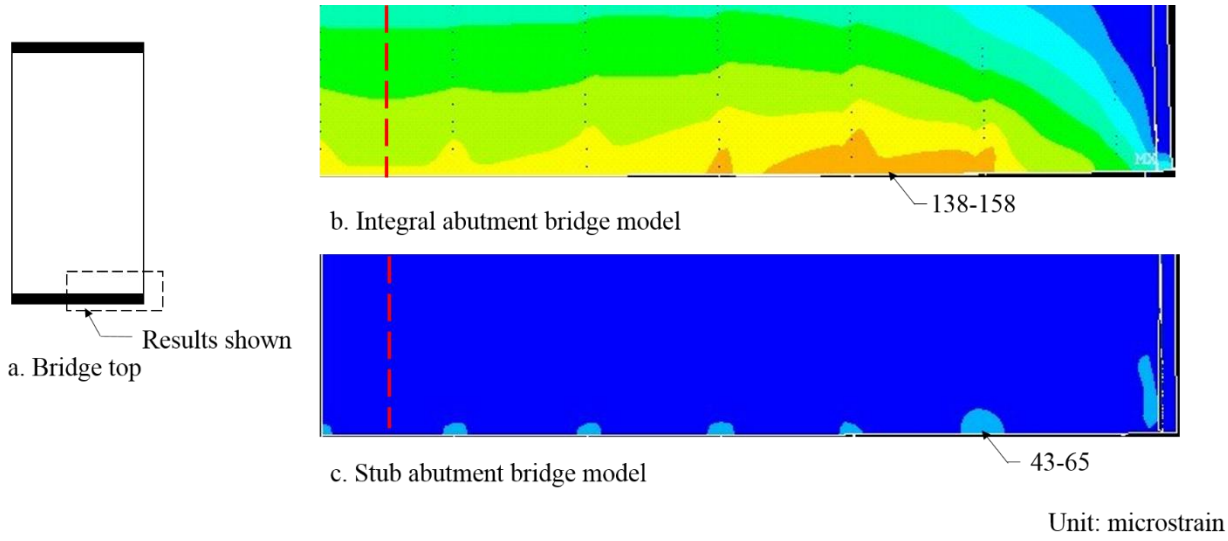

Figure 96. First principal strain contour plot on integral abutment bridge model and stub abutment bridge model

6.4 Pier Type

The influence of two different pier types was studied: fix pier and expansion pier. Based upon details commonly utilized by the Iowa DOT, the major behavioral difference between the

www.manaraa.com

types of pier is that the expansion pier releases the translations in transverse and longitudinal directions between the girder and pier cap, while in the fixed pier, the girder and pier cap move together transversely and longitudinally. Table 7 shows how the fixed pier and expansion pier were simplified in the FEM.

Table 7. Simplification of bearing over pier cap in FEM

Pier type	Translation			Rotation		
	Transverse direction	Longitudinal direction	Vertical direction	Transverse direction	Longitudinal direction	Vertical direction
Expansion Pier	Free	Free	Fixed	Free	Free	Free
Fixed Pier	Fixed	Fixed	Fixed	Free	Free	Free

Figure 97 shows the first principal strain contour plot on the top surface of the deck on the expansion pier bridge model and the fixed pier bridge model. By comparing both plots, it appears that pier type has no significant influence on the strain in the deck near the abutment.

www.manaraa.com

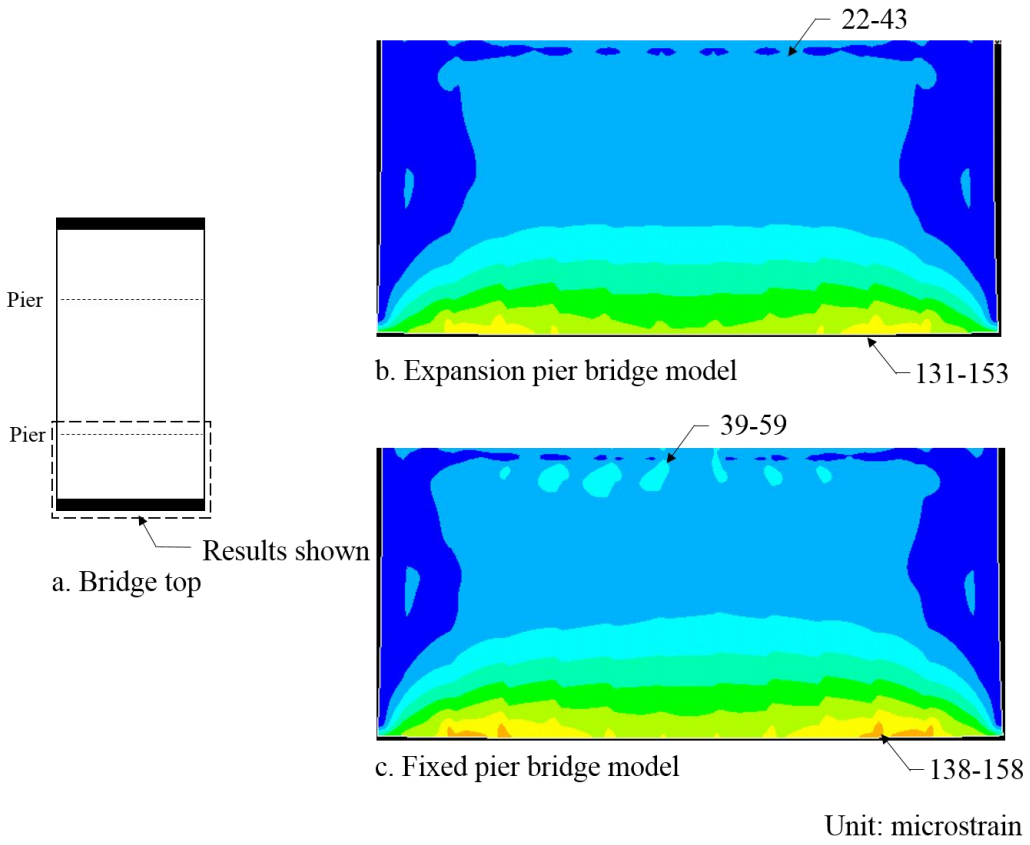

Figure 97. First principal strain contour plot on expansion pier bridge model and fixed pier bridge model

6.5 Span

To study the influence of the number of spans, a one-span bridge model and a three-span bridge model were developed and compared. Figure 98 presents the first principal strain contour plots for the one-span model and for the first span of the three-span bridge model. As shown in the figure, the one-span bridge has a somewhat higher deck strain than the three-span bridge model. However, compared with the magnitude of the strain value, the strain difference between both bridge models appears insignificant.

www.manaraa.com

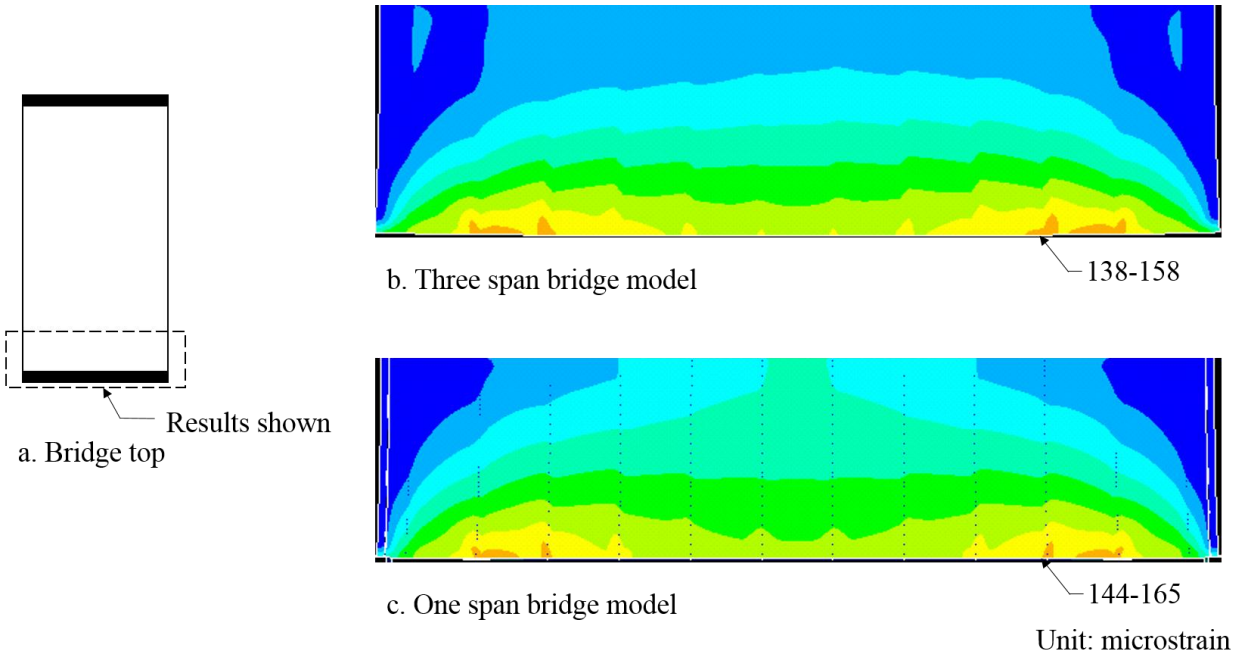

Figure 98. First principal strain contour plot of deck of one-span bridge model and three-span bridge model

6.6 Girder Type

With help from the Iowa DOT, an equivalent steel girder (shown in Figure 99) design was established such that the concrete girder on Bridge #605220 could be replaced with a structurally equivalent steel beam. These equivalent girders were then used to study the effect of girder types by replacing the concrete girders with the steel girders in a geometrically identical analytical model.

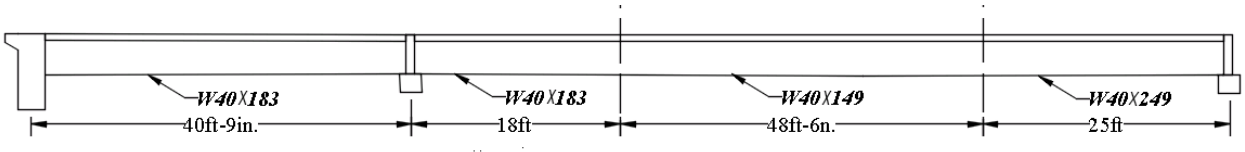

Figure 99. Equivalent steel girder

www.manaraa.com

Figure 100 compares the first principal strain distributions on the deck from the steel girder bridge model and concrete girder bridge model. As can be seen there is virtually no difference between the two models in terms of the deck first principal strain value.

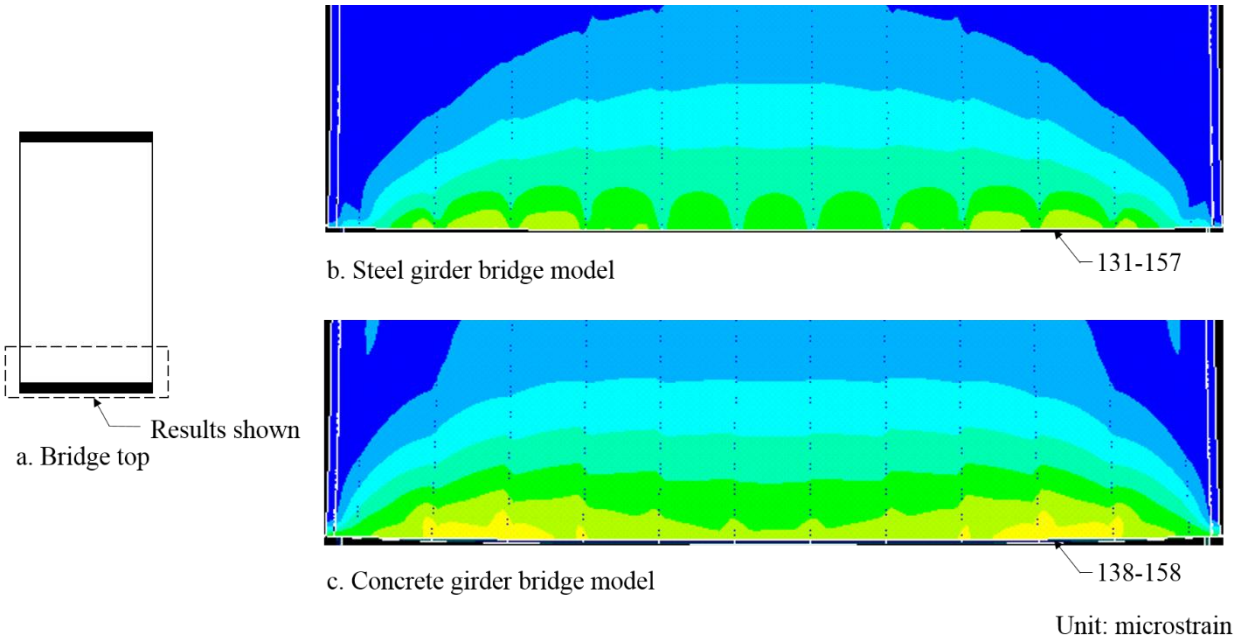

Figure 100. First principal strain contour plot of deck of steel girder bridge model and concrete girder bridge model

6.7 Girder Spacing

Two different girder spacing were analytically studied to evaluate the influence of girder spacing on deck strain. One girder spacing was the original girder spacing of 88.375 in. and the other girder spacing (176.75 in.) was twice that. It must be pointed out that no other changes to the model were made to account for the impact of an increased girder spacing (e.g., required girder size). Figure 101 shows the first principal strain contour plots for both the one-girder-spacing model and double-girder-spacing model. For both models, the maximum tensile strain on

www.manaraa.com

the top surface of the deck was around 140 microstrain. No obvious difference in strain between the two bridge models was observed.

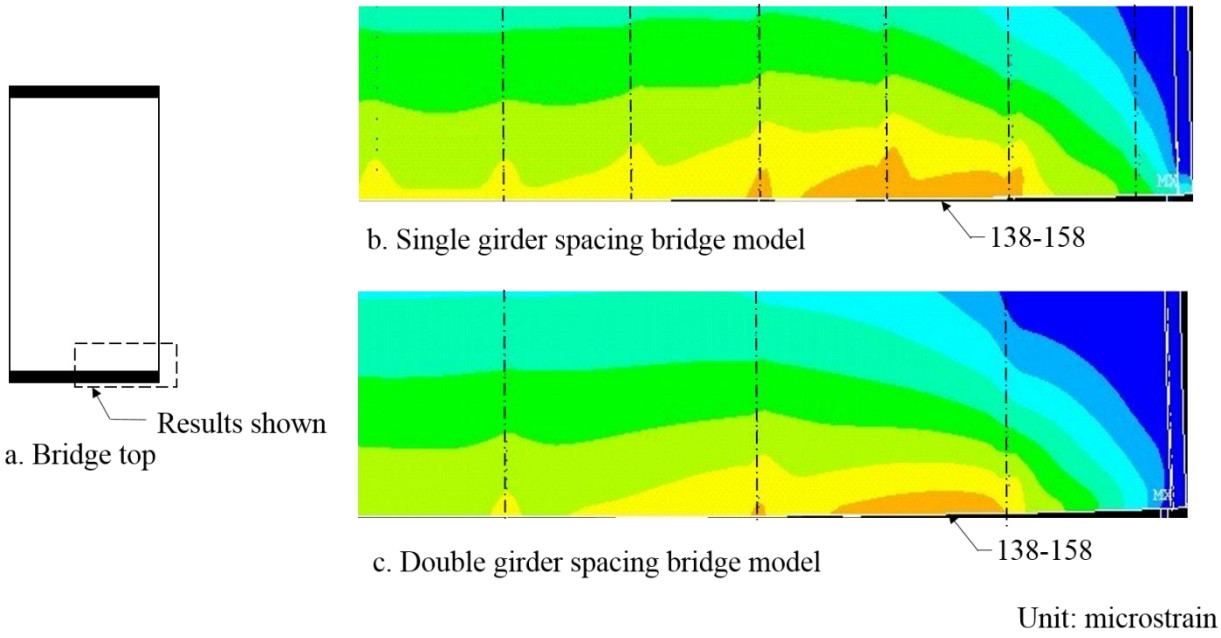

Figure 101. First principal strain contour plot of deck of one-girder-spacing bridge model and double-girder-spacing bridge model

www.manaraa.com

CHAPTER 7. RESULTS VALIDASTIONS AND POTENTIONAL SOLUTIONS

In this chapter, the simple search of bridge deck crack condition was conducted to validate parametric study results. Three potential solutions that may help to reduce the tensile strain in the deck were also preliminarily investigated and are described.

7.1 Deck Cracking of In-Place Bridges

7.1.1 Search on 40 bridges with single type of abutment

To further validate the parametric study results in Section 6.2, a search of bridge inspection reports from "Structure Inventory and Inspection Management System (SIIMS)" was conducted. The bridge inspection review focused on the likely most important factors – width, skew, and abutment type.

Crack maps from bridge inspection reports were used to qualitatively evaluate the likelihood for deck cracking. The bridge search resulted in 40 bridges in Iowa, with 20 integral abutment bridges and 20 stub abutment bridges. For each type of bridge, 10 narrow bridges (around 40-ft) and 10 wide bridges (around 80-ft) were selected. For each bridge width, five skewed bridges and five non-skewed bridges were selected. However, only three wide stub abutment bridges with high skew were found. Relevant bridge inspection parameters are shown in Table 8 and Table 9.

www.manaraa.com

Table 8. Bridge inspection results on integral abutment bridge

No.	FHWANO	Deck Width	Skew	Crack Map	Comments on cracks on top surface of deck near abutment (Based on the crack maps from reports)	Longitudinal or diagonal crack width	Longitudinal or diagonal cracks leach
1	14281	40	0				
2	606905	40	0	X	3-6 longitudinal cracks		
3	606685	40	0	X	7-10 longitudinal and diagonal cracks		
4	16331	40	0	X	No cracks		
5	19421	40	0	X	Extensive longitudinal and diagonal cracks		X
6	32581	40	45	X	1-3 longitudinal and diagonal cracks		
7	43241	40	45	X	2-4 longitudinal and diagonal cracks		
8	49661	40	45	X	Extensive longitudinal and diagonal cracks		X
9	609575	40	45	X	1-3 longitudinal and diagonal cracks		
10	609565	40	45	X	No cracks		
11	20841	75	1				
12	43561	78	0				
13	42391	86	0	X	No cracks		
14	605220	87.2	2	X	Extensive longitudinal and diagonal cracks	"1/16in"	X
15	42181	95	0.4				
16	609165	71	10	X	5-10 longitudinal and diagonal cracks		
17	609160	83	45				X
18	700060	113	35	X	3-5 diagonal cracks		
19	504510	92.5	20	X	2-3 diagonal cracks		
20	607635	73	27	X	7-10 longitudinal and diagonal cracks	"hairline"	

www.manaraa.com

Table 9. Bridge inspection results on stub abutment bridge

No.	FHWANO	Deck Width	Skew	Crack Map	Comments on cracks on top surface of deck near abutment (Based on the crack maps from reports)	Longitudinal or diagonal crack width	Longitudinal or diagonal crack leach
1	601235	40	0	X	No crack		
2	48231	40	0		No crack map included report was found		
3	21841	40	0	X	1 longitudinal crack		
4	605830	40	0	X	1-2 longitudinal crack		
5	211161	40	0	X	No crack		
6	30121	40	45	X	1-2 diagonal cracks		
7	30091	40	45	X	No crack		
8	51311	40	45	X	3-4 cracks at obtuse angle corner		
9	51301	40	45	X	No crack		
10	607730	40	47	X	2-3 longitudinal cracks		
11	700150	77	0		No report found		
12	44691	82	0		No crack map included inspection report was found		
13	604440	72	0				
14	23440	84	0		No bridge record in SIIMS		
15	700110	86.3	0				
16	609905	84	11				
17	600765	85	9		No bridge record in SIIMS		
18	504605	80	17				
19							
20							

For the integral abutment bridges in Table 8, there was no observed significant relation between bridge width and deck cracking, and no apparent relation between bridge skew and deck cracking was found. However, the inspection reports and/or crack maps consistently indicated that inspectors observed deck cracking within nearly all integral abutment bridges. At the same time, no significant crack issue was observed for any of the stub abutment bridges regardless of width nor skew. These results appear to match the FEM results in Section 6.2. They are also

www.manaraa.com

consistent with the literature review results in Chapter 2. From this, one may conclude that the predominant factor influencing deck strain, and therefore the likelihood for deck cracking, is the type of abutment. One can probably also conclude that the reason that integral abutments result in greater deck strain is due to the additional restraint afforded by the structural details. This fact, coupled with the fact that the deck are consistently at different temperatures, leads the research team to believe that the most likely cause of longitudinal deck cracking is a combination of restraint conditions coupled with thermal behavior differences.

7.1.2 Deck crack condition on a bridge with two different abutment

In addition to conducting the search on bridges with single type abutment, the research team also tried to looking for the bridges with both integral and stub abutment, although the information for such bridge is very less. Bridge #608585, located at the north-west of Mt Pleasant, IA is a 220 ft long three span bridge with 36 degree skew. The traffic on the bridge is in east-west direction. The east abutment is an integral abutment, and the west abutment is a stub abutment. Figure 102 shows the deck top crack condition near the abutment on the bridge #608585. It is obvious that on the integral abutment side more cracks develop in the deck than the other side of the bridge. This observation matches with the parametric study results in Section 6.3 that high strain in the deck only occur on the integral abutment bridge, which gives research team more confidence on the conclusion that the restraints from integral abutment is one of the major reason causing the high strain and cracks in the deck near the abutment.

www.manaraa.com

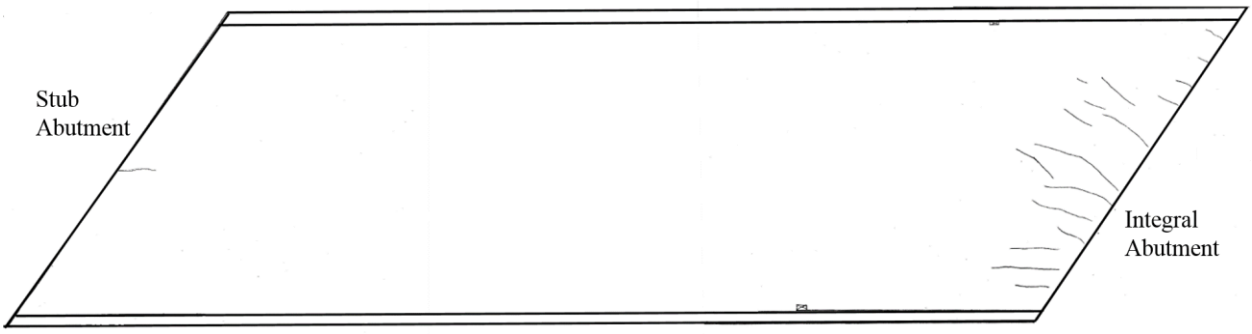

Figure 102. Deck top crack map on Bridge #608585

7.2 Potential Solutions to Reduce Longitudinal Cracks

After the parametric study, additional work utilizing the bridge FEM was completed. Of specific interest was the conduct of a preliminary study of means to reduce strain (cracking) in the deck.

7.2.1 Isolation of abutment from soil

Since the large strain in the deck near the abutment is due to a combination of abutment restrain and the temperature difference between the abutment and the deck, a conceptual temperature isolation pad shown in Figure 103 might prevent heat transfer from the soil to the abutment.

www.manaraa.com

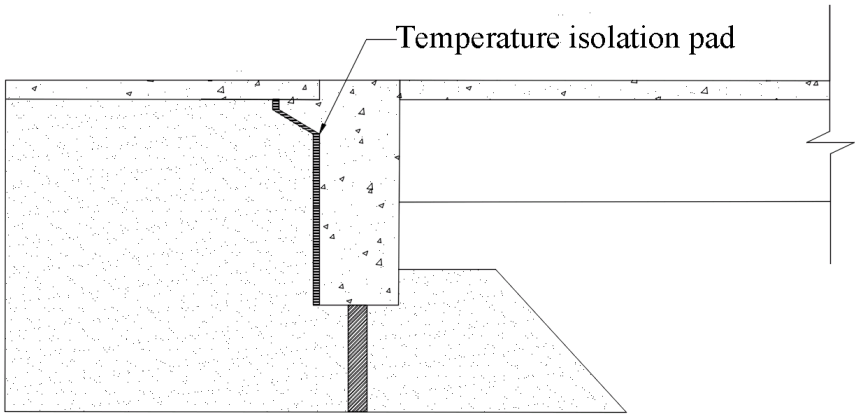

Figure 103. Temperature isolation pad configuration and position

If the temperature isolation pad is fully functional, the temperatures on the abutment and the deck will be similar. In this case, the whole bridge will be under the same temperature change. To study this, an extreme uniform temperature change (-113°F) from summer to winter was applied on the FEM.

Figure 104 shows the first principal strain distribution on the top surface of the deck. As the plot shows, the strain in the deck near the abutment remote from the stress concentration point is greatly reduced from 150 microstrain (shown in Figure 89) to 10 microstrain (shown in Figure 104). The strain concentration at the corner of the deck is not considered significant since for this preliminary study as no temperature isolation pad was theoretically placed at the wing wall so there was a significant temperature difference at the wing wall.

www.manaraa.com

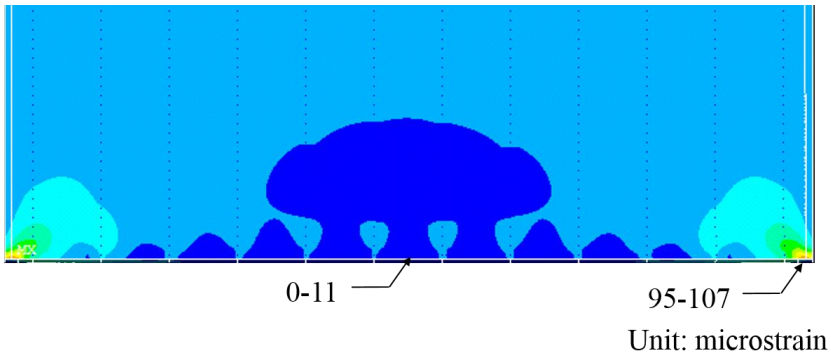

Figure 104. First principal strain distribution plot on deck due to uniform temperature changes - 113 °F

7.2.2 Vertical expansion joints on abutment

To release the high strain in the deck the addition of vertical expansion joints in the abutment was theoretically considered. In the analytical model, two expansion joints with three different spacing were applied. The nodes on the expansion joints were separated to simulate the expansion joint. The top node at the expansion joint was connected to the deck (shown in Figure 105). Three different arrangements were studied, with the distance between the expansion joints being 24-ft, 39-ft, and 53-ft (shown in Figure 106 to Figure 108).

Figure 106 to Figure 108 show the first principal strain contour plot on the top and bottom surfaces of the deck resulting from the conceptual case of a bridge with an expansion joint in the abutment. On the top surface of the deck, stress concentrations were observed at the top of the expansion joint, which was caused by how the connection between the vertical expansion joint and the deck at the top node was modelled. Beyond these stress concentrations, the strain was lower than the strain on the model without the expansion joint. Comparing the first principal strain contour plots from the three different models, placement of the expansion joints

www.manaraa.com

affects the locations of the maximum strain in the deck. However, to put these expansion joints into practice, more would be required to determine how to actually implement such a solution.

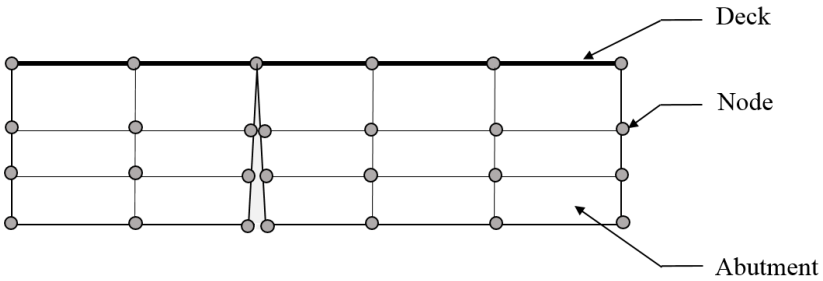

Figure 105. Separation of the abutment on the FEM

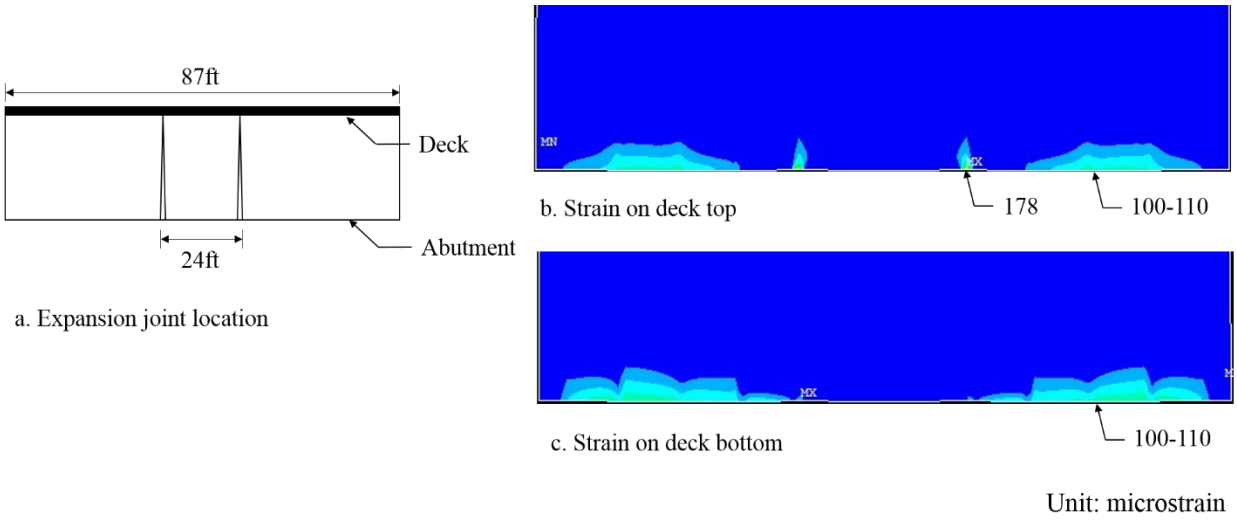

Figure 106. First principal strain for the model width 24 ft spacing joint

www.manaraa.com

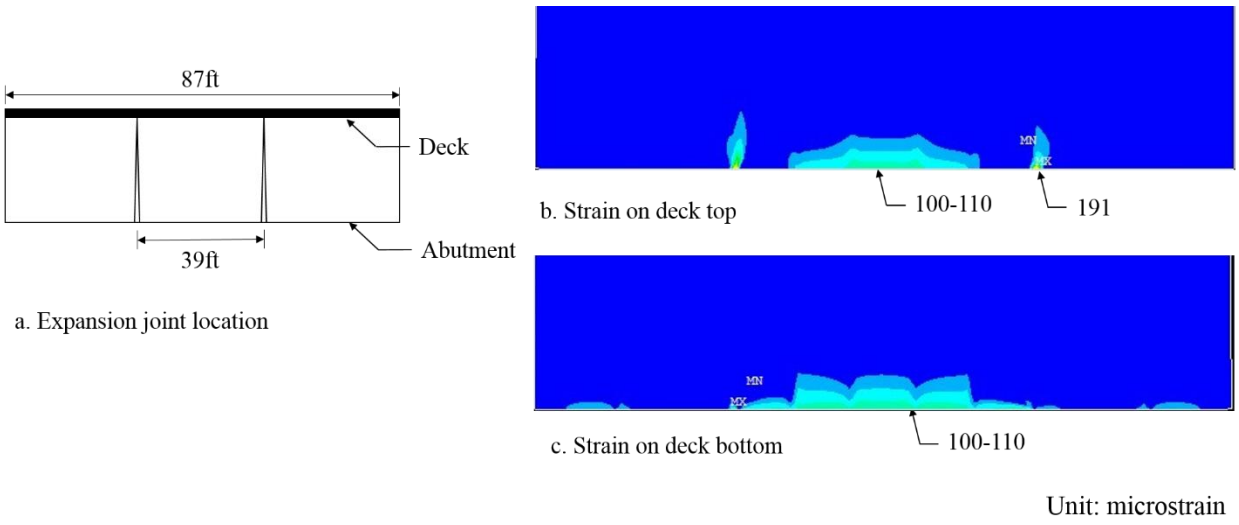

Figure 107. First principal strain for the model width 39 ft spacing joint

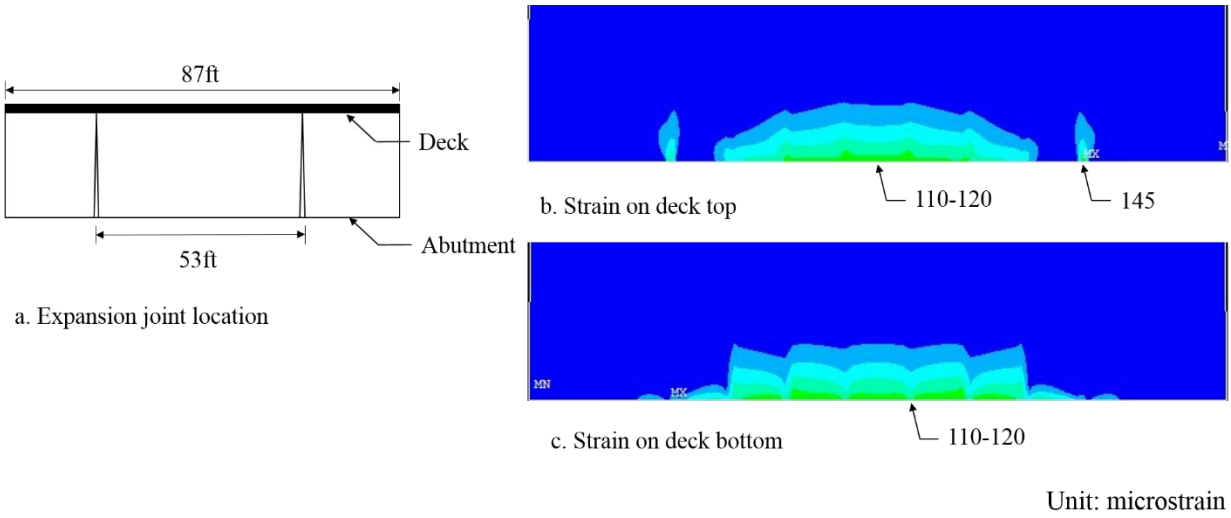

Figure 108 First principal strain for the model width 53 ft spacing joint

7.2.3 Increasing the amount of temperature and shrinkage steel in the deck

One of the problems studied in this project was the longitudinal cracks in the deck near the abutment perpendicular to the transverse steel in the deck. Gilbert indicated that the shrinkage and temperature reinforcement required for a fully restrained slab could be double that required by ACI 318. He showed that the Australian code requires two to three times more

www.manaraa.com

shrinkage and temperature reinforcement than the minimum required by ACI 318 (Gilbert 1992). Hence, further increasing the temperature of the steel in the deck may be a solution to reducing those cracks.

By the AASHTO code, the area of temperature reinforcement per foot required for this concrete bridge deck is 0.142 in^2/ft (0.135 percent). The reinforcement percentage for this bridge deck specified by ACI code is 0.2 percent. The Australian code gives a minimum steel reinforcement percentage of 0.945 percent, and Gilbert suggests using at least 0.284 in^2/ft (0.27 percent) for a fully restrained slab.

Figure 109 and Figure 110 show the transverse and longitudinal reinforcement steel arrangement in the deck provided by Iowa DOT. The reinforcement percentage for the transverse steel is one percent (1.01 in^2/ft). In the longitudinal direction, the reinforcement steel percentage is 0.8 percent (0.81in^2/ft).

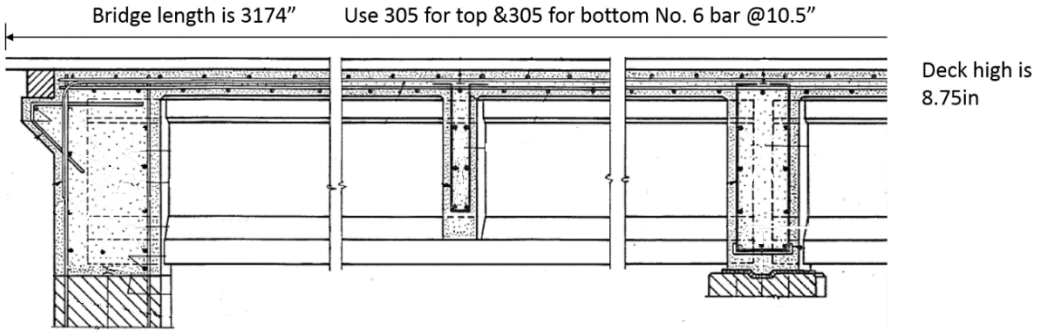

Figure 109. Transverse reinforcement arrangement in deck

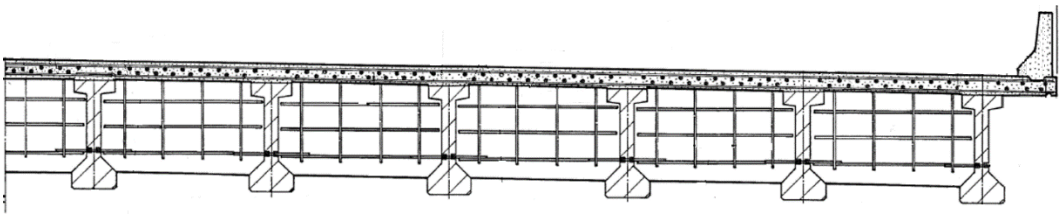

Figure 110. Longitudinal reinforcement arrangement in deck

www.manaraa.com

Comparing the reinforcement ratio with the minimum recommendation from ACI, AASHTO, the Austrilian code and Gilbert, it appears that Bridge #620550 has sufficient temperature of the steel in both transverse and the longitudinal directions. Hence, further increasing the amount of steel was not studied further.

www.manaraa.com

CHAPTER 8. STUDY OF DIAGONAL STEEL

8.1 Problem Statement and Background

Problem Statement

Bridge inspection experience indicated that the opening width of diagonal cracks at the corner of the deck is usually larger than the width of longitudinal cracks at the middle of the deck. The leaking problem through those diagonal cracks is more severe than it is on the longitudinal cracks. Furthermore, on the integral abutment bridge, the diagonal cracks are more prevalent than the longitudinal cracks. Figure 111 compares a longitudinal crack with a diagonal crack at the bottom of the deck on bridge #605220 in Waterloo. The inspection results on newly constructed bridges revealed that often, when longitudinal cracks have not yet occurred, diagonal cracks have already existed.

Figure 111. Typical longitudinal and diagonal cracks at the bottom of deck

www.manaraa.com

Additionally, the FEM results in Chapter 5 indicated higher tensile strain at the corner of the bridge deck than in the middle of the bridge deck. Figure 112 is a top view of the bridge deck which shows the first principal strain contour plot on the top surface of the deck near the abutment on an integral abutment bridge FEM. The maximum strain at the corner of the deck is from 129 to 146 microstrain, while near the abutment at the center line, the tensile strain ranges from 109 to 127 microstrain. Hence, the cracking at the corner of a continuous deck is more severe than that near the abutment at the center line.

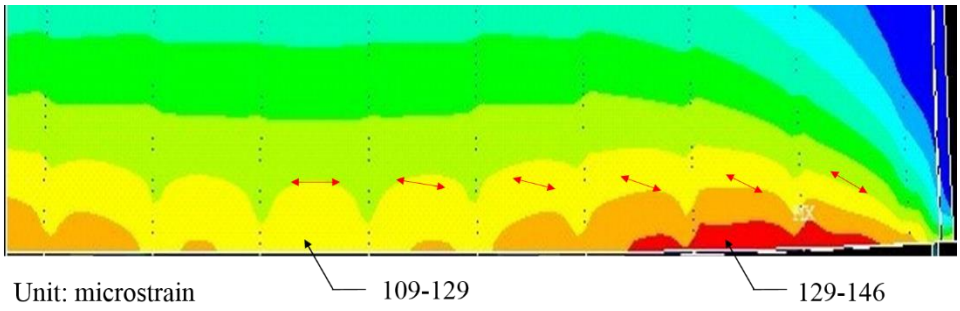

Figure 112. First principal strain on the top of the deck near abutment

Background

Stringer and Burgueno used an experimentally calibrated non-linear FEM to predict the cracks on the jointless bridge deck on an integral abutment bridge and semi-integral abutment bridge. The parametric study results showed that change of the amount, spacing and size of transverse and longitudinal reinforcement has minimal effect on bridge performance (Strainge and Burgueno 2012).

However, in Stringer's research, although the spacing and size of transverse and longitudinal reinforcement steel were changed, the study of orientation of reinforcement steel was

www.manaraa.com

not included. Furthermore, the FEM used in the parametric study had no ability to model the cracks, so, a post-crack analysis which could include a study of crack width was not conducted.

8.2 Objective and Introduction

The main objective of this chapter was to study the effect of diagonal reinforcement steel on the performance of the bridge deck. First, the effect of diagonal steel regarding the reduction of the deck strain was studied with a non-crack model. Second, a simple diagonal crack was modeled into the FEM to study whether crack width can be reduced by diagonal steel. The loading used in this chapter is the annual temperature loading (see annual temperature loading details in Section 5.5.3).

8.3 Effect on Bridge Strain

To study the effect of diagonal steel on bridge deck strain, different diagonal steel sizes and spacing were incorporated into the FEM. In total, four models were used in this section, and three of them had diagonal steels. Table 10 shows the diagonal reinforcement details of each model.

Table 10. Model details for the study of diagonal steel

Model No.	Diagonal steel type	Spacing (in.)	Angle to longitudinal bar (°)
1			No Diagonal Steel
2	No.5	12	45
3	No.6	6	45
4	No.9	6	45

Figure 113 shows the first principal strain contour on the top surface of the bridge deck for those four models. Although the maximum strain region decreased as more steel was placed into the deck, the maximum strains in the deck from these four models were all about 135 to 155

www.manaraa.com

microstrain, indicating that the deck would crack no matter how much reinforcement steel was placed into the deck.

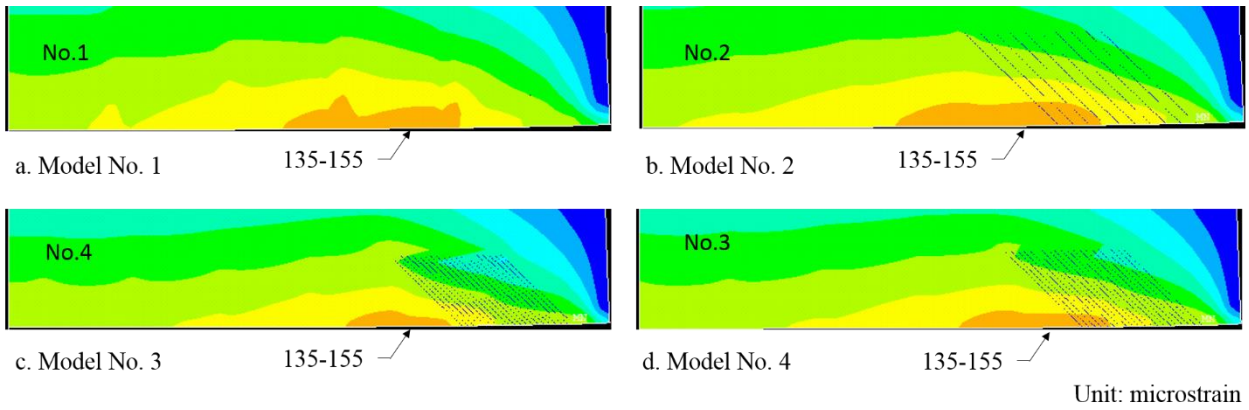

Figure 113. First principal strain contour for the study of diagonal steel

8.4 Effect on Diagonal Cracks

In this section, the effect of diagonal steel after a diagonal crack has formed at the corner of the deck was studied. Rather than creating a crack on the whole bridge model, a simple deck-abutment model was created to simulate deck behavior near the abutment. The simple model was validated by comparing the strain magnitude and the strain direction in the deck with the original full bridge model. A diagonal crack was then created at one corner of the bridge deck on the simple model.

8.4.1 Simple model validation

Since the parametric study results indicated that the longitudinal and diagonal cracks in the deck near the abutment is induced by the temperature difference between the deck and the abutment, and that the main restraints on the bridge deck come from the abutment rather than

www.manaraa.com

other bridge components such as girders and piers, the model used in this section contained only the abutment and the deck in one span (shown in Figure 114 and Figure 115).

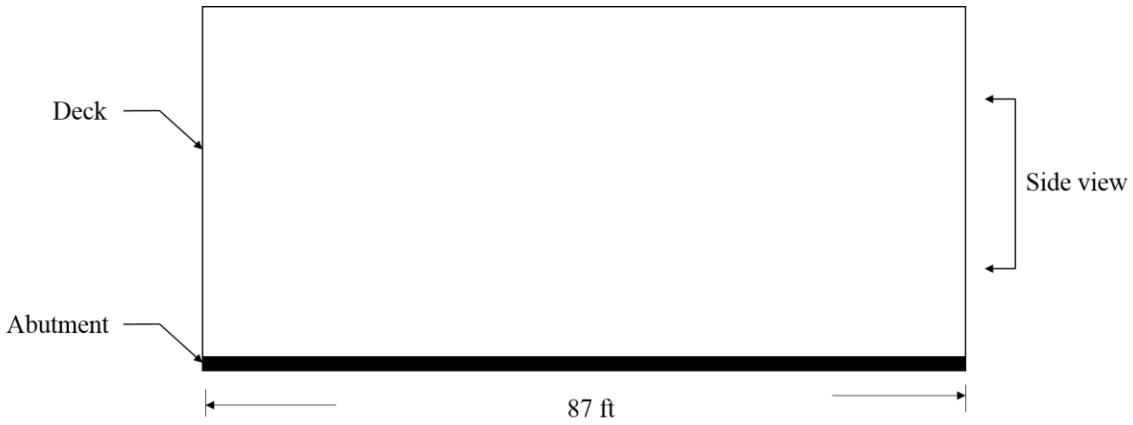

Figure 114. Top view of the simple model

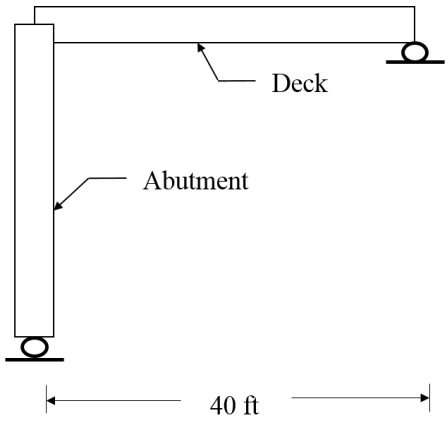

Figure 115. Side view of the simple model

The support conditions at the bottom of the simple abutment model were kept the same as the original full bridge model, which had only vertical supports at each pile location (shown in Figure 115). Since the pier diaphragm and pier type had little effect on the deck strain near the abutment, only simple vertical support was used at each corner at the far end of the deck. The material properties used on the simple model were the same as those in the full bridge model, and reinforcement steel was also smeared into the concrete.

www.manaraa.com

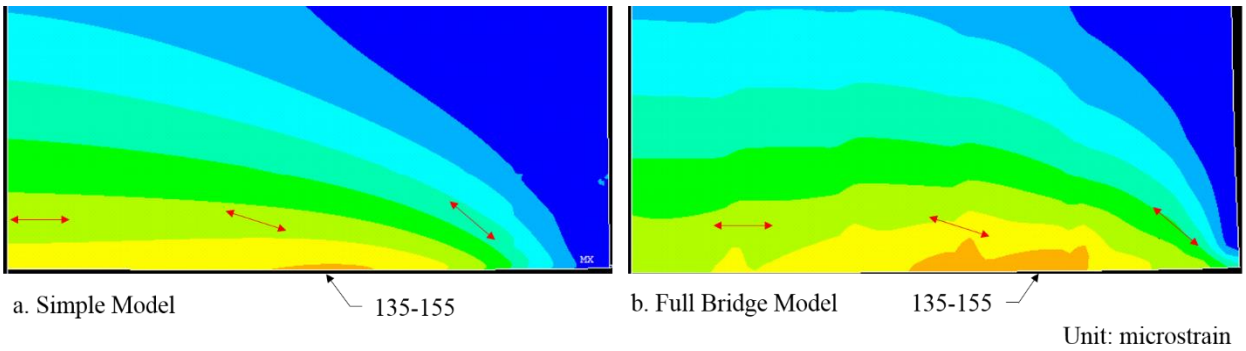

Figure 116. Validation of the simple model

Figure 116 compares the first principal contour plot at the top of the deck between the simple model and the full bridge model. The strain directions from those two models were the same, and the strain magnitudes differ by only 10 microstrain. Hence, the simple model will be effective in representing the deck cracking near the abutment of the full bridge model.

8.4.2 Analytical study

Initially, one simple model (Model-1 shown in Table 11) with only longitudinal and transverse steel was built. The crack was created 45 degrees from the abutment and was perpendicular to the first principal strain direction at the deck corner (shown in Figure 117). The length of the crack was 8.5 ft (shown in Figure 117). The crack at the corner of each model was formed by separating the elements along the crack edge and duplicating nodes at the same location. Longitudinal and transverse steel in the deck was modeled by discrete bar elements in this section.

www.manaraa.com

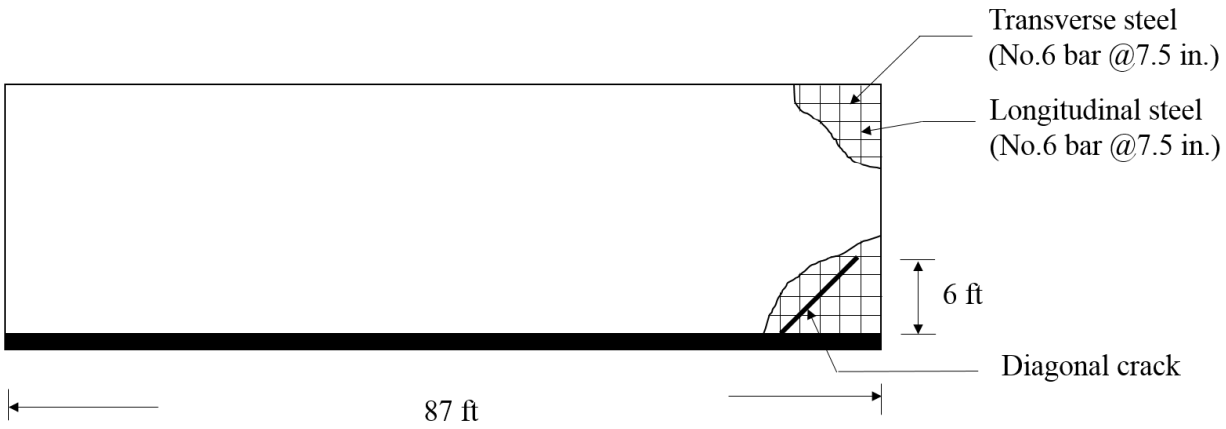

Figure 117. Crack geometry and reinforcement steel distribution on Model-1

The deformed shape near the diagonal crack, due to annual temperature loading, is shown in Figure 118. The upper part of the two edges of the crack overlapped, but this could not happen on a real bridge. Thus, the second and third models were created with the upper part of the crack closed, and a new crack length of 5.6 ft.

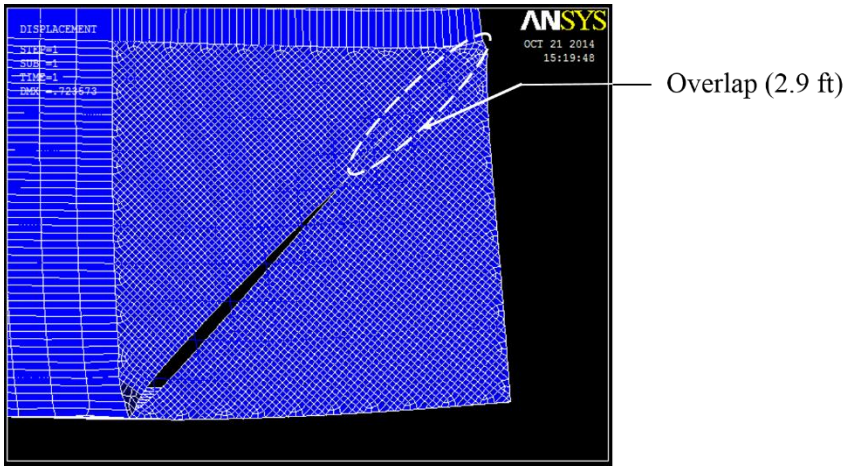

Figure 118. Deformed shape near the diagonal crack

To study the effect of diagonal steel on diagonal crack width, two simple models, each with one diagonal crack at the right corner but with different steel arrangements, were formed. The diagonal cracks were created 45 degrees from the abutment (shown in Figure 119), and the lengths of the cracks were 5.6 ft for both models.

www.manaraa.com

Model-2, as a reference model, had only longitudinal and transverse steel. Model-3 had diagonal steel cross the crack at the corner, as shown in Figure 119. The diagonal steel in the deck was also modeled by discrete bar elements. Detailed information about the diagonal reinforcement steel for each model is listed in Table 11.

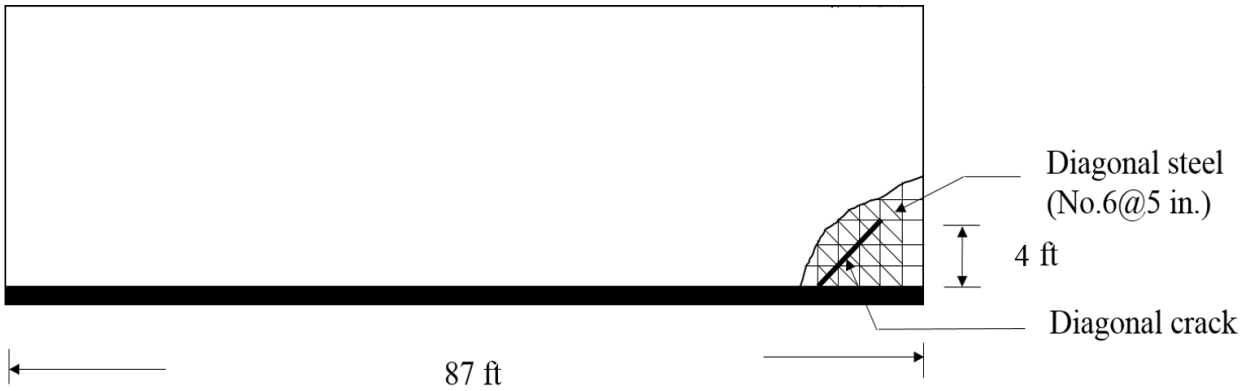

Figure 119. Crack geometry and reinforcement steel distribution on model-3

In the region immediately adjacent to the crack, the concrete and steel stresses vary considerably, and there exists a region of slip between the concrete and steel. The slip length between the concrete and steel was calculated by equation (6) (Gilbert 1992).

$$S_o = \frac{d_b}{10\rho} \qquad (6)$$

S_o – Slip length between concrete and steel (8 in.)

d_b – Diameter of reinforcement steel (0.75 in.)

ρ – Reinforcement ratio ($A_s/A_c \approx 0.01$)

www.manaraa.com

Table 11. Simple model diagonal steel details and analytical results

NO.	Crack length (ft)	Diagonal steel type	Diagonal steel spacing (in.)	Slip length (in.)	Crack width (in.)
Model-1	8.5	No diagonal steel		8	------
Model-2	5.6	No diagonal steel		8	0.0040
Model-3	5.6	No.6	5	8	0.0024

Table 11 shows analytical results for the crack width opening for both models. The maximum crack width from the model without diagonal steel in the corner of the deck was 0.0040 in., while the maximum crack width from the model with diagonal steel was 0.0024 in. The No.6 bar @ 5 in. decreased the crack width by 40 percent. Hence, diagonal steel was very effective in minimizing crack width.

8.5 Conclusions

Diagonal steel at the corner of the deck is not effective in significantly reducing the high strain in the deck. Deck cracks will occur similar to those on a non-diagonal-steel deck, even with a large amount of steel. However, diagonal steel is very effective in reducing crack width after cracks occur. Crack width can be reduced by 40 percent, according to this analytical work.

www.manaraa.com

CHAPTER 9. CONCLUSIONS AND RECOMMENDATIONS

This chapter presents a summary of the project approach, the measured and analytical results, conclusions drawn from those results, and recommendations. Limited information is presented here and additional details can be found in the preceding chapters.

9.1 Summary

9.1.1 Summary of field testing

Field testing, which included live-load and long-term testing, was conducted on Bridge #605220 which is located near Waterloo, IA to provide general behavior information and to provide data for the calibration of an analytical model that would be the focal point of much of the research. The bridge was selected based upon the results of detailed bridge inspection results of five candidate bridges and other factors (including traffic, location, etc.). Bridge #605220 is a 264.5 ft long four-span bridge with a small 1.5 degree skew. The bridge consists of an integral abutment and 12 pre-stressed concrete girders.

Live-Load Testing

In total, 60 BDI strain transducers were installed on Bridge #605220 during live-load testing. Twenty-four transducers were placed near the south abutment and south pier and twelve transducers were placed at mid-span of the second span. At each instrumented location, one transducer was attached on the side of the top flange, and a second transducer was attached at the bottom surface of the bottom flange.

www.manaraa.com

During live-load testing, a three-axle Iowa Department of Transportation snooper truck was driven across the bridge at a crawl speed (approximately 3 mph) to induce a pseudo-static load on the bridge. In total, five load cases with different transverse vehicle positions were utilized to obtain the strain data which was used for general study of bridge behavior and for calibration of the subsequently described FEM. For each load case, the truck moved from south to north.

The live-load testing demonstrated that the bridge effectively acted in a symmetric manner. It was also found that only those gauges on the three to four girders nearest the truck had significant readings, which were then used for the calibration of a FEM. It was also observed that the strain values at the top flange gauges are very small indicating that the cross-section neutral axis is very near the top flange.

Long-Term Testing

Long-term testing focused on studying the behavior of the bridge deck near the abutment during temperature changes since previous bridge inspection results and technical literature indicated that most longitudinal and diagonal cracks were observed in that region. The long-term monitoring plan provided strain, displacement, and temperature data for the calibration and validation of the FEM.

During long-term testing, vibrating wire strain gauges were used to measure the load-induced strain at the bottom of the deck resulting from restrained temperature changes. Three cross-sections - abutment section, middle-span section and pier section-were selected to capture the strain data. The abutment section is 54 in. from the surface of the south abutment. Six bays near the east side of the bridge were selected for strain monitoring. In each bay a strain gauge was attached in the middle of the bay between the two girders. The middle-span section is

www.manaraa.com

located in the middle of the first span on the south side of the bridge. The pier section is 54 in. from the south side of the first pier in the south side of the bridge. In both the middle span section and the pier section, vibrating strain gauges were attached in the 1st bay, 3rd bay and 5th bay on the east side of the bridge.

Four vibrating-wire long-range displacement meters were used to measure the relative longitudinal and transverse displacement due to thermal changes in the first span of the bridge. Two displacement meters were installed at the bottom of the deck in two exterior bays near the first interior girder to measure the relative longitudinal displacement in the first span on the south side of the bridge. The other two displacement meters were used to measure the relative displacement in the transverse direction. One of them was placed at the bottom of the girder on the surface of the abutment on the south side of the bridge. The other one was installed at the bottom of the girder on the surface of the pier in the first span on the south side.

To characterize the thermal conditions at the bridge the temperature at the bottom of the deck was measured by the thermistor housed within each vibrating wire strain gauge. The temperature at the mid-depth of the deck and within the abutment were also measured using a Geokon 3800 thermistor placed at mid-depth of the deck and just below the surface of the abutment.

The long-term testing results showed that the temperature at the bottom of the deck is generally very uniform throughout the bridge and that changes that occur at mid-depth of the deck are the same as the bottom of the deck (note that this was important during calibration of the FEM). The front abutment average temperature change was about 2/3 of the temperature change on the bottom of the deck.

www.manaraa.com

9.1.2 Summary of bridge model development

Bridge Model Development

The bridge model developed as part of this research includes discrete idealizations of the deck, girder, diaphragm, abutment, and pier cap. Piles under the abutment and pier columns were idealized by assuming the support conditions. Beam 4 elements were used to model the girder flanges, pier cap and steel diaphragm; Shell 181 elements were used to model the deck, concrete diaphragm, abutment and girder web. The deck reinforcing steel was smeared into the concrete and represented by effective material properties.

Calibration for live-load behavior

To compare the live-load testing result and the FEM result, a percentage difference between the two was calculated. Comparisons of the girder strains initially indicated that the FEM predicted higher strain values than the field testing results. As a result the Young's Modulus of the girders was increased to minimize the percentage difference. After that, FEM with updated Young's Modulus values was used to conduct the numerical analysis for all five load cases.

Validation for long-term behavior

For the FEM thermal loadings, two types of temperature changes were considered. The first is a temperature difference between the deck and the abutment, which was measured during the long-term testing. The second one is the temperature gradient through the thickness of the deck which was ascertained from relevant Iowa DOT temperature data.

www.manaraa.com

The strain comparisons at the bottom of the deck near the abutment showed that the FEM results from those bays without visible cracks are very close to the field testing results, which means that the FEM can be used to simulate deck behavior before cracks occur. The displacement comparison in the transverse direction showed that the FEM is sufficient to simulate relative movement. In the longitudinal direction, the FEM overestimated the change due to the temperature effect. Comparison of the strains near the abutment and the transverse displacement supported the conclusion that the FEM is sufficiently accurate to be used in a parametric study.

Validation for Crack Pattern

To validate the model's ability to accurately predict cracking in the deck, an annual bridge temperature change was estimated based on the long-term testing measurement and historical temperature records from the Iowa DOT. The first principal strain distribution and direction that resulted when using those temperature inputs were large enough to crack concrete and in the orientation that matched the cracking observed at the bridge. Also of importance is the fact that the maximum tensile strain in the deck was predicted to exceed the estimated cracking strain, which means that annual temperature changes may possibly result in deck cracking and deterioration.

Validation for Shrinkage

The strain induced by shrinkage was calculated using the relationship given by the AASHTO code. The resulting shrinkage loading was applied by using the common "equivalent temperature method". Comparing the first principal strain plot the crack map, the first principal strain distribution and direction did not match with the crack maps from bridge inspection results

www.manaraa.com

and low strain was observed in the crack near the abutment on the FEM. Hence, shrinkage loading were not considered as a cause of the cracks on the top surface, and it was not applied during the parametric study.

9.1.3 Summary of parametric study

A parametric study was performed to principally determine the effect of bridge width on deck cracking. Other parameters such as bridge skew, girder spacing, girder type, abutment type, pier type and the number of bridge spans were also studied during the parametric study.

The bridge width influence study was performed on both a skew model and a non-skewed model with three bridge widths. For both the non-skew and skew models, increasing the bridge width increased the maximum strain in the deck by 20-30 microstrain, but this increase is not significant compared to the magnitude of the deck strain values as the maximum strain even in the narrowest bridge width exceeded the cracking strain. This result was consistent with results of bridge inspection and literature review results.

To study the influence of abutment type, two non-skewed bridge FEMs: integral abutment bridge and stub abutment bridge models, were developed. The maximum tensile strain in the deck of the integral abutment bridge model was two to three times higher than the strain in the stub abutment model. The study of the other factors: pier type, girder type, girder spacing and number of spans, showed that these factors have little effect on the strain in the deck near the abutment. Thus, it appears that the likelihood of developing deck cracking/deterioration may be most a function of the abutment type as a result of resulting restraint from thermal expansion and contraction.

www.manaraa.com

9.1.4 Summary of potential solutions

To reduce the tensile strain in the deck, three solutions were preliminarily evaluated using the calibrated FEM. Use of temperature isolation pad was regarded as the most effective solution to reduce the strain in the deck if such a system could actually prevent heat transfer from the soil to the abutment. Adding an expansion joint within the abutment was also observed to reduce the strain in the deck, and the geometric placement of the expansion joints impacts the magnitude and location of the maximum strain in the deck. However, to put these expansion joints into practice, more consideration would be required to determine how to actually implement such a solution. Increasing the amount of reinforcement steel in the deck was also considered as a potential solution but was not studied further since a simple search on minimum temperature steel required by ACI code, ASSHTO code and Australia code indicated that the subject bridge has sufficient temperature steel in the longitudinal and transverse directions.

9.1.5 Summary of diagonal steel study

To study the effect of diagonal steel on the strain at the deck corner, four bridge models with different the diagonal steel arrangement were built. The results showed that the deck would crack no matter how much reinforcement steel was placed into the deck.

Furthermore, the effect of the diagonal steel on the crack width the bridge corner of the bridge was studied on a simple model with only the abutment and one-span-deck. A simple diagonal crack was created at one side of the bridge corner by separating the elements and duplicating the nodes at the same location. The results showed that the diagonal steel is very effective in reducing crack width after cracks occur and the crack width can be reduced by 40 percent.

www.manaraa.com

9.2 Conclusions

Based on the results of literature review, survey and field testing, and the research investigation on the FEM, the following conclusions can be made:

- Longitudinal and diagonal cracking in the deck near the abutment on an integral abutment bridge is due to the temperature differences between the abutment and the deck. Although not likely to induce cracking, shrinkage of the deck concrete may further exacerbate cracks developed from thermal effects.
- Based upon a limited review of bridges in the Iowa DOT inventory, it appears that, regardless of bridge width, longitudinal and diagonal cracks are prevalent in integral abutment bridges but not as much so in bridges with stub abutments.
- The parametric study results show that bridge width and skew have minimal effect on the strain in the deck bridge resulting from restrained thermal expansion.
- Pier type, girder type, girder spacing and number of spans also appear to have no influence on the level of restrained thermal expansion strain in the deck near the abutment.
- Based upon the literature results and research experience, adding more transverse temperature steel in the deck near the abutment will not likely be effective in reducing the strain in the deck.
- The deck would crack no matter how much reinforcement steel was placed into the deck but the diagonal steel is very effective in reducing crack width after cracks occur.

9.3 Recommendations

In general, no practical solution to eliminate deck cracking was found during the research, the following items are suggested to reduce the deck cracking. But for some of them, more research works are required before putting them into practice.

www.manaraa.com

- If deck cracking is a major concern in certain situation, the use of a stub abutment is recommended.
- To obtain a better understanding of bridge deck behavior, a bridge with both integral and stub abutment was recommended for the field testing to measure the thermal loading and behavior of bridge on both integral and stub abutment ends of the bridge.
- Based upon the FEM results, an effective solution to reduce cracking in the deck might be to place an isolation pad between the soil and back side of the abutment. To put it into practice, more research work including the material and placement of the isolation pad should be conducted.
- Vertical expansion joints in the abutment do help to reduce the strain in the deck, and control the maximum strain location in the deck, according to the FEM. However, more research should be conducted to reduce the stress concentration in the deck over the expansion joints.

www.manaraa.com

REFERENCES

AASHTO. 2004. "AASHTO LRFD Bridge Design Specifications, 3rd ed." *AASHTO. Washington. D.C.,.*

Frosch, R., D. Blackman, and R., Radabaugh. 2003. "Investigation of Bridge Deck Cracking in Various Bridge Superstructure System." *Federal Highway Administration-Joint Transportation Research Program.*

Fu, G., J Feng, J. Dimaria, and Y. Zhuang. 2007. "Bridge Deck Corner Cracking on Skewed Structures." *Final report to Michigan department of transportation.*

Gilbert, R.I. 1992. "Shrinkage Cracking in Fully Restrained Concrete Members." *ACI Structure Journal* 141-149.

Greimann, L., B.M. Phares, Y Deng, G. Shryack, and J. Hoffman. 2014. "Field Monitoring of Curved Girder Bridges with Integral Abutment." *Institute of transportation, Iowa state university.*

Kunin, J.K., and S. Alampalli. 2000 . "Integral Abutment Bridges: Current Practice in United State and Canada." *Journal of performance of constructed facilities* Vol.14, No.3.

Lowell Greimann, Brent M. Phares, Yaohua Deng, Gus Shryack, Jerad Hoffman. 2014. *Field Monitoring of Curved Girder Bridges with Integral Abutment.* Ames,IA: Bridge Engineering Center, Iowa State University.

Martin, P., and JR. Burke. 1999. "Cracking of Concrete Decks and Other Problems with Integral-Type Bridges." *Transportation research record 1688.*

Paul, M., A.J. Laman, and D.G. Linzell. 2005. "Termally Induced Superstructure Stress in Prestressed Girder Integral Abutment Bridges." *Transportation Research Record: Journal of the transportation research board* 287-297.

Purvis, R. 2003. "Bridge Deck Joint Performance." *NCHRP synthesis 319, Transportation research board, Washington, D.C.*

Russel, H.G., and L.J. Gerken. 1994. "Jointless Bridge - the Knows and the Unknows." *ACI Concrete International* 16(4),44-48.

Strainge, D.J., and R. Burgueno. 2012. "Identification of Causes and Solution Strategies for Deck Cracking in Jointless Bridges." *Final report to Michigan Department of Transportantion, Michigan State University, Lansing, Michigan.*

TRS1105. 2011. "Tranportation Research Synthesis: bridge deck Cracking." *Minnesota department of transportant.*

www.manaraa.com

www.manaraa.com